science.sciencemag.org/content/366/6466/708/suppl/DC1

Supplementary Materials for

Ancient Rome: A genetic crossroads of Europe and the Mediterranean

Margaret L. Antonio*, Ziyue Gao*, Hannah M. Moots*, Michaela Lucci, Francesca Candilio, Susanna Sawyer, Victoria Oberreiter, Diego Calderon, Katharina Devitofranceschi, Rachael C. Aikens, Serena Aneli, Fulvio Bartoli, Alessandro Bedini, Olivia Cheronet, Daniel J. Cotter, Daniel M. Fernandes, Gabriella Gasperetti, Renata Grifoni, Alessandro Guidi, Francesco La Pastina, Ersilia Loreti, Daniele Manacorda, Giuseppe Matullo, Simona Morretta, Alessia Nava, Vincenzo Fiocchi Nicolai, Federico Nomi, Carlo Pavolini, Massimo Pentiricci, Philippe Pergola, Marina Piranomonte, Ryan Schmidt, Giandomenico Spinola, Alessandra Sperduti, Mauro Rubini, Luca Bondioli, Alfredo Coppa†, Ron Pinhasi†‡, Jonathan K. Pritchard†‡

*These authors contributed equally to this work.
†Corresponding author. Email: pritch@stanford.edu (J.K.P.); ron.pinhasi@univie.ac.at (R.P.); alfredo.coppa@uniroma1.it (A.C.)
‡These authors contributed equally to this work.

Published 8 November 2019, *Science* **366**, 708 (2019)
DOI: 10.1126/science.aay6826

This PDF file includes:

Other Supplementary Materials for this manuscript include the following:
(available at science.sciencemag.org/content/366/6466/708/suppl/DC1)

Tables S1 to S4 (Excel)

Table of Contents

Supplementary Text

Determination of dates for time periods and study individuals

Date ranges for time periods were determined based on archaeological and historical information about the local region. The locations and time periods of all sites are reported in Fig. S1 and Table S1.

- **Mesolithic (ME)**: 10,000 BCE-6,000 BCE
- **Neolithic (NE)**: 6,000 BCE-3,500 BCE
- **Copper Age (CA):** 3,500 BCE-2,300 BCE
- **Bronze Age (BA):** 2,300 BCE-900 BCE
- **Iron Age & Roman Republic (IA):** 900 BCE-27 BCE
- **Imperial Rome (IR):** 27 BCE-300 CE
- **Late Antiquity (LA):** 300 CE-700 CE
- **Medieval & Early Modern (MD):** 700 CE-1800 CE

Chronological dates for individuals in the study were determined using a consensus of AMS dating and archaeological and historical inference. For AMS dating, 1 gram of dense petrous bone was aliquoted and sent to the W.M. Keck Carbon Cycle Accelerator Mass Spectrometer Lab at the University of California at Irvine. These were calibrated using the intCal13 calibration curve using the OxCal interface (https://c14.arch.ox.ac.uk/oxcal/OxCal.html)

A single date estimate for each individual in the study was determined by the average of lower and upper estimates of the 95% confidence interval when using AMS dates, and the average of the lower and bound inference dates when using archaeological and historical context for dating. The full 95% confidence intervals are reported in Table S2.

DNA extraction and library preparation

The 134 ancient genomes reported in this study (127 ancient from central Italy described in the main text and 7 Bronze/Copper Age Sardinians also released with the data) represent a subset of samples screened from 30 archaeological sites in central Italy and Sardinia.

We isolated and finely ground the cochlear regions of the petrous bones in a dedicated clean room facilities at University College Dublin (April - November 2017) and the University of Vienna (Feb - Dec 2018) following the protocols described in (*37*, *38*). DNA was extracted from 50 - 60 mg of powder following, with the Zymo-Spin V column binding apparatus replaced with a high pure extender assembly from the High Pure Viral Nucleic Acid Large Volume Kit (Roche) as in (*39*, *40*).

DNA was eluted in 50 µl 10 mM Tris-HCl, 1 mM EDTA, 0.05% Tween-20, pH 8.0. 12.5 - 25 uL of DNA extract was used to prepare partial uracil–DNA–glycosylase (UDG) double stranded libraries as described in (*41*). After a partial (30 minute) UDG treatment, library preparation followed a modified version of the Meyer and Kircher 2010 protocol (*42*): the initial DNA fragmentation step was not required and MinElute PCR purification kits (Qiagen) were used for all library clean-up steps. Libraries were double-indexed with Accuprime Pfx Supermix. The PCR cycling conditions were as follows: an initial denaturation at 95°C for 5 min followed by 12 cycles of 95°C for 15 seconds, 60°C for 30 seconds and 68°C for 30

seconds with a final elongation at 68°C for 5 min. After indexing, the libraries were purified using the MinElute system (Qiagen) and eluted in 25uL of 1 mM EDTA, 0.05% Tween-20.

Libraries were screened based on Qubit concentration and visual validation of Bioanalyzer peaks for an initial low coverage (MiSeq or NextSeq) screening run.

Sequencing read processing and sample screening

Samples were initially sequenced to low coverage on MiSeq or NextSeq for screening. Following demultiplexing of the sequencing libraries, reads were trimmed, aligned, filtered for quality, and deduplicated.

First, adapters were removed from reads using Cutadapt (v1.14) (*43*). Then, for each sample, reads were processed further (a) with the 2 base pairs at either end of the reads trimmed off and (b) without trimming. Since partial UDG treatment was performed on the libraries, a damage signature consisting of elevated C>T transitions on the 5' end and G>A transitions on the 3' end should remain at the ends of reads. Therefore, analyzing untrimmed, aligned reads would allow us to assess the amount of the ancient DNA damage signature present in a sample, and to use this as a criteria for authenticating that the sample DNA is ancient. Other than the variable trimming parameter for the ends of the reads, all other parameters remained the same in downstream processing.

Following variable trimming, reads were filtered for minimum length of 30, then aligned to hg19 using bwa (0.7.15-r1140) (*44*), with seed length disabled (-l 350). For each sample, aligned reads were sorted by coordinate using Picard's SortSam (version 2.9.0-1-gf5b9f50-SNAPSHOT) and read groups were added using Picard's AddOrReplaceReadGroups (version 2.9.0-1-gf5b9f50-SNAPSHOT) (http://broadinstitute.github.io/picard/). Reads with mapping quality < 25 (including unaligned reads) were filtered out. For higher coverage sequencing runs, this process was parallelized by splitting raw fastq files and merging after alignment, sorting, and quality filtering. Duplicates were removed using samtools rmdup (http://www.htslib.org/doc/samtools.html) (*45*). Genome-wide and chromosomal coverage were assessed using depth-cover (version 1.0.3, https://github.com/jalvz/depth-cover).

Samples were screened and selected using the following criteria: 1) >10% reads aligned to the hg19 build of the human genome; 2) a C>T mismatch rate at the 5'-end and G>A at the 3'-end of the sequencing read of 4% or above (characterized with mapDamage v2.0.8) (*46*); 3) library complexity estimates indicating that at least coverage of 0.5x would be achievable with further sequencing, 4) with a contamination level <= 3%. Contamination rates were estimated with three methods: 1) damage pattern and polymorphism in mitochondrial DNA with Schmutzi (*47*), 2) atypical ratios of coverages of X and Y chromosomes to autosomes calculated with ANGSD (*48*) and 3) for male samples, high heterozygosity on non-pseudo-autosomal region of the X chromosome (chrX:5000000-154900000 in hg19) with the "contamination" tool in ANGSD (*48*).

134 (127 Roman/central Italian, 7 Sardinian) samples passed our quality controls and were further sequenced on HiSeq2000, HiSeq4000 or Novaseq 76-bp single end runs. Adapter trimming and alignment were carried out as described above for the screening runs. Sample information including percent endogenous, C>T rates, and contamination estimates are summarized in Table S2.

Calling pseudohaploid genotypes for ancient Italian individuals

Pseudohaploid genotypes for study samples were called following the pipeline suggested by and tool provided by Stephan Schiffels (https://github.com/stschiff/sequenceTools). First, read coverage of a select SNP set was performed using samtools mpileup (version 1.4). For maximum overlap with published ancient and modern samples, variants were selected based on those used in the Human Origins panel and in the modern reference panel published along the Lazaridis et. al. 2014 data (*12*), resulting in a total of 481,259 SNPs. A filter of minimum base and mapping quality of 30 (--min-BQ and --min-MQ) were also applied during samtools mpileup. Next, pseudohaploid genotypes were called by randomly choosing one allele from each site where there was read coverage, using pileupCaller. Data was output in eigenstrat format. This same procedure was performed for a few published ancient samples for which only fastq or bam data (as opposed to already called pseudohaploid genotypes) were available.

The 134 (127 Roman and 7 Sardinian) samples that passed quality filters have minimum of 39% (186,710) of SNPs and a median of 73% (349,979) SNPs covered with non-missing pseudohaploid calls.

Curating a reference dataset of published modern and ancient individuals

We downloaded and merged data from a collection of genetic diversity datasets. The majority of published modern and ancient samples used were already compiled by David Reich's Lab (*49*). Most of the samples were based on capture sequencing of ~590k targeted SNPs in the Human Origins panel. To this, we added recently published ancient samples from the Phoenician, Iberian, and Lebanese populations (Table S4) (*18*, *28*, *32*). For WGS-based studies, we called pseudo-haploid datasets using the same pipeline as for Italian samples.

For the Chromopainter analysis, we merged Spanish and British populations from the 1000 Genomes (*50*), Jewish populations from Behar *et al.* (*51*), Italian populations from Fiorito *et al*. (2016) (*52*), and Eurasian populations from the Globetrotter dataset (*53*) (Table S4). Samples from the latter three datasets were imputed using the Michigan imputation server (https://imputationserver.sph.umich.edu/index.html#!).

Assessing imputation accuracy for low coverage ancient genomes

To assess imputation accuracy, the same procedure above was performed on a high coverage ancient genome (NE1) *(54)* downsampled from 22x to approximate coverage levels ranging from 0.1x to 5x for chromosome 22. Downsampling was performed using samtools view with the -s parameter. Genotypes were called and imputed from downsampled bam files. Genotype consistency was measured by calculating the proportion of imputed genotypes that were consistent with reads in the full sample bam file (for sites where >10x coverage; Figs. S2 and S3).

Genotype imputation for ancient Roman and published modern individuals

In order to perform haplotype-based analyses, and leveraging the fact that low-coverage whole genome data can be imputed with relatively high accuracy (*54–56*) , we also performed genome-wide imputation

on the study samples. First, genotypes and likelihood scores were obtained using GATK UnifiedGenotyper (*57*) for variants at >0.01 minor allele frequency (MAF) in the 1000 Genomes global reference panel (*50*). The following parameters were used: --min_base_quality_score 30 --output_mode EMIT_ALL_SITES --allSitePLs --alleles <reference_panel> --genotyping_mode GENOYTPE_GIVEN_ALLELES -R <hg19 reference fasta>). We used UnifiedGenotyper instead of more recent genotype callers, such as HaplotypeCaller, because it has the option to output genotype likelihood scores. The likelihood scores model some of the uncertainty of the genotype due to the low coverage of the study samples, making them the preferred input (as opposed to called genotypes) for imputation.

For imputation, we used Beagle v4.0 (*58*). More recent versions of Beagle and other imputation software do not have an option to impute on genotype likelihood or probability scores. The reference panel (1000 Genomes) and the recombination maps used can be found on the Beagle website (https://faculty.washington.edu/browning/beagle/b4_1.html). The following parameters were used: gprobs=true, impute=true, gl=<input genotypes from UnifiedGenotyper> ref=<Beagle imputation reference panel>, map=<GRCh37 recombination map>.

Inference of mitochondrial DNA haplogroups and contamination

Since all libraries were treated with partial-UDG, a deamination signature of > 0.04 remain the last 2 bp on each end of a read (also a criteria used in sample screening). In the main pipeline used for genotype calling, two base pairs on each end are trimmed. However, for determining mitochondrial contamination and the endogenous mitochondrial genome, these untrimmed reads were used to extract only reads with a damage signature. The endogenous consensus mitochondrial genome was called simultaneously while estimating mitochondrial contamination using schmutzi (*47*). Sequencing reads were aligned to the revised Cambridge Reference Sequence (rCRS) mitochondrial genome (NC_012920.1).

First deamination and a contamination estimate based on it were estimated using the contDeam tool in schmutzi with the following parameters: length of expected deamination set to 2 (--lengthDeam 2) and library type set to double strand (--library double). Second, the main schmutzi program was used to 1) estimate contamination based on a haplogroup frequency database in conjunction with the deamination estimates from contdeam and 2) to assemble the endogenous consensus MT genome informed by contamination. Base quality filtering of 30 (--qual 30) and the --uselength parameter were both used. We found that using a global haplogroup frequency database did not provide any additional information than using the eurasian database, both provided by schmutzi. We also ran schmutzi with both a set deamination rate of 0.05 (based on results from Mapdamage during screening of samples) and with the rate estimated by contDeam.

The output of this pipeline is a contamination estimate based on deamination rates, a contamination estimate based on haplogroup frequencies, a contaminant MT genome, and an endogenous MT genome.

Haplogroups for the consensus endogenous genomes were called using the command line version of Haplogrep (v2.1.20) (*59*) (Table S2; Fig. S4). Contamination estimates are reported along with X chromosome contamination estimates, where possible (for males).

Mesolithic (10,000-6,000 BCE; n=3)
All three mesolithic individuals have haplotypes from the U group, two from the U5 subgroup and one from U8. In a study of the neolithic expansion in Europe, 83% of European hunter-gatherers (n = 23)

were shown to have U haplotypes, compared to 12% of farmers (n = 105)(*60*). More specifically, haplogroup U5 (along with U2) represent the majority of mitochondrial variation in Western Hunter-Gatherers (WHG), Eastern Hunter-Gatherers (EHG), and Scandinavian hunter-gatherers (SHG)(*14*).Thus the Italian Mesolithic individuals reported here have typical mitochondrial haplogroups compared to contemporaneous Europeans.

Neolithic and Copper Age (6,000-2,300 BCE; n=13)
Three Neolithic individuals reported here have mitochondrial haplotypes in the U group, three in the K group, and one of each in the H, N, and T groups. The three Copper Age individuals have N, K, and I haplogroups. The K haplogroup is thought to be a marker of the neolithic expansion as it is nearly absent in hunter-gatherers and at the highest levels in the Near East (*61*). Isern shows that the frequency of K decreases with increasing distance from Syria (used as a proxy for the origin of farming) and with increasing time since the introduction of farming into Europe.

Individuals with H, N, and T haplogroups are also consistent with published findings on haplogroups present during the Neolithic period in Europe. Although nearly absent among Mesolithic hunter-gatherers, Haplogroup H was present among ~19% Early Neolithic Europeans, and has been found to have increased in frequency over the course of the Neolithic expansion (*62*). Today, it represents > 40% of European mitochondrial variation, the most common haplogroup amongst present-day Europeans. Haplogroup N1a1, representing haplogroups of one Neolithic and one Copper Age individual in the Roman time series, has been reported at frequencies only as high as ~9% (German Early Neolithic, n = 160) among Neolithic European populations (*63*). The frequency of N1a1 does not seem to noticeably increase in subsequent time periods, as it is found at ~7% in central European Bronze Age populations, and ~2% in the Yamnaya. The T haplogroup is present at <3% frequency in European Neolithic groups from France, Germany, and Iberia. The I haplogroup (which is present in one Copper Age Roman individual) is virtually absent among European Neolithic groups, although found at ~11% frequency in Early Bronze Age central Europeans previously studied.

Iron Age and Roman Republic (900-27 BCE; n=11)
Among the 11 Iron Age and Roman Republic individuals in the time-series reported here, the mitochondrial haplogroups H (n=5, 45%), I (n=2), K (n=1), U (n=1), and T (n=2) are represented. In a study of 15 individuals from Botromagno, in southern Italy, from the same time period (800-500 BCE), *Emery et. al.* found similar frequencies of the H haplogroup, at ~46% (7/15 individuals) (*64*). In contrast to Iron Age individuals studied here, the U haplogroup was found at much higher levels in Botromagno individuals, at 40% (6/15 individuals). Among the Botromagno Iron Age individuals, haplogroups V and J (both n = 1) were also represented, however they were not present in any of the 11 Iron Age individuals reported here.

Imperial Rome (27 BCE - 300 CE; n=48)
Among the 48 Imperial Roman individuals reported here, the most frequent haplogroups are H (n=10), U (n=11), and T (n=10), all haplogroups present since the Neolithic period, according to the Roman time-series reported here. Similarly, in a study of 30 individuals from Vagnari in southern Italy during this period, the H haplogroup was also common at 40%, present in 12 out of 30 individuals, as was the T haplogroup (n=5) (*64*). Surprisingly, the U haplogroup was not present among the Vagnari Roman era individuals, despite being present in 23% of Imperial Roman individuals reported here.

Haplogroups J (n=3), which was not found in individuals of preceding time periods, and K (n=2) are found at lower frequencies. Along with haplogroups H and T, J and K are also typical of Eurasian populations. Both J and K are present at similar frequencies (n=2 each) in the individuals from Vagnari during the same period.

Haplogroups D, HV, R, and X are represented by one individual each from the Imperial Roman period, and interestingly, are not found in preceding time periods. Among the Vagnari individuals, haplogroups D (n=2), HV (n=1), and X (n=2) are also present at low frequencies.

The D haplogroup is considered to be of East Asian origins. R78, the only individual in the time series representing this haplogroup, projects closely to some eastern Mediterranean populations (Turkish Jews, Cypriots, and Greeks) in PCA (Fig. S15), although not as closely as some other individuals of the same time period. Although rare among modern Europeans, Prowse et. al. found that one out of ten individuals from this same time period (2nd-4th century CE) in Vagnari (southern Italy) had the D mitochondrial haplogroup (*65*).

Individual R132, notable for having substantial African ancestry, has a haplotype (R0a2j) belonging to a sister clade, R0, of haplogroup H. The R0 clade has also been found in a Phoenician Lebanese individual dated to 539–330 BCE (*66*). For present-day populations, one study found that the R0a subgroup is found at nearly 40% frequency in the Arabian peninsula, and at 11% and 22% in Yemenite Jews and Ethiopian Jews, respectively (*34*, *67*). Another study that analyzed individuals from the 1000 Genomes Project, found the R haplogroup to be virtually absent in European, African, and admixed American populations, although fairly common in East Asian and Indian populations (of note Middle Eastern and North African populations are not represented in the 1000 Genomes Project) (*68*).

Late Antiquity (300 CE - 700 CE; n=24)

As in previous periods, haplogroup H (n = 8, 33%) is the most frequent among Late Antique individuals, followed by T (n=6), K (n=3), U (n=2), and J (n=2). Haplogroups HV, I, and L are all represented by one individual each. All haplogroups, except L, are common among Eurasian populations. R30 is the only individual in the time-series with a haplotype from this group, specifically subgroup L4, which is rare globally (<0.5%, 12/2504) and found almost exclusively in African populations based on populations in the 1000 Genomes Project (*68*). However, even in the African populations studied, L4 low frequencies even in African populations studied (2.4%, 12/497). Nevertheless, Prowse et. al. showed that 1 out of 10 individuals at Vagnari in southern Italy had an L haplogroup (*65*).

Medieval and Early Modern (700 CE - 1800 CE; n=28)

In contrast to the increasing frequency of the H haplogroup in preceding time periods, only 2 Medieval and Early Modern individuals (~8%) in the Roman time series have the H haplogroup. Haplogroups HV (n=4, 17%), T (n=3) and U (n=3) are the most frequently observed; followed by H and J (two individuals each); and I, K, N all with one individual each.

With the exception of haplogroup N, all others are fairly common in present-day European populations. Haplogroup N is present at highest frequencies in Asian groups, compared to other populations in the 1000 Genomes Project (*68*). Of note, one Neolithic and one Copper Age individual have N haplogroups, along with individual R59 from the Medieval period.

Inference of Y-chromosome haplogroups

We determined the haplogroup assignment of each male individual by examining his genotype at known SNPs informative of Y-chromosome haplogroups (Table S2; Fig. S5). The list of informative SNPs on the Y chromosome was downloaded from the International Society of Genetic Genealogy website (https://isogg.org/tree/; Version 14.62, April 2019). We pruned out SNPs that are on the same position but

characterized with inconsistent alleles by keeping only one record with the ancestral or derived allele matching with the GRCh37/hg19 reference sequence. We called genotypes of our samples at Y-linked SNP positions in 1000 Genomes (phase 3) (*50*) using reads with mapping quality scores ≥30 and bases with quality scores ≥30. We then identified the Y-haplogroup for each sample by using yhaplo software (https://github.com/23andMe/yhaplo) (*69*) with the updated list of informative SNPs from ISOGG. Because the subgroup labels (e.g., R1b1a1a2a1a2) updates constantly and cannot be compared across studies, we reported the haplogroups with the representative derived alleles (e.g., R-M269) in Table S2 and Fig. S5.

In Table S5, we summarized the Y-chromosome haplogroup information of each individual in Mesolithic to Iron Ages as well as additional ancient individuals who belong to the same haplogroup. Below is a brief discussion of the Y-chromosome haplogroup results in light of contextual information of other ancient populations in Europe and the Near East.

Mesolithic (10,000-6,000 BCE; n=3)

All three Mesolithic individuals are assigned to the I-M436 (I2a2) haplogroup, with two of them further classified into the I-M223 (I2a2a) subclade. The I haplogroup has been found in western hunter-gatherer (WHG) populations from many parts in Europe, including individuals from the Grotte du Bichon in Switzerland (11,820-11,610 calBCE), France (11,140-10,880 calBCE), and Germany (7,460-7,040 calBCE)(*15*, *70*). In particular, several Mesolithic hunter-gatherers from the Iron Gates between Serbia and Romania (dated to as old as 8,000 BCE) belonged to the specific I-M223 (I2a2a) haplogroup (*14*). Therefore, the I-M436 haplogroup appears typical and widespread in Europe before the Neolithic transition, which is consistent with the similarity of the three Mesolithic Italian individuals to other WHGs based on autosomal SNPs.

Neolithic (6,000-3,500 BCE; n=4)

The four males in Neolithic period carry three distinct haplogroups: G2a, J and R1b. Haplogroup G2a was a dominant lineage in Neolithic northwestern Anatolia farmers (6,500-6,000 BCE), making up 8 out of 13 characterized Y-chromosomes, and at least three individuals belonged to the specific clade of G-L91 (G2a2a1a2)(*13*). This haplogroup is also found in a late Neolithic individual from northern Greece (*17*). Interestingly, the G2a2a1a2 haplogroup was also the one carried by the Tyrolean iceman Ötzi (3,484-3,104 calBCE) (*71*), illustrating its prevalence in Italy in the Neolithic age.

The J haplogroup, specifically J2a, is also found in one of the 13 Anatolian male farmers characterized in (*13*). Therefore, the appearance of these G2a and J2a haplogroups in Neolithic central Italy can be explained by the previously known large-scale migration of farmers from the Near East into Europe and the striking ancestry transition in our dataset (Fig. 2). Furthermore, the predominance of G2a and presence of J also hold true for early farmer populations in the Balkans (*14*). This echoes our finding from qpAdm modeling that the Mesolithic-to-Neolithic genetic transition in central Italy can be modeled as addition of Neolithic ancestry from the Balkans (northern Greece, Croatia, Macedonia, Serbia; Table S8).

The R-M343 (R1b) is the most common haplogroup in modern western Europe. Although the high frequency of R-M343 is thought to largely reflect the migration of pastoralists from the Pontic-Caspian steppe into Europe during the late Neolithic and Bronze Ages, subtypes of R-M343 without the M269 derived allele were already present at low frequency in Europe before that time, for example, in a

Mesolithic individual found Villabruna in northern Italy (c. 12,000 calBCE) (*15*), some Mesolithic hunter-gatherers from the Iron Gates between Serbia and Romania (*14*), an early Neolithic individual in Spain (c. 5,000 calBCE) (*10*) and several early Neolithic individuals from Ukraine (*14*). Therefore, the presence of the R-M343 haplogroup in early farmers in central Italy is not surprising and could reflect persisting lineages that were present in local hunter-gatherers. Interestingly, R6, the person that carries R-M343, is also the one with the highest amount of WHG ancestry among all Neolithic and Copper Age individuals based on autosomal SNPs (Fig. 2; Fig. S24). Therefore, the R-M343 (R1b) haplogroup observed in R6 is compatible with a model in which Neolithic farmers in central Italy result from admixture between local hunter-gatherers and incoming Near Eastern farmers, without involving any Steppe ancestry.

Copper Age (3,500-2,300 BCE; n=2)

In addition to the G2a haplogroup that has already been seen in Neolithic individuals, we also observe a new haplogroup H in Copper Age individuals. Individual R1014 carries five derived alleles (M2936, M2942, M2945, M2955, M2992, M3035) characteristic of the H-haplogroup as well as 35 ancestral alleles that are incompatible with the H3 subgroup, 50 incompatible with with H1b1 and 13 incompatible with H1b2. Therefore, R1014 most likely belongs to an ancestral H haplogroup or the H2 (H-P96) branch, the latter of which is present at low levels in modern-day West Asia and Sardinia as well as in early farmers in Neolithic Anatolia (c. 6,500-6,200 BCE) (*13*) and Copper Age Bulgaria (3,336-3,028 BCE) (*14*). It is possible that H haplogroup (most likely H2) was already present in Neolithic central Italy, although we were not able to capture it in our limited Neolithic samples of only four males; under this scenario, the observed H haplogroup can be explained by the migration of Near Eastern farmers during Neolithic transition. Alternatively, it could be introduced into Italy after the Neolithic transition by later genetic exchanges with the Balkans or the Near East between 6,000 BCE and 3,500 BCE.

Iron Age (900-27 BCE; n=7)

The Iron Age witnessed a striking shift in the distribution of Y-chromosome haplogroups compared to previous periods, indicative of large-scale immigration before the Iron Age (our dataset did not contain any Bronze Age individual from central Italy). Five of the seven male individuals in this time period belong to the R-M269 (R1b1a2) group, which is not observed the nine earlier male samples. Unlike the general R-M343 (R1b) haplogroup, the R-M269 subgroup is thought to be tightly associated with Steppe-related ancestry, as it was absent in ancient individuals in western Europe before 3,000 BCE but found in all Bronze Age Yamnaya males from Russia (c. 3,500-3,000 BCE) (*10*), >90% males associated with the Beaker-complex in Bronze Age Britain (c. 2,700-2,500) (*72*) and nearly 100% males in Iberia after 2,000 BCE (*18*). Therefore, the appearance of R-M269 at high frequency (5 out of 7) in central Italy is consistent with the arrival of Steppe ancestry detected based on autosomal SNPs (Fig. 2), via migration of Steppe pastoralists or intermediary populations in the preceding Bronze Age.

The other two Iron Age males, R474 and R850, belong to J-M12 (J2b) and T-L208 (T1a1a) haplogroups respectively. As discussed above, the J haplogroup and its J2a subclade have already been present in early farmers in Italy, the Balkans, and Anatolia (*13*, *14*). In addition, a Bronze Age individual from Croatia (1631-1521 calBCE) belonged to the J2b2a haplogroup (*14*) and carried exactly the M314 derived allele that is also found in R474. Therefore,the observed J-M12 (J2b) could be a surviving lineage from local Neolithic populations or due to recent migrations from the Balkans or the Near East. The T1a haplogroup, although absent in our samples prior to Iron Age, has previously been found in early farmers in Bulgaria (5,800-5,400 calBCE) (*14*) and Germany (5,500-4,850 BCE)(*13*), so it is possible that it was also present in early farmers in central Italy.

Imperial Period and afterwards (27 BCE - early modern; n=59)

The Y-chromosome haplogroups present in Rome and surrounding regions become highly diverse since the Imperial period, preserving all the aforementioned groups while showing introduction of R1a, J1 and E1b haplogroups in the Imperial period, I1 haplogroup in Late Antiquity and C haplogroup in Medieval and early modern period.

Among those haplogroups that are first seen in the Imperial period, a case of particular interest is E-V12 (E1b1b1a1a1). This haplogroup is present at high frequency across present-day North Africa, especially in Egypt (up to 74.5%), but at low frequency in the Levant, Anatolia, and Mediterranean Europe (*73*). Therefore, E-V12 is thought to have originated in somewhere in North Africa and spread to southern Europe via trans-Mediterranean migrations (*73*). For the two individuals (R113 in Imperial and V59 in Medieval) who belong to E-V12 haplogroup, we did not detect significant evidence of African introgression on autosomes based on *f*-statistics or supervised ADMIXTURE (see the "African Introgression" section below; Fig. S23). One explanation is that these tests are underpowered to detect North African ancestries, which are themselves admixtures of multipl(*74*) and under-represented in current ancient DNA datasets. A non-mutually exclusive explanation is that the Y-chromosomes came from remote African ancestors on the paternal lineage, whose genetic contributions have been much diluted on autosomes.

An intriguing haplogroup observed in Late Antiquity is I-M253 (I1), which is quite common in present-day northern Europe (at 25-40% frequency in Scandinavia)(*75–77*), relatively rare in mainland Italy (~4%) and completely absent in Sardinia (*78*). It is estimated that the I-M253 haplogroup arose 3,200-5,000 years ago in northern Europe (*79*), so the presence of this haplogroup in Imperial Rome could possibly reflect migration from the north into central Italy. R110, the individual who carries the I-M253 comes from Crypta Balbi, a site that used to be a theater courtyard in the Imperial era and transformed for other purposes in Late Antiquity. Interestingly, Lombard-associated ornaments have been excavated at this site, pointing to connections with central Europe. Additionally, five of the seven individuals from this site, including R110, are classified by ChromoPainter into a cluster with more haplotype sharing with central/northern Europeans. Therefore, the I-M253 haplotype observed in Late Antiquity is consistent with the increasing genetic influence from central European populations detected by other analyses (e.g., PCA, *f*-statistics, *qpAdm*).

Lastly, the C haplogroup appears for the first time in our time series in the Medieval period, in individual R1285, who belongs to the C-V222 (C1a2a1) subclade. The late appearance of this haplogroup is a little surprising, as the C lineage is thought to be extremely old and widespread worldwise, and the C1a2 haplogroup has been observed in multiple Neolithic individuals from Turkey (6,500-6,200 calBCE) (*13*, *80*), Spain (5,983-5,747 calBCE) (*13*), Croatia (5,986-5,786 calBCE), Austria (5,500-4,775 BCE), Hungary (5,500-4,775 BCE) (*14*) and even in Paleolithic individuals from Belgium (33,210-32480 calBCE) and Czech (28,760-27,360 BCE) (*15*). Therefore, it is more than likely that the C haplogroup was present in Italy before Medieval era but at relatively low frequency, so it was not represented in earlier samples in our study.

Calculation of conditional heterozygosity

In order to avoid calculating heterozygosity based on variants that are misclassified as heterozygous due to sequencing, genotype calling or imputation errors, we calculated heterozygosity using variants that are already known to be segregating in human populations. Specifically, we focused on 286,138 variable sites that are heterozygous in a San Khomani individual, SA50, in the Globetrotter dataset (*53*). For each individual, we used a read-based method (*14*, *81*) to estimate the conditional heterozygosity by (1)

computing the probability of observing two different alleles, if only two reads are sampled at random at each site; (2) averaging the probabilities across all sites covered by at least two reads; and (3) doubling the averaged probability. Fig. S6 shows the conditional heterozygosity for the study samples.

Kinship analysis and runs of homozygosity

To detect close relatives in our newly collected Italian samples, we applied PLINK (*82*) and KING (*83*) to the imputed genotypes to calculate kinship coefficient. Starting with 12,057,197 autosomal SNPs with global MAFs above 0.01 in 1000 Genomes Project (*50*), we performed linkage disequilibrium (LD) pruning with PLINK v1.9 using "--indep-pairwise 200 25 0.4" and reached a set of 1,490,052 SNPs in which any pair within 200kb are in approximate linkage equilibrium with r_2<=0.4 (www.cog-genomics.org/plink/1.9/)(*82*).

Pairwise kinship coefficients estimated by "--kinship" in KING 2.1.2 (*83*) revealed no close relatives among the 134 ancient Italian individuals (including 127 from central Italian peninsula and 7 from Sardinia). All pairs have kinship coefficients below 0.035, except for R53 and R54, who have an estimated kinship coefficient of 0.0639 corresponding to third-degree relationships (e.g., great-grandparents, first cousins). Both of these two individuals were found in Villa Magna, dated to late Medieval (1280-1430 CE) and inferred to be male. However, they carried distinct mitochondrial (R53: U2e1c1 and R54: H4a1) and Y-chromosome haplotypes (R53: E-V257 and R54: J-Z1296). Given the remote relatedness, if any, in our samples, we kept all 127 individuals in downstream analyses.

To detect recent inbreeding, we called runs of homozygosity in each ancient Italian individual using a read-based approach, which consists of the following steps:

1. Focusing on a set of 286,138 SNP sites that are heterozygous in a San Khomani individual, SA50, in the Globetrotter dataset (*53*), same as the sites used for calculating conditional heterozygosity;
2. For sites that are covered by at least two reads, computing the probability of seeing two different alleles when exactly two reads are sampled at random (using the method described in (*14*) for calculating conditional heterozygosity);
3. For each 2Mb sliding window at a step size of 200kb (for example, chr1:1-2,000,000, chr1:200,001-2,2000,000, chr1:400,001-2,400,000 and so on), if at least 40 sites are covered by two or more reads, calculating the average probability resulted from (2) across all sites in the window (elsewise, the window is not classified due to too much missing data);
4. Calling a window "homozygous" if the average probability of seeing two different alleles is below 0.02;
5. Joining consecutive "homozygous" windows to call ROH tracts;
6. Summing the lengths of ROH tracts of 5Mb or longer.

Nineteen individuals carry at least one ROH segment of 5Mb or longer (Table S6), with only six (R7, R1015, R473, R474, R15, and R11) having more than 30Mb ROH segments in total length. R7, R15, and R11 are the three Mesolithic individuals, who also have low conditional heterozygosity levels (Fig. S6). R15 and R11 only carry 6-7 ROH tracts of intermediate length (<8Mb), which is more consistent with a small historical effective population size (*Ne*) than very recent inbreeding. However, R7 carries many more (26) ROH tracts of at least 5Mb than his contemporaries, with the longest tract as long as 24.8Mb (Fig. S7A). Such long ROH segment suggests recent inbreeding in the past few generations, so the extremely low conditional heterozygosity of R7 (Fig. S6) likely arose from consanguinity on top of small historical population sizes for hunter-gatherer populations (*12*, *14*, *81*).

The other three individuals with relatively long ROH (R1015, R473 and R474) are all in the Iron Age. Evidence for consanguinity is particularly strong for R1015 and R473, who carry ROH segments as long

as 30-40Mb (see Fig. S7BC for examples), which can only arise from union of close relatives. The exact relationships of their parents are uncertain, given the randomness in segregation and recombination, but we are able to make rough inference based on the total ROH length. R1015 carries 157Mb of ROH above 5Mb, which is more than 5% of the genome and compatible with being the offspring of third-degree relatives (e.g., first cousins). R473 has 85.2Mb of ROH tracts of 5Mb or longer, which is compatible with the parents being fourth-degree relatives (e.g., first cousins once-removed).

ADMIXTURE analysis

Unsupervised ADMIXTURE model evaluation. We used ADMIXTURE to interpret the study data as a mixture of ancient source populations (*8*). All modern and ancient Eurasian individuals were included in the ADMIXTURE runs. During initial runs of ADMIXTURE we noticed that clusters were often dominated by modern-day populations with large sample sizes. To avoid bias towards modern-day populations, we downsampled modern populations to 20 individuals. To determine the appropriate populations and number of populations to use as "sources" for supervised admixture, we performed unsupervised admixture for k = 2 through 9, with 5-fold cross validation, and 3 repetitions of each k (with different random seeds). Runs for k = 4 through 7 had the lowest CV error across repetitions (Fig. S8).

Candidate source populations using unsupervised ADMIXTURE. Next, we considered which populations at each k that maximized the proportion for each of the k clusters (Fig. S9). To be considered as an interpretable source population for supervised ADMIXTURE, a population should be ancient (pre-historic period) and consist of more than one individual and individuals of reasonable quality (less than ~75% missingness). Candidate populations are shown for k = 2 through k = 8. In many cases, no single population clearly had the maximum proportion (close to 1) for a given cluster (Fig. S9).

In general, we observe that clusters at each k are broadly defined as follows:

At K = 2:
1. Western Hunter-Gatherers
2. Moroccan Hunter-Gatherer / Early Neolithic

At K = 3
1. Western Hunter-Gatherers
2. Caucasus Hunter-Gatherers/Iran Neolithic
3. Balkans/Anatolian Neolithic

At K = 4
1. Western Hunter-Gatherers
2. Caucasus Hunter-Gatherers/Iran Neolithic
3. Balkans/Anatolian Neolithic
4. Moroccan Hunter-Gatherer/Early Neolithic

At K = 5
1. Western Hunter-Gatherers
2. Eastern Hunter-Gatherer/Steppe Eneolithic
3. Iran Neolithic
4. Anatolian Neolithic
5. Moroccan Hunter-Gatherer/Early Neolithic

At K = 6
1. Western Hunter-Gatherers
2. Eastern Hunter-Gatherer/Steppe Eneolithic
3. Iran Neolithic
4. Malak Presalevets/Iberian Neolithic

5. Greek Neolithic/central Anatolian Neolithic
6. Moroccan Hunter-Gatherer/Early Neolithic

At K = 6 and onward, modern populations (not shown in Fig. S9) tend to maximize proportions for clusters, possibly reflecting recent admixture. Top candidate source populations and cluster proportions for both k = 4 and k = 5 are consistent with known transitions at the start of the Neolithic and Bronze Age periods for published data. The Caucasus Hunter-Gatherers (CHG) component at k = 4 appears to split into Steppe-like and Iranian Neolithic-like components at k = 5, a valuable ancestry distinction, which led us to choose k = 5 as a robust and interpretable k for supervised ADMIXTURE.

The first five populations shown below were chosen as source populations at k = 5 since they clearly maximized the five cluster proportions and have been used previously as source populations in an ancient eurasian context. Eastern Hunter-Gatherers were considered as a population with Steppe Eneolithic when for supervised ADMIXTURE results that included populations with pre-Bronze Age Steppe ancestry.

- **Western Hunter-Gatherers / WHG** (n = 9; 14,776-5,220 BCE): Loschbour_published.DG, Falkenstein, Falkenstein_published_d, Iboussieres25-1, Iboussieres31-2, Rochedane, BerryAuBac, LaBrana1_published.SG, KO1_published.SG, I2158_published (Sicily Oriente)
- **Anatolian Neolithic / Anatolia_N** (n = 24; 6,500-5,845 BCE): Bar31.SG, Bar8.SG, I1100, I1102, I1099, I1103, I1101, I1097, I0744, I1096, I1098, I0708, I0745, I0746, I0707, I0709, I0736, I0726, I0723, I0724, I0727, I1580, I1581, I1583
- **Moroccan Hunter-Gatherers / Moroccan_Iberomaurusian** (n = 4; 13,127-11,900 BCE): TAF010, TAF011, TAF013, TAF014
- **Iran Neolithic / Iran_N** (n = 9; 8,241 - 7,082 BCE): AH1.SG, AH2.SG, AH4.SG, WC1.SG, I1290, I1944_published, I1945_published, I1949_published, I1951_published
- **Steppe Eneolithic / Steppe_Eneolithic** (n = 3; 5,300-4,300 BCE): I0434, I0433, I0122
- **Eastern Hunter-Gatherers / EHG** (n = 2; 6,773-5,541 BCE): I0124, I0211

Moroccan Hunter-Gatherers (Moroccan_Iberomaurusian) were used instead of the Early Neolithic (Moroccan_EN) population due to ~90% missingness in the individuals of the latter population. Steppe Eneolithic was chosen over EHG for the Steppe-like component since it is closer in temporal proximity, but still prior to the estimated entrance of Steppe ancestry into mainland Europe, with respect to understanding the ancient Italian time series reported here. Steppe Early Middle Bronze Age (Steppe_EMBA) could also be a valid choice for the Steppe component. Where samples and populations other than the ancient Italian study samples are presented, both EHG and Steppe_Eneolithic are used as a single source population. Various combinations of these alternatives, including using a sub-Saharan population (Yoruba) as the African source population, were explored, although none proved to be more informative than the chosen source populations for understanding the ancient Italian time-series.

Supervised ADMIXTURE model robustness. For the supervised ADMIXTURE analysis presented at k = 5 (Western Hunter-Gatherer, Anatolia Neolithic, Iran Neolithic, Steppe Eneolithic, Moroccan Hunter-Gatherer), 20 repetitions were performed (with different random seeds) and the repetition with the maximized log-likelihood was chosen. To assess consistency of assigned ADMIXTURE proportions genome-wide we compared the proportions for ADMIXTURE on the full genome, odd chromosomes, and even chromosomes. In general, for a given repetition (random seed), full genome, odd chromosome, and even chromosome ADMIXTURE runs were highly correlated. For the best repetition, odd and even chromosome proportions had a correlation of > 0.93 for the study samples and > 0.98 for all samples, except for the Moroccan Hunter-Gatherer source cluster proportions which were due to the small amount of this ancestry present in the population.

Constructing an ADMIXTURE time series for other regions using published data. Time series are shown for several geographical regions, with samples binned by the time periods in section "Determination of dates for time periods and study individuals". These are shown for unsupervised ADMIXTURE at k = 5 and k = 6, as well as supervised ADMIXTURE at k = 5. For the latter, EHG and Steppe Eneolithic are considered as a single source population since several populations (e.g. in northern Europe and the Steppe) could have Steppe-like ancestry from prior to the Eneolithic period (Fig. S12).

Principal components analysis (PCA)

Setting up the principal component analysis. Principal component analysis (PCA) was performed by projecting ancient study samples onto a PC space constructed based on modern-day individuals. Using smartpca (v16000)(*84*, *85*) and the poplistname option, 574 individuals from 47 present-day populations, with 480,712 snps, previously reported were labeled to create the PC space (*14*). These specific individuals and populations were used in order to recreate the PC space reported previously in several other ancient DNA papers *(67)*. All other samples, both modern and ancient, were projected onto this space (Fig. S14). Given the amount of missingness in the genotypes of ancient samples, the lsqproject option was set to "YES". In addition to using the pseudohaploid study genotypes in PCA, we also performed this procedure for the imputed study genotypes as a quality assessment for the imputation (discussed in the imputation validation section).

Visual representation of PCA. The same principal component analysis was used in all genotype-based PCAs in main and supplement figures (Figs. 2, 3, S14, S15, S17-20). Generally, the PC space shown in full in Figure S14 is cropped to be centered on the study samples from central Italy. Furthermore, modern day populations used to create the PC space are not necessarily those that are labeled (other than in Fig. S14). Select modern and (sometimes ancient) populations are labeled for simplicity and relevance. Furthermore, to reduce visual clutter, populations (other than the ancient Italian samples) are represented either as the 2 standard deviations along each PC (a cross) or a polygon encompassing member individuals. A version of the PCA plot in Fig. 2 of the main text is shown with all ancient Italian samples labeled (Fig. S15).

Variation in principal components and admixture proportions for study individuals in the same time period. To illustrate the spread of samples across the PC space for each time period, we plotted the standard deviation for the first two principal components for the population at each time period (Fig. S16). The first PC roughly mirrors variation along the north to south cline of Eurasia, while the second PC roughly mirrors variation along the east to west cline. The standard deviations of these components in each time period can be thought of as how diverse the population was in this dimension of genetic variation. Populations in the top right corner of the plot, with high SD(PC1) and high SD(PC2), are the most spread out in the PC space, while ones in the bottom left form tighter clusters. Exact locations of Late Antiquity and Imperial Rome samples are dependent on whether outliers are included in the calculation of standard deviation. Regardless, both periods have the highest standard deviations of PC1 and PC2 compared to any other time period.

The standard deviations of ADMIXTURE proportions follow similar trends over time as the standard deviations in PC1 and PC2, although ADMIXTURE proportions are not clearly correlated with either of the first two PCs. The lowest amount of variation across all components (sum of standard deviations) is seen in Mesolithic population, followed by the Copper Age, and then Neolithic. The remaining historic periods (Iron Age onward) have higher overall variation, with the peak being around Late Antiquity.

Across the historic periods the most variation is seen in the Iranian Neolithic component, followed by the Steppe Eneolithic component.

Test for significant principal component variation by archaeological sites. To assess whether variation in the first two principal components could be explained by variation among the archaeological sites, we performed a two-way ANOVA (Analysis of Variance) test of the form $C_1 + C_2 \sim Period + Site$, where Crepresents principal component. Since most sites have individuals from a single period*, time period ($Period$) was also considered as an independent variable on the right-hand side. The order of variables in the regression (i.e., period followed by site) insures that variance in $C_1$and $C_2$is first attributed to time period and then to site. The results of this test show that $Period$ is significant with a p-value $< 2 \times 10^{-16}$, while $Site$ is not significant (p-value > 0.10). This test indicates that, conditional on the time period, archaeological site does not explain additional variation observed in the first two principal components.

*The only two sites with individuals from more than one time period are Marcelino & Pietro (Imperial Rome and Late Antiquity) and Grotta Continenza (Mesolithic, Neolithic, Copper Age).

Diversity of Roman population peaks in Imperial Rome and Late Antiquity in the first two principal components. The average ancestry of Rome went through a series of shifts in different time periods, due to gene flow from a variety of sources. In principle, such ancestry shifts could occur through short pulses of immigration but with the population being well-mixed at most times.

But instead our results emphasize Rome as a highly cosmopolitan population. Within all time periods from the Iron Age onward, our samples include diverse ancestries: especially from the eastern Mediterranean, Europe, and occasionally north Africa, reflecting Rome's extensive trade networks as well as forced movement of people across Europe and the Mediterranean. The extent of variation in ancestry peaks in the Imperial period and Late Antiquity, and declines again toward the present (Fig. 4C; Fig. S16). This indicates high rates of immigration from elsewhere in the empire, and potentially persistent population structure within Rome (as may be the case in Imperial Isola Sacra, where isotope analysis suggests that the individuals of different ancestry may have grown up locally).

Ancient Italian individuals reported in this study and contemporary ancient populations in PCA. To visually depict contemporary ancient populations, we show them omitting modern day populations, including those that form the reference PC space upon which all ancient samples are projected. Due to the high missingness and varying genotyping approaches used in published ancient samples, performing a principal component analysis with only ancient samples would be biased towards technical artifacts, such as genotyping differences and sample quality. Shown here are prehistoric (Mesolithic through Copper Age) study samples and historic (Iron Age onward) study samples projected with their prehistoric and historic contemporaries, respectively (Figs. S17 and S18). To maximize visual distinction, not all published ancient individuals were plotted. Those we found were relevant to our analyses (used in qpAdm modeling or ADMIXTURE analysis) and from geographically relevant regions (e.g. around the Mediterranean) were included.

Continuity of populations in PC space before and after the Imperial era. In some analyses in the paper (e.g. PCA, *qpAdm*), where high quality ancient samples are unavailable or uninterpretable, we refer to the reported ancient Italian study individuals as being "similar to" or "modeled in terms of" modern-day populations. Comparing ancient individuals to modern day populations in this way raises two questions:

1. Are these modern day populations representative or even remotely similar to their ancient predecessors we attempt to approximate?

2. When we observe genetic similarities between the Imperial Roman population (in the city of Rome) and modern day populations, how do we know we this similarity is not due to the genetic influence of ancient Romans or the predecessors of these modern populations.

To investigate this question with the principal component space, we looked at the pre- and post- Imperial-era populations for several regions relevant to this study. We chose to look at Bronze Age populations for the pre-Imperial representation since 1) they post-date the major transitions (Neolithic and Steppe) in Eurasia and 2) there are very few samples available between Bronze Age and Imperial Rome (~900 BCE to 27 BCE). To represent the post-Imperial population, we use present-day populations, with the exception of Germany where we used Medieval German samples since there is no appropriate data for present day.

Indeed, for several regions we do observe discontinuity between pre-Imperial and post-Imperial (generally modern-day) (Fig. S19). However, the shift is not generally in the direction of the Roman era population nor are the shifts large (beyond other populations of the same subcontinental region). Given this, we expect that comparison of ancient Roman samples to modern populations (when ancient ones are not available) can be a reasonable proxy for their recent (last ~3000 years) ancestors.

Consistency of imputed and pseudohaploid genotypes in ADMIXTURE and PCA

Supervised ADMIXTURE for imputed genotypes. To check the integrity of the imputed genotypes for the reported samples, we compared ADMIXTURE and Principal Component Analysis (PCA) between pseudohaploid and imputed genotypes. The same ADMIXTURE procedure described above (see ADMIXTURE section) was performed on imputed genotypes of the reported samples. As with the pseudohaploid analysis, 675 eurasian ancient and modern samples were included with 480,712 snps. This was run on the full imputed genome, as well as only the odd chromosomes and even chromosomes (for all samples included in the analysis), for 20 repetitions (with varying random seeds). The repetition with the highest log likelihood was chosen to represent the imputed ADMIXTURE analysis. Overally, ADMIXTURE proportions were highly correlated and qualitatively the same (a) between pseudohaploid and imputed runs and (b) across odd and even chromosomes and the full genome (Fig. S21). Between the pseudohaploid and imputed full genome runs for the ancient Italian samples, correlations were >0.99 within source populations and when samples are subsetted by time periods.

Principal component analysis for imputed genotypes, compared to pseudo-haploid genotypes. PCA was also performed as described previously (see PCA section) by projecting the imputed genotypes onto the same PC space that the pseudo-haploid genotypes were projected onto. A small shift along PC1 and PC2 from imputed to pseudo-haploid samples is noted (Fig. S22). However, this shift does not negate any inferences made about the genetic affinities of samples to other populations or samples as the relative positions of the imputed samples to each other and to the reference space remains the same.

Calculation of *f*-statistics

We measured shared drift between two groups (or individuals) using the outgroup f_3 statistic (*9*), which measures the length of shared branch between a pair of groups (i.e., shared genetic drift) from outgroup on the phylogenetic tree.

We used the admixture f_3 statistic and the f_4 statistic to detect evidence of gene flow between populations (*9*). In brief, the admixture f_3 statistic tests for "treeness" of the phylogenetic tree, and rejection of the null

model suggests presence of "loop structure" in the tree that represents genetic flow between the tested populations. The f_4 statistic of the form f_4(group1, group2; test, outgroup) detects admixture by examining the symmetry between group1 and group2 with regard to the test population in terms of genetic distance, and significant asymmetry suggests genetic exchange between the test population and the closer group (group1 if the f_4 statistic is positive, and group 2 if negative), despite uncertainty in the direction of gene flow.

Since the f_4 statistic is often used as a test for symmetry, technical differences (methods, coverage, and quality) in assaying genotypes of group1 and group2 may lead to bias or even artificial signals in the results. For this consideration, we primarily used the f_4 statistic to contrast two groups within our study, using it to detect ancestry shifts between time periods, or between groups from different archaeological contexts (such as Etruscan vs. Latin).

We computed the *f*-statistics based on pseudo-haploid genotypes of our samples, using qp3Pop (with "inbreed: YES" unless otherwise specified) and qpDstat (with "f4mode: YES") in the ADMIXTOOLS package (https://github.com/DReichLab/AdmixTools) (*9*). We excluded SNPs at CpG sites to reduce errors in variant calling due to post-mortem damage of methylated cytosines (which cannot be removed by UDG treatment and would appear as T alleles in sequencing).

African Introgression

One particular usage of the *f*-statistics in our study is to test for African introgression for each of the Italian samples with f_3(Test sample; CEU, Yoruba) and f_4(Test sample, CEU; Yoruba, Onge). The f_3 statistic tests whether across the genome, the allele frequency of the test sample is intermediate between those of Finnish and Yoruba, which is unexpected if the test sample, presumably of primarily European ancestry, forms a clade with Finnish with regard to Yoruba in the phylogenetic tree at all genomic loci. Therefore, a significantly negative f_3 statistic provides evidence for African ancestry in the test sample. (In this particular application, we used the imputed diploid genotype data without the "inbreed: YES" option, because qp3Pop cannot calculate f_3 when (1) the target is a single individual and (2) the "inbreed: YES" option.) For the f_4 statistic described above, under the assumption that chimpanzee is an outgroup, a significant positive score suggests more allele sharing between the ancient Italian individual (test sample) and Yoruba than between CEU and Yoruba, thus pointing to African introgression in the Italian individual. This test alone does not exclude the possibility of gene flow in the reverse direction, i.e., from the Italian sample to Yoruba, but this alternative scenario is unlikely given current knowledge about the demographic history of Yoruba and does not produce a significant f_3 statistic as formulated above. Taken together, significant signals in both tests provide strong evidence for African introgression, which is observed for 8 of the 127 Italian samples, including R475 from Iron Age, R80 and R132 from Imperial period (Fig. S23). We obtained qualitatively similar results by substituting Yoruba by Mota (an ancient African found in Ethiopia dated to ~2500 BCE) or Morocco_Iberomaurusian (hunter-gatherers from Morocco dated to 13,000-10,000 BCE) for the African population, and Onge by Papuan for the outgroup. We note that using Yoruba, Mota or Morocco hunter-gatherers as the representative African population is conservative for detecting more recent North African ancestry. We are using conservative estimates, since data is not available from relevant, contemporaneous (e.g. Iron Age and Imperial) populations, such as Carthagians. For instance, *qpAdm* analysis using Late Neolithic individuals from Morocco models R475 as approximately 53% Late Neolithic Moroccan, 30% Italian Copper Age and 16% Steppe Eneolithic, whereas the estimates below show Morocco Iberomaurusian and Yoruban to be around 8 - 10% ancestry proportion for this individual.

The Afican introgression signal we observe in the time series may reflect increased seafaring in the Mediterranean prior to Iron Age. Phoenician seafaring prowess had resulted in a network of colonies

across North Africa, engaged in trans-Mediterranean trade. Carthage, which began as a Phoenician trade colony in 1234 BCE, became the dominant naval state in the Mediterranean, with territory spanning North African, Sardinia, Sicily, and Iberia (*26*). Egypt had been involved in trans-Mediterranean and trans-Saharan trade networks for over a millennium by the start of the Iron Age. And trans-Saharan trade routes, made easier by a greener, less arid Sahara than today, connected the states and communities of North Africa and the Mediterranean with their Saharan and Sub-Saharan counterparts (*86*).

Admixture modeling with *qpAdm*

As an extension to the f_4 statistic, *qpAdm* (*10*, *87*) evaluates the goodness of a proposed admixture model (with a small p-value indicating a poor fit) and estimates the admixture proportions in a regression framework. This method relies on the rationale that if a target population can be modeled as a mixture of several source populations, the f_4 statistic of this target population with regard to any outgroup populations can be expressed as a linear combination of the f_4 statistics of the source populations to the same outgroup populations. More formally, *qpAdm* tests whether the matrix of f_4 statistics between a specified set of "left" populations (the target and all proposed source populations) and a set of diverse "right" populations (i.e., the outgroup populations) has a rank lower than the number of proposed source populations and, if so, whether the estimated mixture proportions from regression are biologically possible (i.e., between 0 to 1).

We carried out *qpAdm* analyses on pseudo-haploid genotypes (except for modern samples) using *qpAdm* in the ADMIXTOOLS package (*10*, *87*) with the option "allsnps: YES". Similar to f_4-statistics calculation, we excluded SNPs at CpG sites to avoid genotyping errors. We consider models with p-values>0.05, which indicates a small deviation of data from the model expectation, to be consistent with the data. We caution that the p-values are not comparable across models, because different source populations differ in sample size and coverage (i.e., the number of SNP sites covered by at least one read), so there is differential power to evaluate the goodness of the model fit. In other words, a working model with a greater p-value is not necessarily better or more likely than another working model with p>0.05.

We performed admixture modeling of ancient Italians for each time period separately. For each time period, we performed two or more rounds of admixture modeling. We first tested 1-way models with only one source population, where the source is an ancient population earlier than or of the same age as the target samples. We then tested two-way admixture models with the Italian samples in the preceding period as one source and another ancient population as the other source. If any of the proposed source populations were already in the pre-defined "right" (outgroup) set, we removed them from the "right" set and used the remaining populations as the outgroup populations. This modeling strategy assumes continuity in the genetic makeup of Italians since the Mesolithic Age and greatly reduces the search space. Although other two-way models which do not involve the preceding local population may also provide good fits, we consider them to be biologically unlikely and thus did not test those models.

As the *qpAdm* analysis results depend on the selection of the outgroup populations, we tested the robustness of the admixture models by using two different sets of outgroup panels for each analysis (see below for more details). Unless otherwise specified, we consider a model to be acceptable if it has p>0.05 with both the "right" sets. Although a very small p-value strongly indicates that a model is poorly fit and should be rejected, the threshold for acceptance is somewhat arbitrary; we occasionally also consider models with 0.01<p<0.05 to be marginally acceptable.

1 From the Mesolithic to the Iron Age

We first defined a set of 13 "right" populations (ANC13) that are genetically diverse and most of which predate our Italian samples. This ANC13 "right" set includes (with the sample size indicated by the number in the parentheses): Anatolia_N (25), CHG (2), EHG (4), ElMiron (1), Iran_Ganj_Dareh_N (3), Jordan_PPNB (1), MA1 (1), Mbuti (10), Natufian (6), Ust_Ishim (1), Vestonice16 (1), WHG (6), Russia_Yamnaya_Samara (9).

To increase the power to differentiate between models, we expanded this "right" set to 17 ancient populations (ANC17):
Anatolia_N (25), CHG (2), EHG (4), ElMiron (1), GoyetQ116-1 (1), Iran_Ganj_Dareh_N (3), Jordan_PPNB (1), Kostenki14 (1), MA1 (1), Morocco_Iberomaurusian (6), Mota (1), Natufian (6), Ust_Ishim (1), Vestonice16 (1), Italy_Villabruna (1), WHG (6), Russia_Yamnaya_Samara (9).

For each analysis, we fitted models with both ANC13 and ANC17 as the "right" set, and reported the results under ANC17 for working models (generally $p>0.05$) under both "right" sets. Numbers in parentheses following each population indicate the number of individuals included in the group and the number of SNP sites with data available. Populations with fewer than 50,000 SNPs available for analysis are not considered for *qpAdm* modeling, due to lack of power to reject the admixture models.

1.1 Mesolithic (10,000-6,000 BCE)
Potential source populations considered: CHG, China_Tianyuan, EHG, ElMiron, France_Ranchot88_published, France_Rigney1_published, GoyetQ116-1, Italy_Continenza, Italy_Villabruna, KO1, Kostenki14, LaBrana1, Latvia_HG, Lithuania_Mesolithic, MA1, Morocco_Iberomaurusian, Mota, Natufian, Norway_Mesolithic.SG, Norway_N_HG.SG, NW_Iberia_Meso, Romania_Iron_Gates_HG, SE_Iberia_Meso, Serbia_Iron_Gates_HG, Sicily_OrienteC_HG_published, Sweden_Mesolithic.SG, Sweden_Motala_HG, Switzerland_Bichon.SG, Ukraine_Mesolithic, Ust_Ishim, Vestonice16, WHG, WHG

Although PCA and supervised ADMIXTURE indicate that Mesolithic hunter-gatherers in central Italy can be modeled as 100% WHG, one-way models with the hunter-gatherer from Villabruna in north Italy (dated to 12,230-11,830 calBCE) (*15*) or western hunter-gathers (WHG) from Luxembourg (*12*), France or Germany (*15*) as a group provide poor fits to the data ($p<1e-12$). This suggests subtle but significant genetic differentiation between hunter-gatherers in central Italy and other WHG groups.

Interestingly, based on one-way *qpAdm* modeling, our three hunter-gatherers form a clade with a previously reported hunter-gatherer from Grotta de Continenza (dated to 8,920-8,750 calBCE) (*70*) and with a hunter-gatherer from Grotta d'Orient in Sicily (dated to 14,776-9,873 BCE) (*14*). The also project closer to each other in PCA, indicating genetic similarity between hunter-gatherers from southern and central Italy. However, both of these two samples have very low coverages (5,077 and 21,669 SNPs respectively), which limits our power to detect genetic differentiation.

1.2 Neolithic (6,000-3,500 BCE)
Potential source populations considered: Anatolia_N, Anatolia_N_Boncuklu.SG, Anatolia_N_Kumtepe.SG, Anatolia_N_Tepecik_Ciftlik.SG, Austria_LBK_EN, Bulgaria_Dzhulyunitsa_N, Bulgaria_Krepost_N, Bulgaria_MP_N, Bulgaria_N, Bulgaria_Varna_EN1, Bulgaria_Varna_EN2, Bulgaria_Varna_EN3, CHG, China_Tianyuan, Croatia_Cardial_N, Croatia_Impressa_EN, Croatia_Sopot_MN, Croatia_Starcevo_EN, Croatia_Starcevo_LN, Czech_N, Denmark_LN.SG, Denmark_MN_B.SG, EHG, ElMiron, England_N, Estonia_Comb_Ceramic_N.SG, Estonia_EMN_Narva, Estonia_MN_CCC, France_MN, France_Ranchot88_published, France_Rigney1_published, Germany_MN, GoyetQ116-1, Greece_N, Greece_Peloponnese_N, Greece_Peloponnese_N_out, Hungary_ALPc_Tiszadob_MN, Hungary_LBK_MN, Hungary_Lengyel_LN, Hungary_Starcevo_EN, Iberia_EN, Iberia_MN, Iran_Ganj_Dareh_N,

Iran_Tepe_Abdul_Hosein_N.SG, Iran_Wezmeh_N.SG, Ireland_MN.SG, Israel_PPNB, Italy_Continenza, Italy_Iceman_MN.SG, Italy_Villabruna, Jordan_PPNB, KO1, Kostenki14, LaBrana1, Latvia_HG, Latvia_LN_CW, Latvia_MN, Latvia_MN_Comb_Ware.SG, Lithuania_EMN_Narva, Lithuania_LBA.SG, Lithuania_LN, Lithuania_Mesolithic, MA1, Macedonia_N, Morocco_EN, Morocco_Iberomaurusian, Morocco_LN, Mota, Natufian, NE_Iberia_MLN, N_Iberia_MLN, Norway_Mesolithic.SG, Norway_N_HG.SG, NW_Iberia_Meso, NW_Iberia_MLN, Poland_BKG.SG, RMPR_ME, Romania_EN, Romania_Iron_Gates_HG, Russia_Shamanka_EN.SG, SE_Iberia_Meso, SE_Iberia_MLN, Serbia_EN, Serbia_Iron_Gates_HG, Serbia_N, Serbia_Starcevo_EN, Sicily_OrienteC_HG_published, Sweden_LN.SG, Sweden_Mesolithic.SG, Sweden_Motala_HG, Switzerland_Bichon.SG, Ukraine_Mesolithic, Ust_Ishim, Vestonice16, WHG

We found two one-way models fit the data of Neolithic individuals: Serbia_Starcevo_EN (p=0.19) and Anatolia_N_Boncuklu (p=0.06), indicating relatively high genetic similarity between these populations and Neolithic Age central Italians.

We also found several two-way admixture models that can explain the Mesolithic-to-Neolithic transition in central Italy by adding to the local population 93-97% ancestry of Neolithic population from central Anatolia (Boncuklu) (*80*), northern Greece (including three samples from Kleitos, Paliambela, Revenia) (*17*), or the Balkans (Croatia, Macedonia, Serbia) (*14*)(Table S7).

By contrast, Neolithic central Italians are poorly modeled (p<1e-5) as a mixture between the local Mesolithic population (RMPR_ME) and farmers from northwestern Anatolia (Anatolia_N), nor can they be modeled as two-way admixture of WHG (from Luxembourg, France or Germany) and Anatolia_N (p<1e-5), although the latter model fits well for early farmers from central Europe (p>0.09 in our *qpAdm* analysis). The admixture modeling results, together with the excess Iran_N component in Neolithic Italians in supervised ADMIXTURE, support additional or alternative source populations with the spread of agriculture into the Italian peninsula.

The significant nested p-values for the RMPR_ME component in the working two-way models suggest that adding hunter-gatherer ancestry significantly improves the model fit. In other words, there is significant evidence for persistence of hunter-gatherer ancestry in central Italy during the Neolithic transition. In fact, the amount of WHG ancestry gradually increased with time among our Neolithic samples (dated to 6,100-5,100 BCE): later individuals shifted towards WHG compared to earlier individuals in both PCA and shown by f_4 statistics in the form of f_4(test sample, Chimp.REF; WHG, Anatolia_N) (Fig. S24). Similar rebound of hunter-gatherer ancestry was previously reported in central Europe, Iberia and the Balkans (*10*, *13*, *17*, *19*, *88*).

1.3 Copper Age (3,500-2,300 BCE)

Potential source populations considered: Anatolia_C, Anatolia_N, Anatolia_N_Boncuklu.SG, Anatolia_N_Kumtepe.SG, Anatolia_N_Tepecik_Ciftlik.SG, Armenia_C, Austria_LBK_EN, Bulgaria_C, Bulgaria_Dzhulyunitsa_N, Bulgaria_Krepost_N, Bulgaria_MP_N, Bulgaria_N, Bulgaria_Varna_EN1, Bulgaria_Varna_EN2, Bulgaria_Varna_EN3, CHG, China_Tianyuan, C_Iberia_CA, C_Iberia_CA_Afr, C_Iberia_CA_Stp, Croatia_Cardial_N, Croatia_Impressa_EN, Croatia_Sopot_MN, Croatia_Starcevo_EN, Croatia_Starcevo_LN, Czech_N, Denmark_LN.SG, Denmark_MN_B.SG, EHG, ElMiron, England_CA_EBA, England_N, Estonia_Comb_Ceramic_N.SG, Estonia_EMN_Narva, France_Bell_Beaker_C, France_MN, France_Ranchot88_published, France_Rigney1_published, Germany_MN, GoyetQ116-1, Greece_N, Greece_Peloponnese_N, Hungary_ALPc_Tiszadob_MN, Hungary_Baden_LCA, Hungary_LBK_MN, Hungary_Lengyel_LN, Hungary_Starcevo_EN, Iberia_C, Iberia_EN, Iberia_MN, Iran_Ganj_Dareh_N, Iran_Seh_Gabi_C, Iran_Tepe_Abdul_Hosein_N.SG, Iran_Wezmeh_N.SG, Ireland_MN.SG, Israel_C, Israel_PPNB, Italy_Continenza, Italy_Iceman_MN.SG, Italy_Villabruna, Jordan_PPNB, KO1, Kostenki14, LaBrana1, Latvia_HG, Latvia_LN_CW, Latvia_MN,

Latvia_MN_Comb_Ware.SG, Lithuania_EMN_Narva, Lithuania_LBA.SG, Lithuania_LN, Lithuania_Mesolithic, MA1, Macedonia_N, Morocco_EN, Morocco_Iberomaurusian, Morocco_LN, Mota, Natufian, NE_Iberia_CA, NE_Iberia_MLN, N_Iberia_CA, N_Iberia_MLN, Norway_Mesolithic.SG, Norway_N_HG.SG, NW_Iberia_CA_Stp, NW_Iberia_Meso, NW_Iberia_MLN, Poland_BKG.SG, RMPR_ME, RMPR_NE, Romania_C, Romania_EN, Romania_Iron_Gates_HG, Russia_Shamanka_EN.SG, Scotland_CA_EBA, SE_Iberia_CA, SE_Iberia_Meso, SE_Iberia_MLN, Serbia_EN, Serbia_Iron_Gates_HG, Serbia_N, Serbia_Starcevo_EN, Sicily_OrienteC_HG_published, Steppe_Eneolithic, Sweden_LN.SG, Sweden_Mesolithic.SG, Sweden_Motala_HG, SW_Iberia_CA, Switzerland_Bichon.SG, Ukraine_Mesolithic, Ukraine_Trypillia_Eneolithic, Ust_Ishim, Vestonice16, WHG

For Copper Age individuals in central Italy, the one-way model with Bulgaria_Dzhulyunitsa_N as the single source provides marginally acceptable fit (Table S8). In addition, we found that the nine Copper/Bronze Age individuals from Sardinia collected in this study form a clade with the three Copper Age individuals from central Italy, at a borderline acceptance level (Table S8). This result, in conjunction with the lack of significant results from f_4 tests for any test population in the form of f_4 (RMPR_CA, RMPR_CA_Sardinia; test, Onge), suggests that Copper Age individuals from central Italian Peninsula and Sardinia are genetically highly similar.

Based on admixture f_3 and f_4 tests (Tables S9 and S10), there is significantly more WHG ancestry in the Copper Age individuals compared to in the Neolithic Age. Consistent with this, we found numerous working two-way admixture models that involve ~6-9% ancestry of a WHG group (or individual) and the preceding local Italians in Neolithic Age. Alternatively, the Copper Age individuals can also be modeled as an admixture of local Neolithic population with 30-80% ancestry of Neolithic groups from various European regions, such as Ireland, Iberia, Germany, France, Poland, and Romania. To discriminate between these models, we adopted a "model competition" approach that was first introduced in (*87*) and also used in (*22*). Specifically, we added each of the potential source populations to the "right" set and tested the fits of models with other proposed source populations. Because the actual source population shares extra drift with the target population, moving it to the "right" set will lead to poor fits (e.g., $p<0.05$) for models with surrogate source populations (i.e., populations that are close to the actual source populations). By performing this analysis, we found that admixture with any "pure" WHG populations cannot explain the data, as the p-values drop below the acceptance threshold, when a group of Middle/Late Neolithic individuals from north Iberia (N_Iberia_MLN) are added to the "right" set. In contrast, models with Neolithic and Copper Age populations from Iberia, Sardinia, and Ireland survive the "model competition" (Table S11), suggesting that the rebound of WHG ancestry in Copper Age is likely due to admixture with farmer populations with higher amounts of WHG ancestry rather than directly with hunter-gatherer groups.

We did not detect any significant differences between the Copper Age individuals (n=3) from central Italy and those from Sardinia (n=7) with f_4 statistics in the form of f_4(RMPR_CA, RMPR_CA_Sardinia; test population, Onge).

1.4 Iron Age (900-27 BCE)

Potential source populations considered: Anatolia_C, Anatolia_EBA, Anatolia_IA.SG1, Anatolia_IA.SG2, Anatolia_MLBA.SG, Armenia_C, Armenia_EBA, Armenia_LBA, Armenia_LchashenMetsamor.SG, Armenia_MBA, Bulgaria_C, Bulgaria_EBA, Bulgaria_IA, Bulgaria_MLBA, C_Iberia_BA, C_Iberia_CA, C_Iberia_CA_Afr, C_Iberia_CA_Stp, Croatia_Early_IA, Croatia_MBA, Croatia_Vucedol, Czech_Bell_Beaker, Czech_Corded_Ware, Czech_EBA, Czech_Protounetice_EBA, Czech_Starounetice_EBA, Czech_Unetice_EBA, Denmark_BA.SG, Denmark_LBA.SG, Egypt_Late_Period, Egypt_New_Kingdom, E_Iberia_IA, England_Bell_Beaker, England_Bell_Beaker_EBA, England_CA_EBA, England_EMBA, England_IA.SG, England_LBA,

England_MBA, Estonia_Corded_Ware.SG, France_Bell_Beaker_C, Germany_Bell_Beaker, Germany_Corded_Ware, Germany_LBK_EN, Germany_Unetice_EBA, Greece_Crete_Armenoi, Greece_Minoan_Lassithi, Greece_Minoan_Odigitria, Greece_Mycenaean, Greenland_Saqqaq.SG, Hungary_BA, Hungary_Baden_LCA, Hungary_Bell_Beaker_EBA, Hungary_LBA, Hungary_Prescythian_IA.SG, Iberia_BA.SG, Iberia_Bell_Beaker, Iberia_C, Iran_IA.SG, Iran_Seh_Gabi_C, Ireland_BA.SG, Israel_C, Israel_MLBA, Italy_Bell_Beaker, Italy_Remedello_BA.SG, Jordan_EBA, Latvia_BA, Lebanon_Canaanite_MBA.SG, Lithuania_BA, Moldova_Cimmerian.SG, Moldova_Scythian.SG, Montenegro_LBA.SG, NE_Iberia_BA, NE_Iberia_CA, NE_Iberia_Greek, NE_Iberia_Hel, Netherlands_BA, Netherlands_Bell_Beaker, N_Iberia_BA, N_Iberia_CA, N_Iberia_IA, NW_Iberia_CA_Stp, Phoenician_IA, Poland_Bell_Beaker, Poland_EBA, Poland_Globular_Amphora, Poland_Unetice_EBA.SG, RMPR_CA, RMPR_CA_Sar, Romania_C, Russia_Afanasievo.SG, Russia_Alan.SG, Russia_Aldy_Bel_IA, Russia_Andronovo.SG, Russia_Early_Sarmatian_IA, Russia_IA.SG, Russia_Karasuk.SG, Russia_Late_Sarmatian.SG, Russia_Okunevo_BA.SG, Russia_Poltavka, Russia_Sarmatian.SG, Russia_Shamanka_EBA.SG, Russia_Sintashta_MLBA, Russia_Srubnaya, Russia_Srubnaya_Alakul.SG, Russia_Tagar.SG, Russia_Yamnaya_Kalmykia.SG, Russia_Yamnaya_Samara, Russia_Zevakino_Chilikta_IA.SG, Scotland_Bell_Beaker, Scotland_CA_EBA, Scotland_LBA, Scotland_MBA, SE_Iberia_BA, SE_Iberia_CA, Sicily_Bell_Beaker, Steppe_Eneolithic, Sweden_BA.SG, Sweden_IA.SG, SW_Iberia_BA, SW_Iberia_BA_Afr, SW_Iberia_CA, SW_Iberia_IA, Switzerland_Bell_Beaker, Turkmenistan_IA.SG, Ukraine_Scythian.SG, Ukraine_Trypillia_Eneolithic

The only well-fit one-way model is with an Iron Age individual from Croatia dated to 805-761 calBCE, suggesting that this individual form a clade with Iron Age central Italians, with respect to all the populations in the "right" set (ANC17). This result, together with those for Neolithic and Copper Age individuals, points to tight connections between Italy and the Balkans from Neolithic to Iron Ages.

For the Copper Age to Iron Age transition in central Italy, admixture f_3 and f_4 tests both point to ancestry input that can be ultimately traced back to west Eurasian Steppe (Tables S13 and S14). This is also supported by admixture modeling results with *qpAdm*: most potential source populations in working two-way models are Bronze or Iron Age populations directly from the Pontic-Caspian Steppe, with one exception being an Iron Age Pre-scythian individual (Scythian is a nomadic culture complex inhabiting in vast areas of the west Eurasian Steppe and north to the Black sea) from Hungary.

In consideration of the inter-individual heterogeneity in this period in PCA and ADMIXTURE, we also performed admixture modeling for each sample separately. Based on the *qpAdm* results for all Iron Age samples collectively, we started by testing a two-way model with RMPR_CA and Russia_Yamnaya_Samara as the source populations and found that it provides reasonable fits ($p>0.05$) for eight of the 11 Iron Age individuals (Table S16) but can be rejected for R437, R850 and R475. We therefore tested for these three individuals alternative one-way, two-way and three-way models, if none of the simpler models fits.

Based on one-way *qpAdm* modeling, R437 forms a clade with an individual from Croatia dated to the early Iron Age. In contrast, R850 forms a clade with an individual from Copper Age Anatolia. These two individuals both came from Latin archaeological context, together with four other samples, who can be modeled as two-way mixtures of Copper Age central Italian and Steppe-related ancestries.

Two two-way models fit well for R437 and R850: RMPR_CA + Armenia_LBA and RMPR_CA + Anatolia_IA.SG. In both models, the incoming source population is temporally proximate to the Iron Age Italian samples, and their geographic locations point to ancestry input from the Near East. Strikingly, R437 and R850 both carry more ancestry from the incoming source than the preceding local population, highlighting the substantial influence of this "eastern" influence on the genetic makeup of central Italians

in Iron Age. Furthermore, the influence of this "eastern" ancestry is not limited to R437 and R850, as R1016 and R1015 can also be modeled as RMPR_CA + Anatolia_IA.SG, and R1016 (but not R1015) as RMPR_CA + Armenia_LBA

The location of R475 in PCA indicates that she (biological sex inferred based on sex chromosome and autosome coverages) carries more Neolithic Anatolian or African ancestry than her contemporaries. Further f_4 analysis reveals that R475 shares more alleles with Moroccan hunter-gathers and less alleles with Anatolia farmers, compared to other Italian Iron Age individuals. We were not able to model R475 with any one-way models or as any two-way mixtures with one source being the Copper Age location population, but two three-way models with an African population as one of the sources provide reasonable fits (p>0.03): RMPR_CA + Russia_Yamnaya_Samara + Mota and RMPR_CA + Russia_Yamnaya_Samara + Mota.

Interestingly, although Iron Age individuals were sampled from both Etruscan (n=3) and Latin (n=6) contexts, we did not detect any significant differences between the two groups with f_4 statistics in the form of f_4(RMPR_Etruscan, RMPR_Latin; test population, Onge), suggesting shared origins or extensive genetic exchange between them.

2 From Imperial period onward

To further increase the power to find best fit models for samples in Imperial era and later in *qpAdm* analysis, we defined an additional "right" (outgroup) population set consisting of 18 diverse modern populations (MOD18) (with the sample size indicated by the number in the parentheses):

Ami (10), Basque (29), BedouinB (19), Biaka (20), Bougainville (2), Chukchi (20), Eskimo_Naukan (12), Han (43), Iranian (38), Ju-hoan_North (5), Karitiana (12), Mbuti (10), Papuan (14), Russian (22), Sardinian (27), She (10), Ulchi (25), Yoruba (30).

As for earlier time periods, we performed *qpAdm* admixture modeling for Italian individuals sampled in Imperial era and later in a stepwise fashion. Having observed the high inter-individual ancestry diversity in Iron Age and after, we did not test one-way models, as a positive result (p>0.05) would only indicate that the average ancestries of the sampled individuals from the two populations happened to be similar. Instead, we tested two-way models for individual in each time period, proposing the two sources to be preceding Italian samples in last period and another ancient population (Iron Age onward) or a modern population. We considered a model to be acceptable if it has p>0.05 with both ANC17 and MOD18 as the right set, and reported the results under MOD18, unless otherwise noted.

2.1 Imperial period (27 BCE to 300 CE)

Potential source populations considered: Anatolia_C, Anatolia_EBA, Anatolia_IA.SG1, Anatolia_IA.SG2, Anatolia_MLBA.SG, Armenia_C, Armenia_EBA, Armenia_LBA, Armenia_LchashenMetsamor.SG, Armenia_MBA, Bulgaria_C, Bulgaria_EBA, Bulgaria_IA, Bulgaria_MLBA, C_Iberia_BA, C_Iberia_CA, C_Iberia_CA_Afr, C_Iberia_CA_Stp, Croatia_Early_IA, Croatia_MBA, Croatia_Vucedol, Czech_Bell_Beaker, Czech_Corded_Ware, Czech_EBA, Czech_Protounetice_EBA, Czech_Starounetice_EBA, Czech_Unetice_EBA, Denmark_BA.SG, Denmark_LBA.SG, Egypt_Late_Period, Egypt_New_Kingdom, E_Iberia_IA, England_Bell_Beaker, England_Bell_Beaker_EBA, England_CA_EBA, England_EMBA, England_IA.SG, England_LBA, England_MBA, England_Roman_MiddleEast.SG, Estonia_Corded_Ware.SG, France_Bell_Beaker_C, Germany_Bell_Beaker, Germany_Corded_Ware, Germany_LBK_EN, Germany_Unetice_EBA, Greece_Crete_Armenoi, Greece_Minoan_Lassithi, Greece_Minoan_Odigitria, Greece_Mycenaean, Greenland_Saqqaq.SG, Hungary_BA, Hungary_Baden_LCA, Hungary_Bell_Beaker_EBA,

Hungary_LBA, Hungary_Prescythian_IA.SG, Iberia_BA.SG, Iberia_Bell_Beaker, Iberia_C, Iran_IA.SG, Iran_Seh_Gabi_C, Ireland_BA.SG, Israel_C, Israel_MLBA, Italy_Bell_Beaker, Italy_Remedello_BA.SG, Jordan_EBA, Latvia_BA, Lebanon_Canaanite_MBA.SG, Lithuania_BA, Moldova_Cimmerian.SG, Moldova_Scythian.SG, Montenegro_LBA.SG, NE_Iberia_BA, NE_Iberia_CA, NE_Iberia_Greek, NE_Iberia_Hel, Netherlands_BA, Netherlands_Bell_Beaker, N_Iberia_BA, N_Iberia_CA, N_Iberia_IA, NW_Iberia_CA_Stp, Phoenician_IA, Poland_Bell_Beaker, Poland_EBA, Poland_Globular_Amphora, Poland_Unetice_EBA.SG, RMPR_CA, RMPR_CA_Sar, RMPR_IA, Romania_C, Russia_Afanasievo.SG, Russia_Alan.SG, Russia_Aldy_Bel_IA, Russia_Andronovo.SG, Russia_Early_Sarmatian_IA, Russia_IA.SG, Russia_Karasuk.SG, Russia_Late_Sarmatian.SG, Russia_Okunevo_BA.SG, Russia_Poltavka, Russia_Sarmatian.SG, Russia_Shamanka_EBA.SG, Russia_Sintashta_MLBA, Russia_Srubnaya, Russia_Srubnaya_Alakul.SG, Russia_Tagar.SG, Russia_Yamnaya_Kalmykia.SG, Russia_Yamnaya_Samara, Russia_Zevakino_Chilikta_IA.SG, Scotland_Bell_Beaker, Scotland_CA_EBA, Scotland_LBA, Scotland_MBA, SE_Iberia_BA, SE_Iberia_CA, Sicily_Bell_Beaker, Steppe_Eneolithic, Sweden_BA.SG, Sweden_IA.SG, SW_Iberia_BA, SW_Iberia_BA_Afr, SW_Iberia_CA, SW_Iberia_IA, Switzerland_Bell_Beaker, Turkmenistan_IA.SG, Ukraine_Scythian.SG, Ukraine_Trypillia_Eneolithic

Unlike Iron Age individuals that mostly fall close to western Europeans and northern Italians in PCA (Figs 2A and 3C), most of our central Italian individuals in the Imperial period project onto eastern Mediterranean or Near Eastern populations, such as Greek, Maltese, Cypriot, and Syrian. This shift in mean ancestry toward eastern Mediterranean populations is also evidenced by f_4 statistics (Table S20) and admixture f_3 statistics (Table S21).

Only one two-way model, RMPR_IA + Cypriot, provides robust fit (p-value>0.20) to Imperial Italian samples and estimates an admixture proportion of ~80% for Cypriots under both ANC17 and MOD18 outgroup sets (Table S22). This result, at face value, can be easily mis-interpreted as indicating 80% of the inhabitants in Imperial central Italy were immigrants from Cyprus, but this interpretation is problematic for several reasons. First, the genetic makeup of modern Cypriots may not represent how it was 2000 years ago. In particular, if migration became increasingly prevalent in pre-modern era, which seems plausible, modern populations would become more genetically similar than they were in the past, leading to an overestimated admixture fraction. Second, genetic data of ancient populations in late Iron Age and early Imperial period are sparse, which precludes tests for most of potential source populations based on historical records or geographic proximity. Furthermore, the active commodity and slave trades in the Imperial period may have brought diverse ancestries into the city of Rome from various regions, within or even beyond the empire's territories. The high inter-individual genetic heterogeneity in Rome is supported by the spread the samples in PCA (Fig. 2A) as well as the presence of individuals in five distinct clusters in the ChromoPainter results (Fig. 4). In the scenario of multiple incoming populations, the relatively good fit of the RMPR_IA + Cypriot model should be interpreted as that modern Cypriots closely resemble the (weighted) average of ancestries of all incoming source populations.

In addition to RMPR_IA + Cypriot, two other two-way models featuring Anatolia_MLBA and Iraqi_Jew, respectively, give relatively good but less robust fits (i.e., p>0.01 under MOD18 but not under ANC17). For similar reasons as elaborated above, the precise identity of the source populations and the admixture fractions should not be interpreted literally. Nonetheless, these relatively well-fit models all support a strong genetic influence of the eastern Mediterranean populations on the genetic composition of the city of Rome in the Imperial period.

2.2 Late Antiquity (300-700 CE)

Potential source populations considered: Anatolia_Ottoman1.SG, Anatolia_Ottoman2.SG, Bulgaria_IA, Canary_Islands_Guanche_mummy.SG, Croatia_Early_IA, Egypt_Late_Period, Egypt_New_Kingdom, E_Iberia_IA, England_IA.SG, England_Roman_MiddleEast.SG, England_Saxon.SG,

Germany_Early_Medieval.SG, Hungary_Langobard, Hungary_Langobard.SG, Hungary_Prescythian_IA.SG, Iran_IA.SG, Italy_Langobard, Lebanon_MP, Lithuania_Late_Antiquity.SG, Moldova_Cimmerian.SG, Moldova_Scythian.SG, NE_Iberia_c.6-8CE_ES, NE_Iberia_c.6CE_PL, NE_Iberia_c.8-12CE, NE_Iberia_Greek, NE_Iberia_Hel, N_Iberia_IA, Phoenician_IA, RMPR_IA, Russia_Alan.SG, Russia_Aldy_Bel_IA, Russia_Early_Sarmatian_IA, Russia_IA.SG, Russia_Late_Sarmatian.SG, Russia_Sarmatian.SG, Russia_Tagar.SG, Russia_Zevakino_Chilikta_IA.SG, SE_Iberia_c.10-16CE, SE_Iberia_c.10-16CE_Afr, SE_Iberia_c.10-16CE_Afr2, SE_Iberia_c.3-4CE, SE_Iberia_c.5-8CE, Serbia_Medieval_Gepidian.SG, South_Africa_1200BP.SG, South_Africa_400BP.SG, Sweden_IA.SG, Sweden_Viking.SG, SW_Iberia_IA, Turkmenistan_IA.SG, Ukraine_Scythian.SG

In this time period, the average ancestry of our Italian samples shifts substantially toward mainland Europe and starts to approximate that of present-day Italians, as illustrated in PCA (Fig. 3D) and formally tested by f_4 statistics (Table S23). Consistent with these findings, the Late Antiquity individuals can be modeled as a two-way mixture of the preceding local ancestry (RMPR_IR) and 41% ancestry from late Imperial German or 38% ancestry from modern Basque (Table S24).

Additionally, our Italian samples in Late Antiquity can be approximated by two-way mixtures of preceding Imperial samples and one of several modern populations from central and northern Italy ($p>0.04$). These results can be loosely interpreted as the genetic makeup of Late Antique individuals being intermediate between those of Imperial and modern individuals. In other words, there are both continuity and consistent shifts in the ancestry of central Italians since the Imperial period.

2.3 Medieval period and onward (700-1700 CE)

Potential source populations considered: Anatolia_Ottoman1.SG, Anatolia_Ottoman2.SG, Bulgaria_IA, Canary_Islands_Guanche_mummy.SG, Croatia_Early_IA, Egypt_Late_Period, Egypt_New_Kingdom, E_Iberia_IA, England_IA.SG, England_Roman_MiddleEast.SG, England_Saxon.SG, Germany_Early_Medieval.SG, Hungary_Langobard, Hungary_Langobard.SG, Hungary_Prescythian_IA.SG, Iran_IA.SG, Italy_Langobard, Lebanon_MP, Lithuania_Late_Antiquity.SG, Moldova_Cimmerian.SG, Moldova_Scythian.SG, NE_Iberia_c.6-8CE_ES, NE_Iberia_c.6CE_PL, NE_Iberia_c.8-12CE, NE_Iberia_Greek, NE_Iberia_Hel, N_Iberia_IA, Phoenician_IA, RMPR_IA, Russia_Alan.SG, Russia_Aldy_Bel_IA, Russia_Early_Sarmatian_IA, Russia_IA.SG, Russia_Late_Sarmatian.SG, Russia_Sarmatian.SG, Russia_Tagar.SG, Russia_Zevakino_Chilikta_IA.SG, SE_Iberia_c.10-16CE, SE_Iberia_c.10-16CE_Afr, SE_Iberia_c.10-16CE_Afr2, SE_Iberia_c.3-4CE, SE_Iberia_c.5-8CE, Serbia_Medieval_Gepidian.SG, South_Africa_1200BP.SG, South_Africa_400BP.SG, Sweden_IA.SG, Sweden_Viking.SG, SW_Iberia_IA, Turkmenistan_IA.SG, Ukraine_Scythian.SG

Illustrated in PCA, the ancestry shifts of central Italians toward European populations continue into Medieval and early modern periods. Although these shifts are no longer significant by f_4 statistics, admixture f_3 statistics show clear introgression signals for ancient and modern central/northern European populations (Table S25). Consistently, multiple two-way admixture models fit well the data of central Italian individuals dated to 700 CE and afterward: the target population can be modeled as mixtures of local central Italians in Late Antiquity and ~15-29% ancestry from one of the ancient European populations below: English in Roman or Saxon periods (50-900 CE) (*89*), Langobards from Hungary (400-600 CE) (*35*), an individual from Lithuania (50-650 CE) (*90*), individuals from Pla de l'Horta (but not L'Esquerda) in northeastern Iberia dated to the 6th century (*18*), Late Antiquity/Medieval individuals from Germany (350-1500 CE) (*91*), or Swedish Vikings (780-1200 CE) (*92*)(Table S26). Alternatively, many modern central/northern European populations also serve as reasonable source populations in two-way admixture models. Although we lack the resolution to differentiate these working models and take

caution in interpreting the results, it is clear that the genetic makeup of central Italians continues to approach Europeans and pull away from eastern Mediterraneans in the Middle Ages.

Detection of genetic outliers by f_4 statistics

With the substantial ancestry shifts throughout time in mind, we aim to detect genetic outliers for each time period relative to the overall ancestry of the corresponding population. To achieve this, we took a recursive procedure to identify the most significant outlier sequentially: (1) in each round, we calculated the f_4 statistics for each sample in the form of f_4(Test individual, contemporaries; ancient source, Onge), where "*contemporaries*" represents all other (n-1) samples in the same period as the test individual, and "*ancient source*" is one of five distinct ancient populations that represent typical ancestries: WHG, Anatolia_N, Morocco_Iberomaurusian, Russia_Yamnaya_Samara, Iran_Ganj_Dareh_N, Natufian; (2) we then identified the most significant f_4 statistic among all n*6 tests based on the z-scores and calculated its p-value after Bonferroni correction; (3) if the corrected p-value is below 0.001, we considered the corresponding test individual a genetic outlier and removed them from the time period; (4) we repeated steps (1)-(3) until none of the remaining samples in one time period had a significant f_4 statistic (i.e., corrected p-value<0.001). The Bonferroni correction and significance threshold are overly stringent on purpose to avoid calling outliers who only differ subtly from the other individuals in the same period. By this approach, we identified a total of 11 outliers in five time periods (Table S27) and then modeled their ancestries by *qpAdm* with one-way or two-way models (contemporary non-outliers + another ancient or modern population)(Table S28).

ChromoPainter analysis

Observing the high levels of inter-individual ancestry heterogeneity in Imperial Rome (Fig. 3C,D), we sought to characterize the fine-scale genetic structure of the population by assessing haplotype-sharing, using ChromoPainter (v 2.1.3) (*11*). In detecting subtle population structure, ChromoPainter is more sensitive than allele frequency-based methods such as PCA. For each target individual, ChromoPainter infers the most closely related individuals at each genomic locus based on shared haplotype segments ("chunks").

We performed this analysis across 475 individuals:

- 134 ancient Italian individuals (127 central Italians and Romans reported in main paper and 7 ancient Sardinians)
- 341 present-day individuals from 31 modern Mediterranean, Eurasian, and North African populations, with 11 individuals each, from the Globetrotter dataset (*53*)

A set of 997,710 non-missing snps were used. Default parameters were used for EM iterations and estimation (s1emits:10, s1minsnps:10000, s1snpfrac:0.1, s1indfrac:1). Running the main ChromoPainter software results in a co-ancestry matrix with 475 rows and 475 columns (Fig. S25), where individuals defining columns are "donors" and individuals defining rows are "recipients". Each value in the matrix describes copying of haplotype segments from the donor to the recipient. To reduce the effects of phasing errors in this analysis, we use the total length of the shared haplotype segments rather than the number of segments.

Principal component analysis (PCA) was performed on the co-ancestry matrix (Fig. S27). Individuals with similar haplotype donating and receiving profiles cluster closely together. The PCA of the co-ancestry matrix has a high concordance with the PCA previously described, where pseudo-haploid

genotypes of ancient individuals are projected onto a reference PC space created by present-day individuals (Fig. 2).

We measured the genetic affinity between an ancient Italian individual and a present-day population by summing the total length of the haplotype segments "copied" from individuals of the present-day population to the recipient ancient individual.

Allele frequencies for alleles of functional importance

Genomic time-series can be useful in understanding how the frequencies of functional alleles change in a population, which can potentially be used to detect signals of natural selection. However, the identification of selection signals must account for ancestry changes (e.g. by migration) occurring in the population. In this study, we only looked at the genotypes for individuals across our time-series for alleles that have prior evidence for selection and functional importance (*13*). Therefore, this is not intended to demonstrate selection on alleles in the Roman population.

Social Status in Imperial Rome

While ancient Rome was a highly stratified and hierarchical society, mobility between status groups and the shared use of necropolises across classes limits our ability to use status as a factor in analyses.

During the Imperial period, it is thought that slaves comprised roughly a third of the city's population (*93*) with freed slaves and non-elites (arranged into a number of social hierarchies) making up the majority of the remaining population. While the aristocracy constituted only a small percentage of the population, they are overrepresented in historical accounts, as they controlled political, military and cultural institutions (making them highly visible to contemporaneous writers and also allowing them to commission inscriptions and texts, such as Virgil's Aeneid, commissioned by Augustus) (*94*). However, archaeological, bioanthropological and biomolecular approaches, including this study, have allowed researchers to examine the population of Rome beyond the aristocracy.

Even within this highly stratified society, mobility between groups was possible, and wealth was not directly linked with status. For instance, the opulent tomb of Marcus Vergilius Eurysaces the Baker belonged to a wealthy freed slave. Additionally, the Roman elites and non-eiltes were often buried in the same necropolises, limiting our ability to infer social status based on burial context. For many of the individuals in this study, we do not have direct information (such as burial inscriptions) about individuals' identities.

Given the confounding factors mentioned above, we could not analyze status as a factor in this study, but we do believe that these individuals represent a diverse range of ancient Roman society, as they were sampled from a variety of contexts (in Rome itself, as well as rural, agricultural, and maritime contexts).

Supplementary Site and Archaeological Details

ANAS (Azienda Nazionale Autonoma delle Strada)

Date range: 100 - 300 CE
Individuals: R66, R67, R68, R69, R70, R71, R72, R73

The ANAS necropolis is situated in a southern suburb of Rome and was uncovered during road building (by the Azienda Nazionale Autonoma delle Strada, ANAS) in the area of the present day Acilia (Rome). The necropolis consists of 8 individuals, mostly adults, and is dated to the II-III century CE. The graveyard was associated with a small rural center of farmers and possibly with a nearby villa. Paleodietary analysis of the inhumated has been previously studied (*95*). The human osteological material is currently stored at the Museo delle Civiltà in Rome.

Ardea

Date range: 800 BCE - 500 BCE
Individuals: R850, R851

Located 4 kilometers from the Tyhrennian coast, Ardeatine territory consists of a large flat area with a maximum height of about 80-90 m s.l.m., which descends towards the sea with a series of successive terraces (*96*, *97*). The area was once the main urban center of the Rutuli, a population belonging to the "Latin lineage", as featured in the Aeneid (7.409-411) (*94*) .

Past archaeological research campaigns, as well as those in progress, carried out by the Superintendency for the Archaeological assets of Lazio, and by F. Di Mario direct, have allowed the discovery of sites, structures and finds of considerable importance, demonstrating how the Ardeatine territory is still extraordinarily rich in historical and artistic elements: their study
is starting to provide interesting data for more knowledge of this part of the ancient Lazio (*97–101*). Early evidence for the town's inhabitation dates back to the late Bronze Age (*102*, *103*). Ardea was part of the Latin League confederation and first became a Roman colony in the 5th century BCE. It is mentioned in the first Roman-Carthaginian treaty (3.22.24) as Ardea was one of the towns that refused to aid Rome in the Second Punic Wars (*104*).

The skeletal materials come from a necropolis (Campo del Fico) and from the area of the sanctuary, and are dated VIII and VI century BCE. The location of the site is not far from the sea and in connection with an important seaport, Castrum Inui, which gave Ardea a strategic role in controlling coastal routes in the pre-Roman Lazio region (*102*).

The two excavation campaigns conducted in 1981 and 1982 by E. Tortorici and L. Crescenzi brought to light 24 buried individuals (11 males 10 females and 3 infants) in both the necropolis area and the cult area (*101*).

Boville Ernica

Date range: 700 BCE - 600 BCE
Individuals: R1021

Boville Ernica, known in the past as “Bauco”, is situated on a steep hill overlooking the surrounding Liri, Cosa and Sacco valleys (*105*, *106*). Pre-Roman occupation of the site is evidenced by Italic archaeological findings and Pelasgic walls, characteristic of the people of the Bronze Age Aegean (*107*, *108*). The name of the city refers to the nearby temple on Monte Fico thought to be dedicated to the agricultural deity Bove, where votive statuettes featuring oxen have been found.

Cancelleria - The Basilica of San Lorenzo in Damaso

Date Range: 771 calCE - 1411 calCE
Individuals: R1219, R1220, R1221, R1224, R1283, R1285, R1290, R1287, R1288, R1289, R1286

The Basilica of San Lorenzo was erected by Pope Damaso (366-384 CE) in south-western Campo Marzio, reusing part of an architectural complex in which it is possible to recognize the buildings of the *factio prasina*, one of the four factions of the circus (*109–111*). The Basilica, with three naves, occupied a large area largely coinciding with that of the courtyard of the Palazzo della Cancelleria, in one of the most central areas of Rome, halfway between Piazza Farnese and Piazza Navona.

Probably as early as the sixth century CE there are numerous burials (subsequently reworked several times) that are carried out in the area of the church, in particular in a vast environment located close to the south side of the building (*112*).

A radical transformation of the Basilica is recorded in the second quarter of the 11th century CE following a fire, of which extensive traces have been found. In addition to conspicuous transformations of a structural nature, the floor of all the sections of the Basilica was raised by about 1 m. In the church, starting from this date until its destruction, numerous burials were built including several masonry ossuaries. New changes to the structure of the church were made during the second half of the fifteenth century. The numismatic artifacts found have allowed us to date, at the beginning of the last quarter of the fifteenth century, a large mass grave in which hundreds of burials were deposited (SU17, SU30 and SU471). In the way of organizing the burials it is likely to recognize the effects of a plague epidemic which we know to have struck the city between 1476 and 1479 CE, a hypothesis that would also be confirmed by the study of skeletal remains. In 1489 CE the building of the Palazzo della Cancelleria begins and the church is totally destroyed. The population of this necropolis covers most of the Middle Ages and is representative of the population of Rome of this period.

Casale del Dolce

Date range: 1 CE - 400 CE
Individuals: R123, R125, R126, R128

The archaeological site of Casale del Dolce is located on the southern border of Anagni, positioned on a limestone formation terrace on the eastern bank of the Sacco river.
In this area, there is little data regarding the production economy and its transformation from the fifth millennium to the third century BCE. This site is a fundamental reference point due to the breadth of the investigated area and the multiplicity of structural remains.

The presence of a prehistoric settlement in the area was reported by I. Biddittu (1976-1977; 1990), who in Mola Santa Maria had recovered archaeological materials, later published by Guidi and Pascucci (*113*), probably coming from a burial in the cave and from the remains of a village 500 meters further east (*114*).

A short distance from the excavated area, in Vadolargo and in Sgurgola -Valle Anagnina, other Eneolithic burials have been identified.

Archaeological investigations that began in November 1995 and concluded in February 1997 have allowed us to investigate an area of 2 hectares and led to the identification of the necropolis (*115*). This is relevant to the last phase of occupation of the site and consists of tombs located mainly in area A: 6 funerary structures have been identified, two of which are isolated while the other 4 are adjacent. An additional 7 are completely isolated at the northern end of the town near area C. The funerary structures presented multiple burials layered over time.

The site in fact presents, as the materials show, an occupation that goes from the Eneolithic to Late Antiquity (*116*). The four individuals from Casale del Dolce reported in this study date back to the Imperial / Late Antique period (1 - 400 CE) and come from the excavations of area C. One individual, who is not part of this study, was identified with leprosy (*117*). Isotopic analysis shows a relatively low amount of meat consumption at the site, with a few outlier individuals who appear to be consuming high amounts of marine resources (*118*).

Castel di Decima

Date range: 900 BCE - 700 BCE
Individuals: R1016

The necropolis of Castel di Decima is located along the Via Pontina (SS48) between approximately 18 and 20 km, on the southern outskirts of Rome, after Tor dei Cenci, along the route of the ancient Via Laurentina which connected Rome to Lavinio (*119*, *120*). It was identified in 1953, with the recovery of partially damaged funerary objects, then a rectification of the path of the road and partially explored in a systematic way from 1971 to the end of the 1990s. On the occasion of the doubling of the road and the construction of houses the site was subject to archaeological protection. The excavations in the necropolis were directed by the two archaeological Superintendencies of Ostia Antica and Rome, competent for the territory, respectively to the west and east of the Via Pontina.

The excavations at Castel di Decima returned about 400 pit inhumations, dating back to a period of time between the beginning of the eighth century BCE and the end of the seventh century BCE. Apart from some tombs found devoid of objects or previously disturbed, they have all provided funerary objects of particular interest, among which some of considerable wealth emerge, attributable to figures of aristocratic rank and their family groups which characterize the Lazio and Tyrrhenian societies in general from the Orientalizing period (*121*).

The type of argillaceous-ferrous soil has not generally allowed the preservation of the skeletal remains of which only the teeth are preserved and traces of the long bones and skull, except for rare cases in which the outline of almost the entire skeleton is preserved, but with the bones which, while retaining their shape, are completely decalcified and very crumbly, especially in the distal parts. In these cases, the skeleton was recovered inside the blocks of earth that contained them. The gender of individuals is therefore almost always has been determined by the composition of funerary objects. The materials recovered by the Superintendency of Ostia Antica are kept at the EUR Civilization Museum, those recovered by the Superintendency of Rome at the National Museum of Terms in Rome.

Celio

Date range: 400 CE - 600 CE
Individuals: R35, R36

The excavations inside the Military Hospital of Celio (Rome), conducted by the Archaeological Superintendence of Rome, took place above all from 1986 to 2000 and were of a preventive nature, compared to a wide-ranging project of building and functional renovation of the nineteenth-century hospital (*122*, *123*).

The excavations have revealed archaeological elements whose chronology extends from the archaic age up to the 7th century CE. However, the most numerous testimonies regard the phases of occupation that are concentrated between the first century of the empire until the V-VI century CE.

Structures attributable above all to dwellings with ground-floor shops, complexes with storage and market functions and large aristocratic domus (also equipped with private baths) have been identified and partly excavated. These residences were built in the age of the Antonine emperors (in the second half of the II century CE), were then restructured in the IV century (when they were bought by families of the high pagan aristocracy) and finally abandoned around the second half of the V century CE, like many others of the structures mentioned above.

The main discovery, and the only building investigated in full in the hospital area, is the Basilica Hilariana, schola (home) of the religious college of the Dendrophori and place of worship of Cibele and Attis. The complex visible today, located at a slightly higher level, dates back to the time of Antoninus Pius and has a series of building and stratigraphic phases that last until the end of the 4th century CE.

The schola was taken from the Dendrophores around 415 CE, due to the imperial measures that hit the still active pagan religious corporations, and was then partially occupied by precarious manufactures between the middle of the 5th and the middle of the 6th century CE. The final abandonment and collapse occurred around the beginning of the seventh century CE.

Centocelle Necropolis, Rome (Suburbium)

Date Range: 1 CE - 400 CE
Individuals: R50, R49, R51, R47

The area of the ancient *Centumcellae*, in a south-eastern suburb of Rome, next to the Via Labicana (within modern day Centocelle, Rome), extends for more than 30 hectares and preserves a rich archaeological record ranging from the 6th century BCE to the 6th century CE. Among the many monuments and sites so far investigated, the necropolis of Centocelle is associated with a Roman imperial Villa (*Ad Duas Lauros*) and is dated to the IV-V century CE.
The necropolis consists of 61 inhumations and the individuals possibly pertained to the inhabitants of the Villa. The preliminary bioarchaeological survey is published in (*124–127*). Dietary analysis of the inhumated through compound specific isotope analyses (CSIA) performed on single amino acids is currently in progress. The human osteological material is currently stored at the Museo delle Civiltà in Rome.

Civitanova Marche

Date range: 27 BCE - 300 CE
Individuals: R835, R836

The skeletal remains come from the excavation carried out in the mid-1970s by the Archaeological Superintendency of the Marche of the ancient Roman city of Cluana (*128*). There is no archaeological publication of the excavation, the information comes from the anthropological study of this necropolis published in an article together with the study of three other contemporary necropolises. The tombs are dated to the 4th century AD. The particular characteristic that they have is that of the presence in each tomb of several individuals, even if the dimensions of the tomb were always constant and independent of the number of skeletons they contained. The 35 tombs contained 181 individuals, of whom 119 adults and 62 sub-adults. The tombs had very poor grave goods.

Civitavecchia

Date Range: 700 BCE - 600 BCE
Individuals: R473, R474, R475

La Mattonara is an Iron Age Etruscan necropolis near the coastal town of Civitavecchia, on the Tyrrhenian Sea (*129*, *130*). Archaeological evidence, such as storage rooms for traded goods and pits for salting and preserving seafood, suggests the economy of this and other coastal Etruscan towns was based on long-distance trade and the exploitation of marine resources (*131*). Civitavecchia later served as a major Roman port (built between 103 and 110 CE) and was known at the time as Centum Cellae.

Crypta Balbi

Date Range: 400 CE - 600 CE
Individuals: R105, R106, R107, R108, R109, R110, R104

The area of the Crypta Balbi is a significant sector of the current historic center of Rome flanked by the modern via delle Botteghe Oscure (*132–134*). Extended about one hectare, the area contains the remains of a public building of the Augustan age (Crypta Balbi) attached to a theater. In medieval times the ancient ruins were transformed into a castle (Castrum aureum) where a church was built (S. Maria domine Rose). During the late Middle Ages the perimeter of the area was gradually occupied by private settlements (houses and vegetable gardens), until it hosted a monastery in the Renaissance with a new church (S.Caterina dei Funari), which still exists today. During the twentieth century the monastery was demolished and later even the houses were abandoned. Archaeological excavations started in 1981 led to the opening of the new Crypta Balbi Museum annexed to the archaeological site.

During the excavations some areas have been identified that have received funerary depositions of burials referable to the centuries of late antiquity and the Middle Ages.

Grotta Continenza

Date Range: 10100 BCE - 2877 calBCE

Individuals: R11, R7, R15, R2, R3, R8, R10, R9, R6, R4, R5

The Continenza Cave is located in the territory of the former Fucino Lake, at 713 meters above sea level and has returned a sequence of 9 meters thick. The upper levels are from the Roman period, below which there are levels of the Copper Age, of the ancient Neolithic to imprinted ceramics (6,590 to 6,170BP), followed by mesolithic (Castelnovian) levels, so far unknown in central Italy (7,230 BP), and Sauveterrian (9,650 BP). The sequence ends with levels of the final epigravettian in which it is possible to recognize several phases thanks to the variations of the faunas and the size of the lithic industries (10,200 to 12,831 BP)(*135*, *136*).

Numerous burials have been found in the cave: those of the ancient Neolithic were upset by clandestine excavators but it was possible to establish the presence of over 40 individuals including male and female adults, young people, children and fetuses. Exceptional is the discovery of a cremation complex with two vessels containing the burnt-in remains of two children covered by the remains of a woman, a phenomenon known in Italy only in very few other cases. Human remains were also found in the Castelnovian levels and a part of the female burial was present in the Sauveterrian ones(*137*).

In the sequence of the final epigravettian two male tombs in a circle of stones were discovered, one of which was stretched out with the belly and the face down and headless, and various other human remains. Numerous combustion pits and structured hearths, flint processing areas and meal waste clusters were also found, for which various functions of the cave, dwellings and funerals can be seen (*138*).

In addition to the abundant lithic industry, there were numerous bone and shell ornaments, and bones decorated with geometric motifs as well as painted pebbles.

Isola Sacra necropolis

Date Range: 1 CE - 400 CE
Individuals: R42, R39, R37, R38, R40, R41, R43, R44, R45

The Imperial port town of Portus Romae is located approximately 23 km southwest of Rome, and was a key trading center for the city during the Roman Empire. Portus was the port of Rome, and the uninhibited flow of goods into the metropolis, first and foremost grain, but also other vital foodstuffs, was the highest priority of the imperial government. The prosperity of Portus was tied up with that of the imperial city. The inhabitants of Portus were buried in the necropolis of Isola Sacra, which extends approximately 1.5 km along the road between Ostia and Portus Romae, and was in use from the 2nd to the late 3rd-early 4th centuries CE. People buried in the Isola Sacra were engaged in commerce and business, frequently themselves descended from slaves. The population, those sections of it that are 'visible', was, or appears, relatively egalitarian, in comparison with other Italian towns. There is a missing 'tranche' in the social hierarchy, at the top, where one would expect to locate an aristocracy of office and social prestige (*33*).

Over 2000 individuals have been recovered to-date from the necropolis and are currently stored at the Museo delle Civiltà in Rome. The bioarchaeology of the odontoskeletal collection of Isola Sacra was intensely investigated and a number of contributions has been published, exploring demography (*139*, *140*), diet (*34*, *95*, *141*, *142*), occupational markers (*143*), stress of the infant segment (*144–146*), and paleopathology (*19*, *147–149*).

Marcellino & Pietro

Date Range: 136 calCE - 500 CE
Individuals: R132, R130, R133, R134, R136, R137

The catacombs of Santi Marcellino e Pietro (Saints Marcellinus and Peter) are located about 3 kilometers south of Rome and named after the early Christian martyrs who were thought to be buried there in the 3rd century CE. The catacombs are comprised of roughly 4.5 kilometers of underground tunnels(*150*).

The burials in this study were excavated in 1958 and 1993 and the paleopathology and bioarchaeology of these two excavations (from galleries I7, I8, I9, I11, and Z4) studied as part of a combined report (*151–153*). In this group there is a large number of infants and children (over 20%). The low presence of individuals in old age, together with low values of stature, when compared to the contemporary groups, as well as the high incidence of enamel hypoplasia, suggest that there as the individuals were subjected to widespread metabolic and/or nutritional stress during childhood (*151*).

Martinsicuro

Date range: 930 cal BCE - 839 calBCE
Individuals: R1

Martinsicuro is a coastal site located on the border of Le Marche and Abruzzo on central Italy's Adriatic coast. It is a proto-Villanovan village, situated on a hill above the Tronto river, dating to the late Bronze Age and Early Iron Age(*154*). Excavations at the site have been limited, but during an excavation in preparation for road construction, a single post-built structure was excavated which contained a rich archaeological deposit of ceramics (*155*). These finds from the site indicate an affinity with contemporaries in the Balkans, suggesting direct trade contacts and interaction across the Adriatic. In particular, the practice of decorating ceramics with bronze elements was shared between the Nin region in Croatia and Picene region of Italy, including Martinsicuro (*156*). These finds also show the conservation and preservation (e.g. as artifacts) of ceramics from the earlier Middle Bronze Age into the Late Bronze Age and Early Iron Age.

Mausoleo di Augusto

Date Range: 300 CE - 700 CE
Individuals: R31, R30, R32, R33, R34

Between 2007 and 2011, the Capitolina Superintendency for Cultural Heritage conducted preventive investigations in the area of the Mausoleum of Augustus, in the center of Rome, as part of a project to redevelop the monument and the surrounding square.

During the excavation in the sector to the south of the Mausoleum, the staircase and the other structures relating to the arrangement of the 1950s were demolished, 20 burials in primary lying in the earth pit were found, to which 2 depositions in secondary position are added. These burials, characterized by an extreme variety and irregularity in the preparation, did not return funerary objects (*157*).

They belong to the already well-known burial ground of the Mausoleum of Augustus, partly excavated in the years 1950-51, on the occasion of the works of arrangement of the area outside the Mausoleum. On that occasion, 23 "cappuccina tombs" were identified, for a total - to date - of 45 depositions. The graves for the

depositions are excavated inside caves that obliterated the paving of the imperial age; at a first examination of the materials, these bays are not prior to the second half of the 5th century CE This chronological indication provides the *terminus post quem* for the dating of the burial ground. It can therefore be said that the cemetery complex found in the area of the Mausoleum of Augustus is, due to its characteristics, an example of the spread, between the second half of the 6th and the 7th century, of vast cemeteries within the Aurelian Walls, in a territory characterized by the alternation of built-up areas and abandoned areas (*158–160*).

Mazzano Romano, Necropolis of Monte Agnese

Date range: 1 CE - 400 CE
Individuals: R1543, R1544, R1545

The necropolis of Mazzano Romano, on Monte Agnese, is located about 50 north of Rome on the border with the Province of Viterbo (*161*). The necropolis is from the Roman imperial period which come from a chamber tomb that has undergone severe remixing due to violations both in ancient and recent times. In total the chamber tomb has returned the remains of at least 20 individuals, of which 16 are adults and 4 sub-adults (*162–164*).

Monterotondo

Date range: 26 BCE - 300 CE
Individuals: R1551, R1547, R1548, R1549, R1550

A town located northwest of Rome along the Via Salaria, making it an important defensive position for Rome (*165*). Early evidence for habitation of the site dates back to the late Bronze Age and it has been suggested that it is heir to the Sabine town of Eretum, mentioned by Virgil in the Aeneid and other ancient writers (*94*). The individuals in the study from Monerotonodo are from Roman occupation of the site in the Imperial period (*166*).

Monte San Biagio

Date range: 3500 BCE - 2500 BCE
Individuals: R1014

Monte San Biagio is a Eneolithic site located in southern Lazio at foothill of Monti Ausoni about 120 km south of Rome near the Tyhrennian coast (*167*). Archaeological finds from the site belong to the Gaudo and the Rinaldone material cultures and indicate a mixed farming economy with small scale polyculture, as well as the development of copper metallurgy and increased specialization of craft production (*168*, *169*). Similarities between the Gaudo culture and Aegean groups suggest ongoing contact between these regions in the Eneolithic.

Palestrina (Antina, Colombella, Selciata)

Date range: 600 BCE - 200 CE
Individuals: R435, R436, R437

Praeneste, modern-day Palestrina, located south of Rome, was one of the largest ancient cities in Iron Age Latium and home to the Praenesti tribe. Praeneste was originally part of the Latin League, a consortium of cities allied for mutual protection, but left to form an alliance with Rome. After Rome was sacked by the Gauls in the 4th cen BCE, Praeneste switched sides again and fought against Rome in the Latin Wars. After defeat by the Roman, Praeneste was incorporated into the growing Roman territory (*170*).

Archaeological evidence attests to the strong trade links Praeneste had across the Mediterranean. One striking example is the silver bowl (Fig. S30) from an Iron Age tomb at Praeneste dating to the 8th/7th century BCE (*3*). Based on stylistic elements, art historians have attributed the bowl to a Carthaginian or Phoenician origin. Interestingly, the hieroglyphic characters serve as a design motif rather than as textual characters. They do not spell anything, perhaps suggesting that the bowl was created for a market that valued their aesthetic, rather than inscriptive, value.

Ripabianca di Monterado

Date range: 5465 calBCE - 5214 calBCE
Individuals: R16, R17, R18, R19

The Ripabianca di Monterado site belongs to the Middle-Adriatic Impressed Ware phase located in a sub-coastal area a few kilometers north of Ancona in the Marche region (*171*). The site was excavated in the early 1960s and returned three primary burials over further fragmentary remains (*172*, *173*). The calibrated dates of the site place it between 5500 and 4900 BC. These dates have been confirmed by those made, in the present study, directly on the skeletons. The ceramics of the site also presents some characters of originality, revealing evident influences coming from contemporary cultural aspects, it also lends itself perfectly to analyze the contact made, around the second half of the sixth millennium-beginning of the fifth century BC, between the Marche area, Central and inland Tyrrhenian Italy and northern Italy referable to the aspect of linear Ceramics (*171*, *174*). These relationships were probably linked to the trade in raw materials, first of all obsidian (*175*, *176*).

S. Ercolano Necropolis, Ostia (Suburbium)

Date range: 400 CE - 600 CE
Individuals: R117, R118, R120, R121, R122

In the perimeter of the small modern sanctuary of S. Ercolano, in the south-eastern suburb of ancient Ostia, two excavation campaigns, in 1988 and 1989 made it possible to awaken interest in an area funerary only previously glimpsed, especially with earthworks completed in the nineteenth century, which then brought to light cremation and burials from the early imperial age to late antiquity, including Christian inscriptions (*177*, *178*).

At the present state of research, it is not possible to have the certainty of the existence of a church before the modern age; in the same way we have for the first time, in the modern age, the mention of the Hagiotoponym of Ercolano (for the small shrine currently visible), certainly a Christian martyr, attested in the 4th century CE (Depositio martyrum), remembered as buried in nearby Portus.

The burials excavated in 1988 and 1989 belong to late antiquity and the early Middle Ages (based on stratigraphic and typological analysis), in a period ranging from the 4th century to the High Middle Ages (*178*). As in the case of the nearby area of Pianabella, it cannot be ruled out that such a densely occupied

cemetery may be linked to one of the suburban ostiense burial churches, indicating an occupation of part of the space of the ancient city that remains to be identified in its configuration housing. The anthro-archaeological study is fundamental in this case and should guide, with the association to the burials from which the bone finds come, the planning of future investigations.

Tivoli Palazzo Cianti

Date range: 1600 CE - 1700 CE
Individuals: R969, R970, R973

An elaborate palace built in Tivoli by the bishop of the Marsica, Giuseppe Cianti in the 1600's. It also functioned as the seat of a Monte di Pietà (mountain of plenty) and a Monte Frumentario (mountains of grain). These institutions were both operated through the Catholic Church - the former to provide loans to parishioners and the second to provide wheat and barley to farmers for sowing. This site was excavated by a team lead by Dr. Mauro Rubini in 2009.

Veio Grotta Gramiccia

Date range: 900 BCE - 800 BCE
Individual: R1015

The site of Veio (Veii in English, Veio in Italian) is a large Etruscan city, located about 18 kilometers north of Rome (*179*). Veio's territories spanned not only the plateau on which was located, but extended from the Tiber River in the south to Monte Sabatini (*180*, *181*). It was one of the most powerful Etruscan city-states and its proximity to Rome resulted in conflicts between the two cities in the Iron Age and Republican periods, until Rome's victory over Veio in 396 BCE (*182*).

Research by the South Etruria Survey and Tiber Valley Project have documented Veio and it's territory. These surveys mapped roads connecting Veio to other important regional cities, such as Rome and Tarquinia, and identified Veientine necropoli (often located along these roads) (*183–185*). One of these, Grotta Gramiccia contains over 800 tombs (*181*). Located on the road between Veio and Tarquinia and Vulci, it is one of the earliest cemeteries of Veio, with tombs dating from the 9th to 7th centuries BCE (*179*, *181*, *186*).

While the burial in this study from Grotta Gramaccia has not been published previously, material finds from elsewhere in the necropolis, as well as other domestic and industrial contexts in Veio offer insights into daily life in Veio and its contacts with other Etruscan groups and the world beyond.

Via Paisiello Necropolis

Date range: 1 CE - 200 CE
Individuals: R111, R113, R114, R115, R116, R131

During the works of preventive archaeology (2014 - 2016) in a building located in Via Paisiello, a vast funeral area with a very long life was found, ranging from the 1st century to BCE. to the IV sec. CE (*180*). The necropolis is located in northern Rome, near Villa Borghese, where in the Roman age the immense Necropolis Salaria extended, of the size of 24 hectares (*187*, *188*). In this excavation many pit graves have been found, tombs with niches, shaped tombs, primary incinerations (*busta sepulchra*),

secondary incinerations inside *ollae* and inside *amphorae*. The remains of real mausoleums and a columbarium in *opus reticulatum*, *hypogea* and perhaps a *ustrinum* have also been identified. The vast area found, connected to an important ancient road system, the *Salaria vetus*, highlighted the skeletal remains of 88 individuals, whose osteological remains are in poor condition. 18 incinerations were also found, of which 6 primary (*busta sepulchra*) and 12 secondary. The cremated individuals are all adults and mostly female.

The inhumation burials represent almost 80% of the examined sample and are almost all primary, the bodies, often supine and North-South oriented, were probably wrapped in a shroud. There are also 7 prone positions. The burials contain a larger number of older adults than sub-adults, and males than females.

Viale Rossini Necropolis

Date range: 1 CE - 200 CE
Individuals: R75, R76, R78, R80, R81

During some urban archaeology works, for the laying of a long water pipeline, carried out in 2008, a necropolis of about 90 individuals was found near Viale G. Rossini, between the intersections of Via G. d'Arezzo and Via A. Bertoloni and a portion of a columbarium in via G. Puccini (*189*). In the necropolis of viale G. Rossini various funerary types are attested including “cappuccine”, both single and multiple, earthy pits, depositions *in formae* and amphora incineration. The excavation of the necropolis has yielded individual depositions and burials in buildings of probable family character. The presence of amphorae and ollas attests the use of both incineration and inhumation rituals, with a strong prevalence of the latter over the former. Among the funerary structures, two had depositions *in formae* inside, another building had both inhumations and incinerations, while in the section other smaller structures could be distinguished, perhaps due to small monuments. The structures had NW / SE orientation and assumed an ancient road network of the same direction. The path of this ancient road is recognized by the scholars Quilici - Quilici Gigli in the direction of the ancient city of *Antemnae* following the route from Porta Pinciana, along the homonymous street and continuing towards via G. Paisiello, via E. de Cavalieri, viale Romania and via di S. Filippo Martire up to the *Antemnae* hill.

Villa Magna

Date range: 820 CE - 1430 CE
Individuals: R52, R53, R54, R55, R56, R57, R58, R59, R60, R61, R62, R63, R64, R65

The 14 individuals from Villamagna derive from the archaeological excavation, conducted between 2006 and 2010, of the Monastery of San Pietro in Villamagna, Anagni (FR) (41.683246, 13.111812) that saw the identification, unearthing and study of 491 individuals (of which 421 were articulated primary burials and 70 were identified through laboratory analysis of loose bone from specific contexts of known chronological attribution) dated from the 8th to the 14th century CE. Though unevenly distributed in the different chronological phases (15 early medieval, 80 Central Medieval, 382 late medieval and 14 of uncertain attribution), somewhat fragmentary and at times incomplete, the samples were well preserved and proved apt for morphological study, isotope analysis and aDNA extraction (*190*, *191*).

Occupation of the site is attested from the beginning of the first century with a succession of at least two Roman Villas; one of which an Imperial one of extreme prestige (*192*). The estate was reoccupied in the 9th Century and in the 10th it was donated by some land owners of Anagni to the monastic order. The

monastery grew in power, as also testified by the addition of a cloister, a porch, a new apse and a grand cosmatesque pavement, only to be suppressed by Bonifacio VIII in 1297. The monks consequently left but occupation of the site continued, as did its funerary use. It was then transformed into a castrum under the control of the cathedral of Anagni and local noble families and once again abandoned in 1478 (*193*, *194*)

The stable isotope analysis conducted on 125 of the 491 individuals from the medieval cemetery at Villamagna showed wide variation in isotopic ratios and slightly higher d13C and d15N values in the Central Medieval individuals. Though this may in part be consequence of the demographic distribution observed (the Central Medieval phase, the one associated to the Monastery and possibly the one that includes the remains of the monks that died at Villamagna, shows a male to female sex ratio of 1.29), it could also reflect differences in diet, status or mobility (*190*).

Supplementary Figures

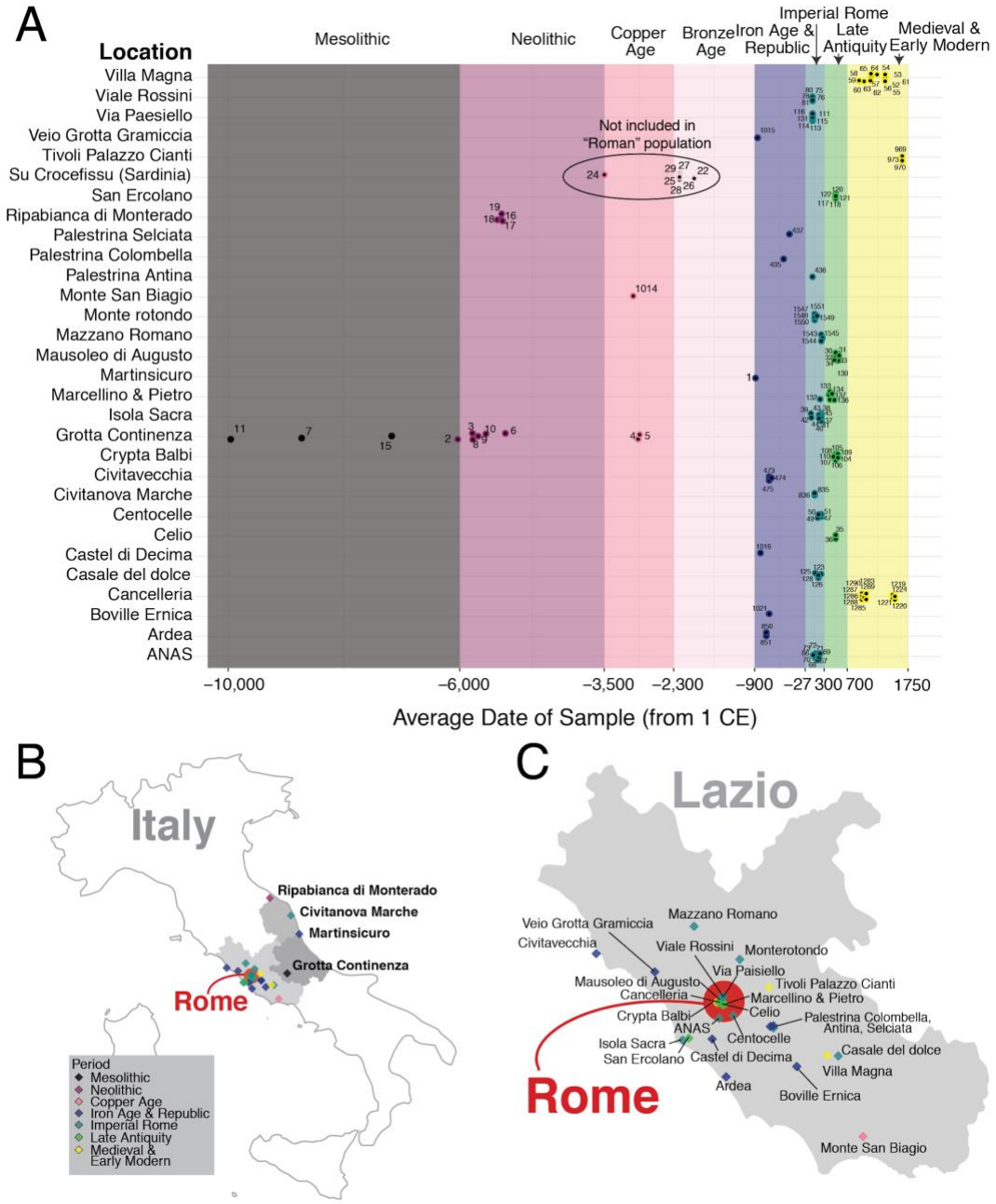

Fig. S1. Locations and time periods of archaeological sites. (**A**) Date ranges for time periods and average dates for samples. The average date for each sample is shown along with ranges for each time period. Sample points are colored based on the time period to which it was assigned regardless of position in time period range. (**B**) Sites locations in Italy, colored by corresponding time period to which the site belongs, with the exception of Grotta Continenza which represents three time periods: Mesolithic (n=3), Neolithic (n=6), Copper Age (n=2); and Marcelino & Pietro which represents two time periods: Imperial Rome (n=1) and Late Antiquity (n=5). (**C**) Zoomed in version of full Italy map to show the province of Lazio.

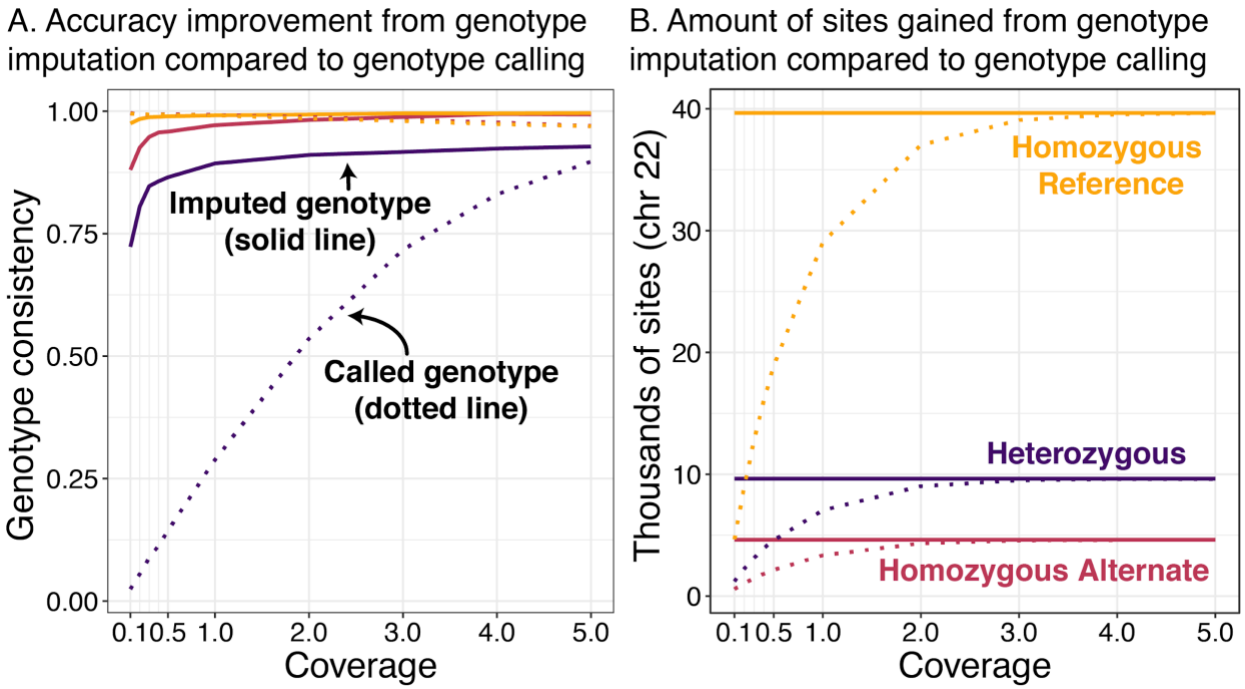

Fig. S2. Genotype calling and imputation compared by genotype accuracy and number of sites. A 22x genome (NE1) (*54*) was downsampled to coverage levels from 0.1x to 5x and imputed at lower coverages. (**A**) The consistency of imputed and called genotypes with the true genotype is shown for heterozygous, homozygous alternate, and homozygous reference genotypes. (**B**) The number of sites are shown for imputed and called genotypes corresponding to the assessment in panel A.

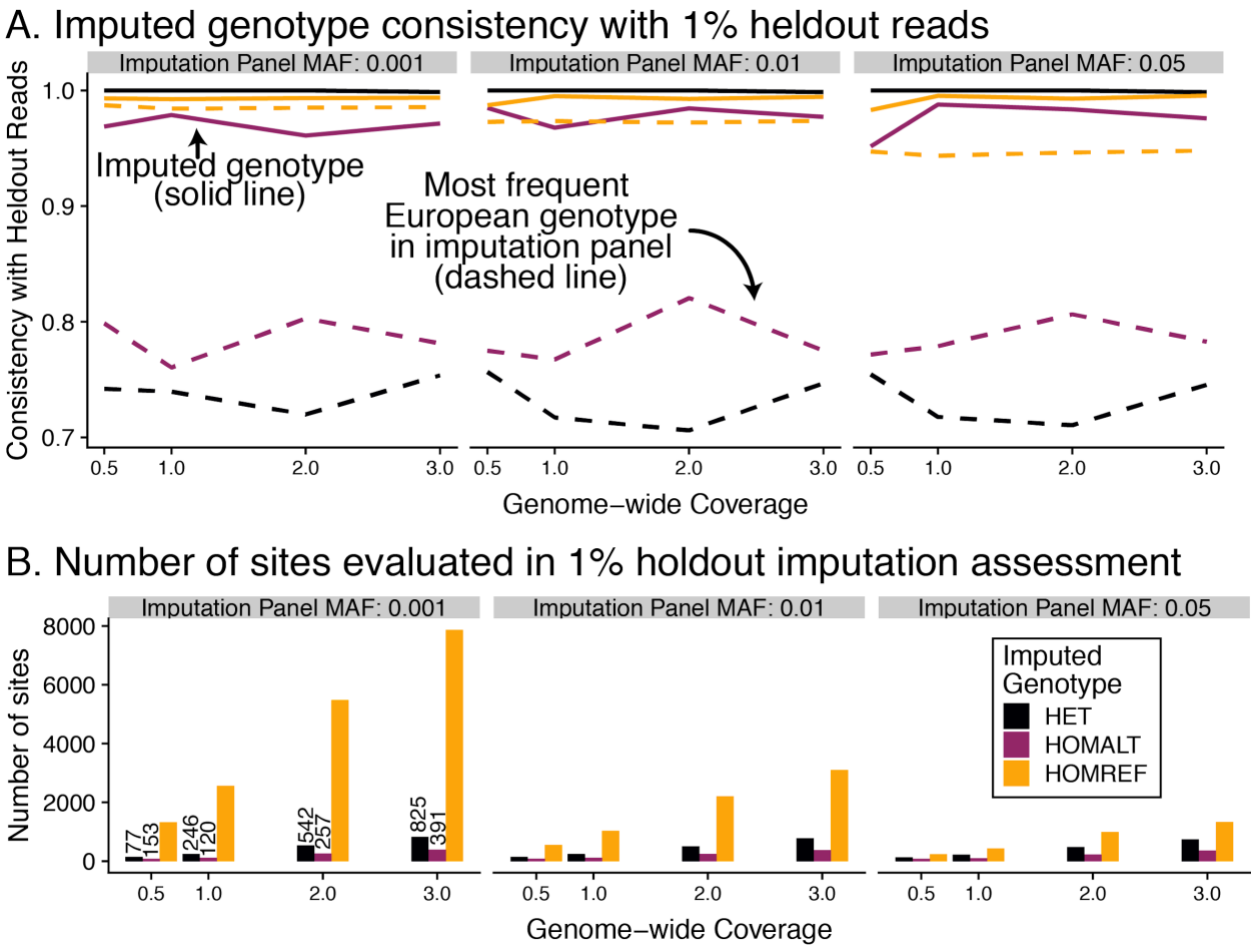

Fig. S3. Imputed genotype consistency with a 1% holdout set of reads. A genome (NE1) sequenced to 22x (*54*)was downsampled to coverage levels of 0.5x to 3x. 1% of reads were held out prior to imputation. Imputed genotypes at sites where reads were held out were assessed for consistency with the true reads. Results are stratification by minor allele frequency (MAF) of the global imputation panel and for heterozygous, homozygous alternate, and homozygous reference genotypes. (**A**) Consistency of genotypes by imputation (solid lines). As a comparison we show the accuracy that would be achieved by naively using the most common European genotypes (dashed lines) in the imputation reference panel. (**B**) The number of sites evaluated in the holdout assessment are shown.

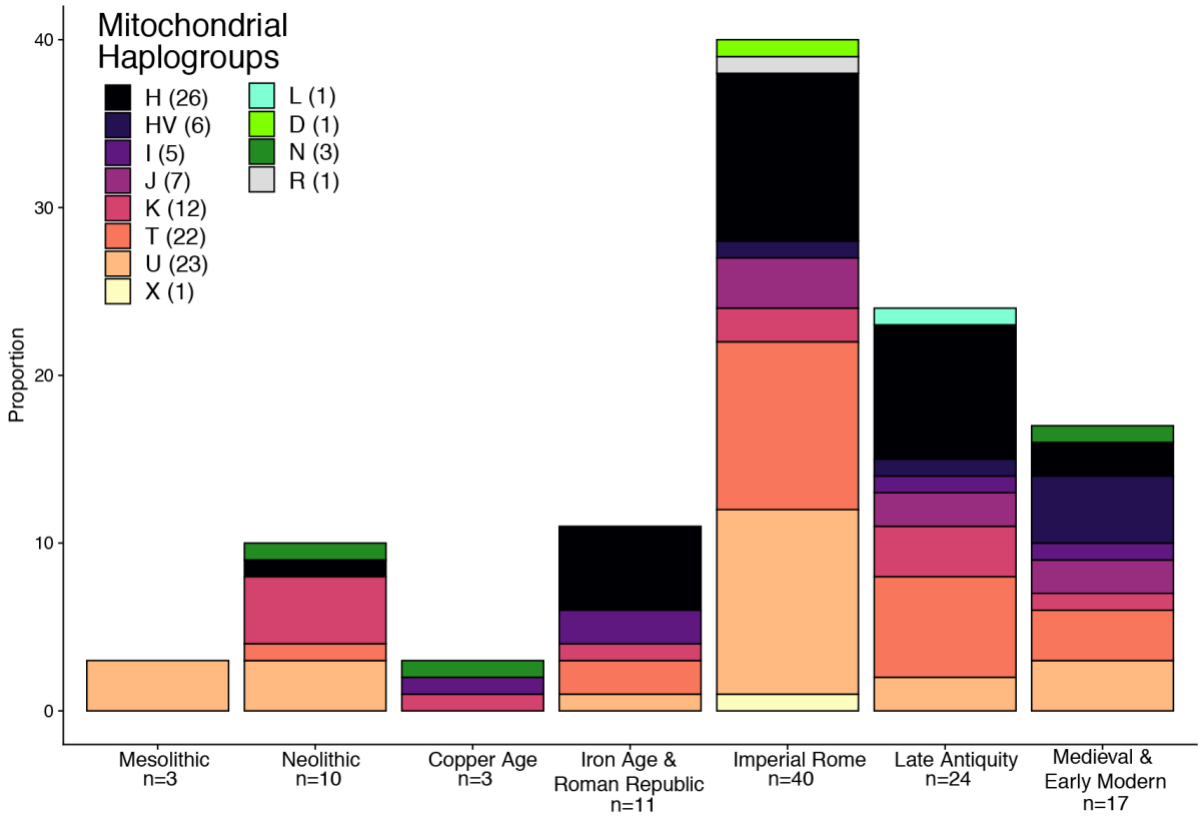

Fig. S4. Mitochondrial haplogroups of ancient Italian individuals.

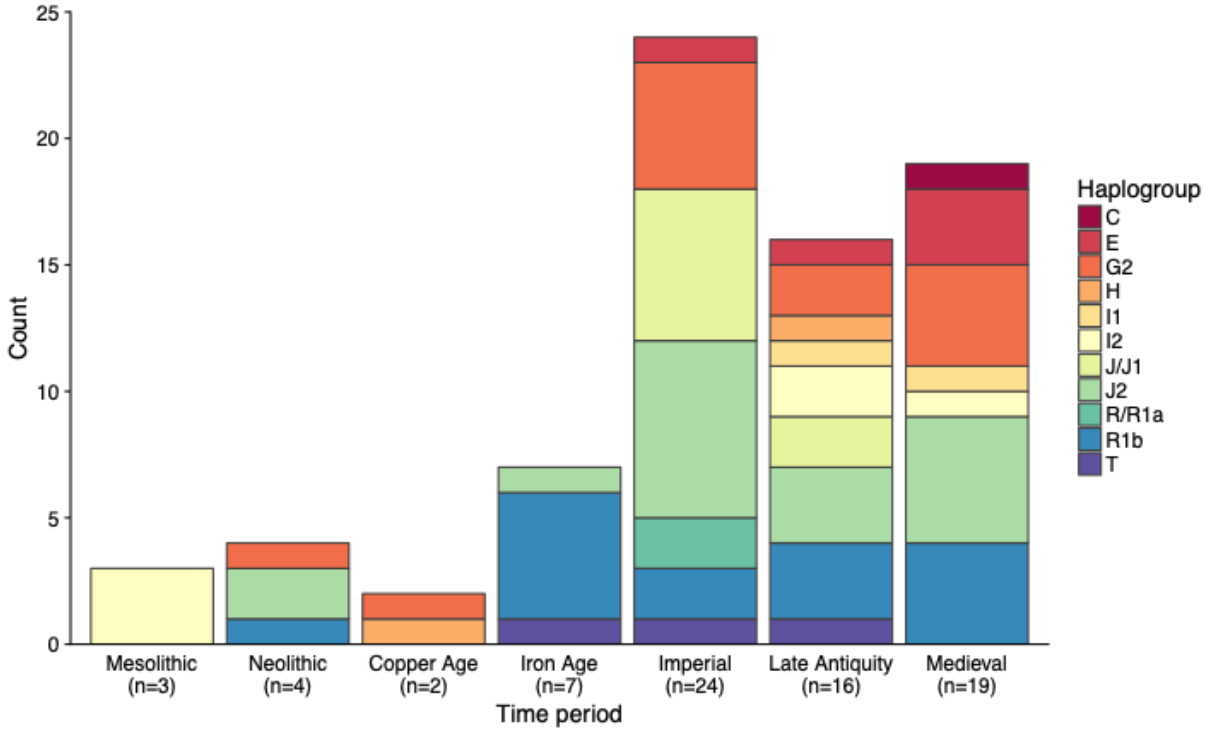

Fig. S5. Distribution of Y-chromosome haplogroups of ancient Italian individuals.

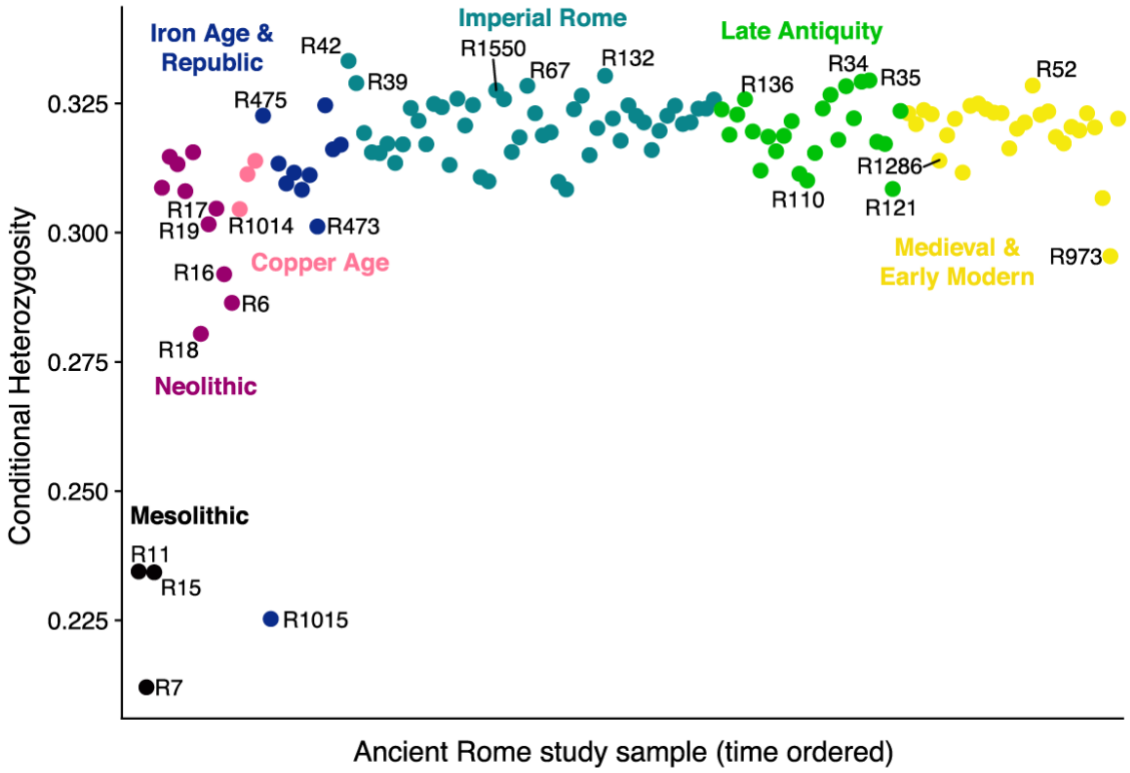

Fig. S6. Conditional heterozygosity for ancient individuals reported in this study. Conditional heterozygosity was calculated per individual at sites that are segregating in a single San Khomani individual with a read-based method (*14*, *81*). Colors represent the time period to which that individual has been assigned. High or low heterozygosity individuals of interest are labeled with their sample ID.

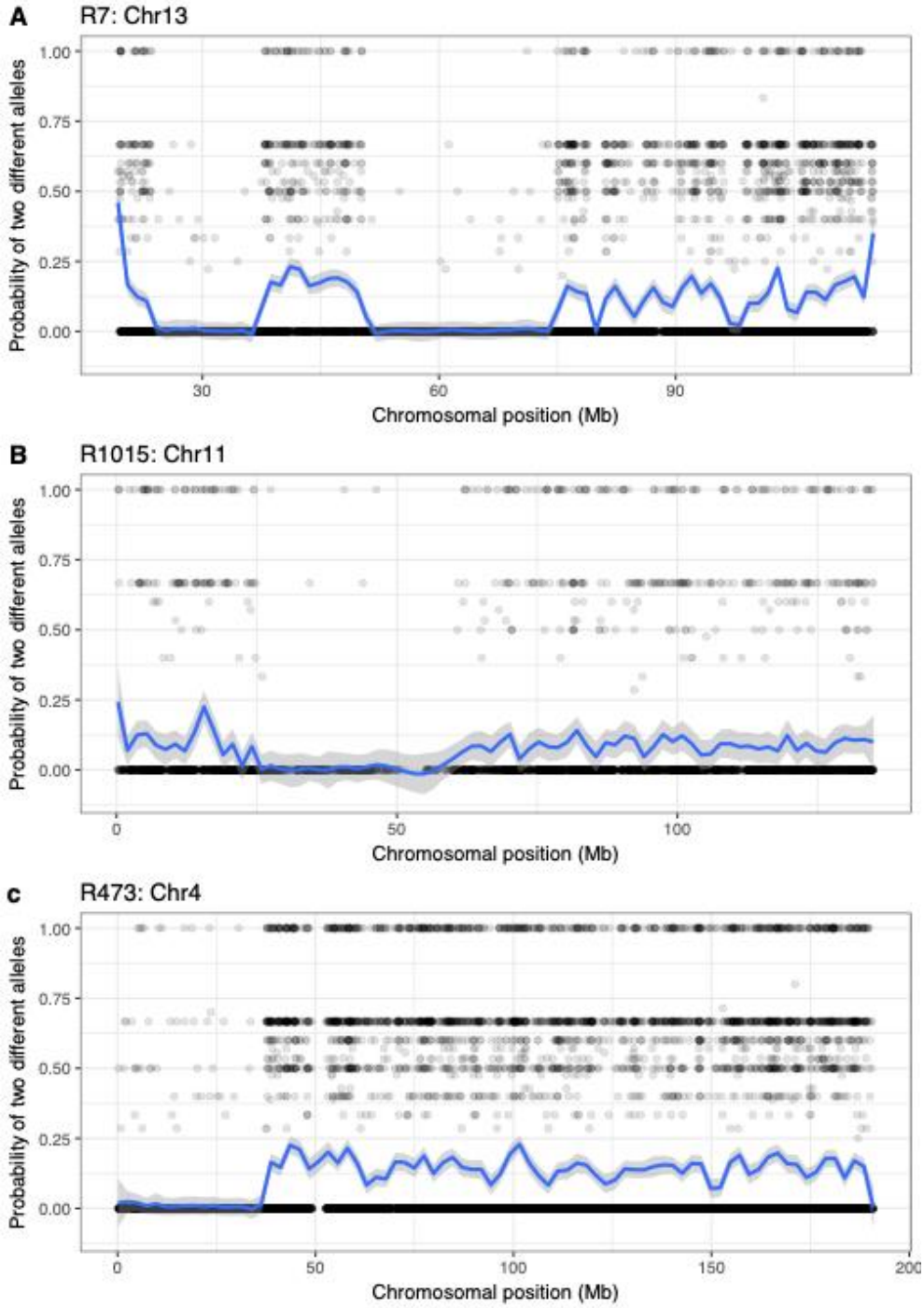

Fig. S7. Examples of long runs of homozygosity (ROH) in three ancient Italian individuals reported in this study. ROH segments are detected by a read-based approach: each dot represents a SNP site covered by at least two reads, and the y-axis is the probability of seeing two different alleles, if exactly two reads are randomly sampled. In blue is the LOESS curve describing the average probability of seeing different alleles in a chromosomal window, so the parts overlapping with the y=0 line indicate ROH segments, with a few dots with estimated heterozygosity>0 potentially due to untrimmed DNA damage or sequencing errors.

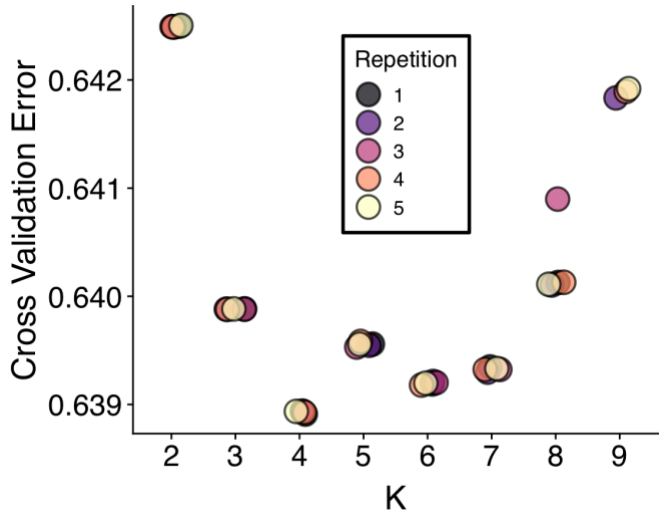

Fig. S8. Cross-validation for unsupervised ADMIXTURE analysis for K=2 to K=9. Unsupervised ADMIXTURE was performed with ancient and modern populations at K=2 to K=9, with 5-fold cross-validation, and 5 repetitions (with varying random seed). Each point (jittered) represents one repetition at a K value.

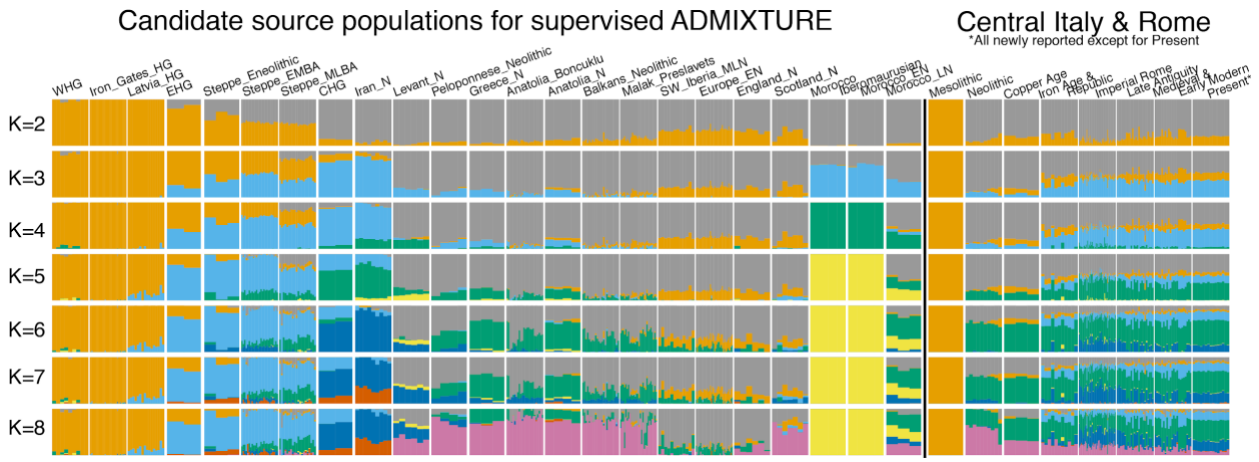

Fig. S9. Unsupervised ADMIXTURE for K=2 to K=8. Runs of unsupervised ADMIXTURE with lowest cross validation error are shown. Only ancient and present-day Eurasian populations were included in all runs. Select published ancient populations with the highest average proportions for a single cluster and with a sample size > 1 are shown across all K. For reference, ancient samples from central Italy and Rome are shown on the right, along with published present-day central Italians. Colors for each cluster are only relevant within each K, although colors/cluster numbers were aligned across runs if possible.

Fig. S10. Unsupervised ADMIXTURE timeline at k=5. Unsupervised ADMIXTURE was performed with ancient and modern populations. Each bar represents the ADMIXTURE proportions for an individual. Each thumbnail includes ADMIXTURE profiles of individuals from that region (column) and date range (row). Time periods and date ranges are based on those used in this study for Rome and Italy.

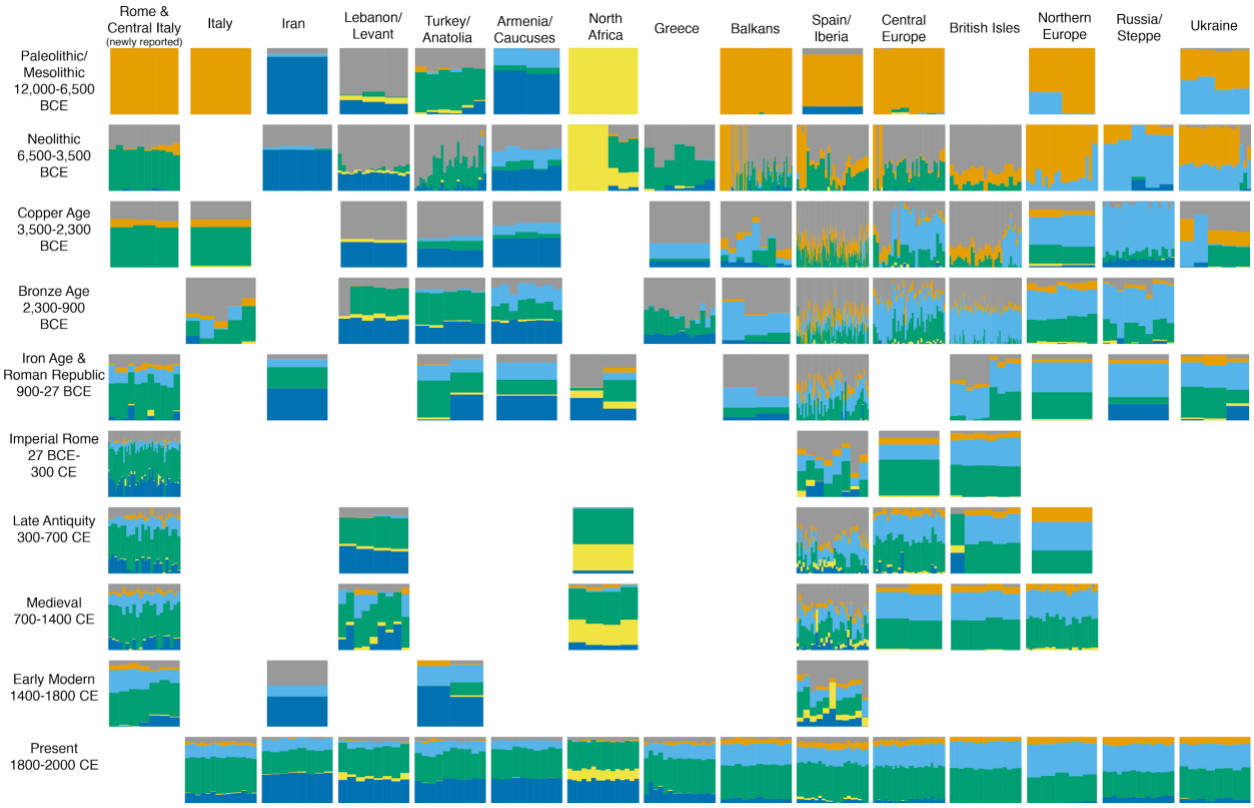

Fig. S11. Unsupervised ADMIXTURE timeline at k=6. Unsupervised ADMIXTURE was performed with ancient and modern populations. Each bar represents the ADMIXTURE proportions for an individual. Each thumbnail includes ADMIXTURE profiles of individuals from that region (column) and date range (row). Time periods and date ranges are based on those used in this study for Rome and Italy.

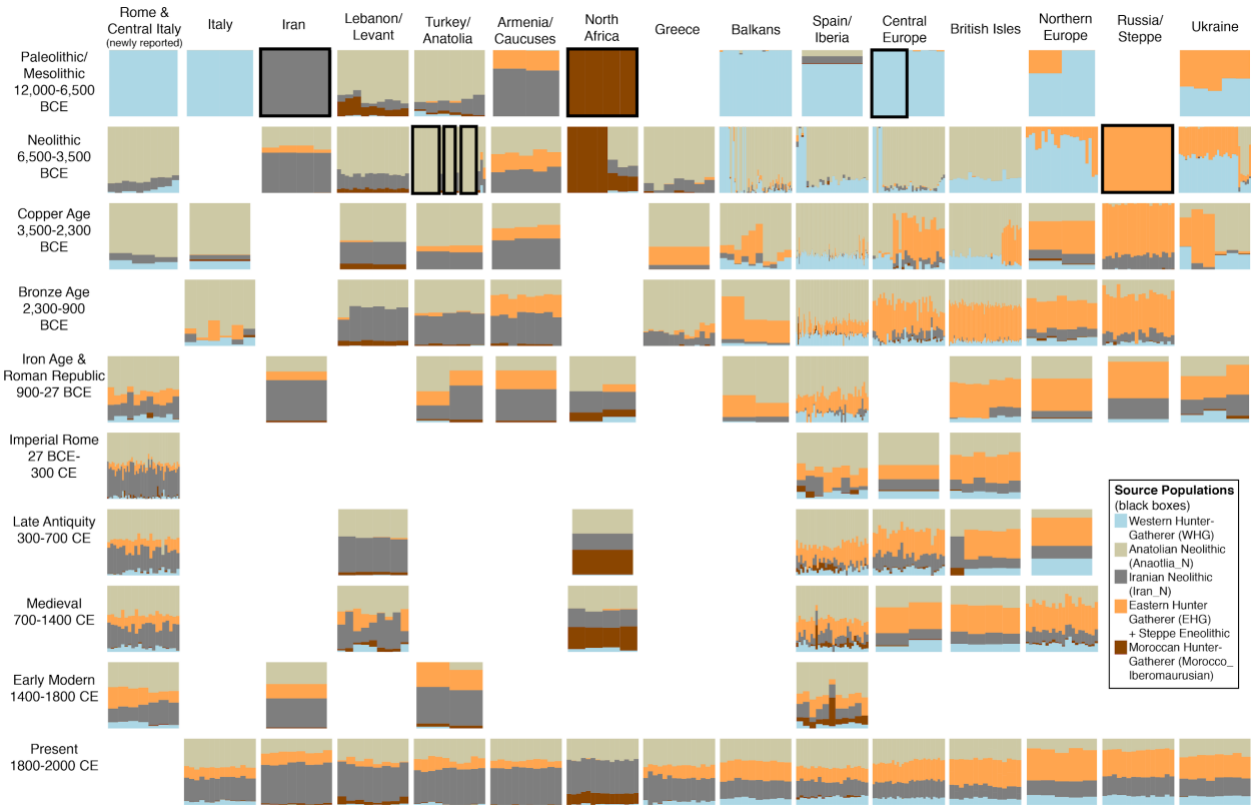

Fig. S12. Supervised ADMIXTURE timeline. Supervised ADMIXTURE was performed with ancient and modern populations and with five source populations: Western Hunter-Gatherers, Northwestern Anatolian Neolithic, Iranian Neolithic, Moroccan Hunter-Gatherer (Morocco Iberomaurusian) and Steppe Eneolithic (denoted by black boxes around corresponding samples). Each bar represents the ADMIXTURE proportions for an individual. Each thumbnail includes ADMIXTURE profiles of individuals from that region (column) and date range (row).

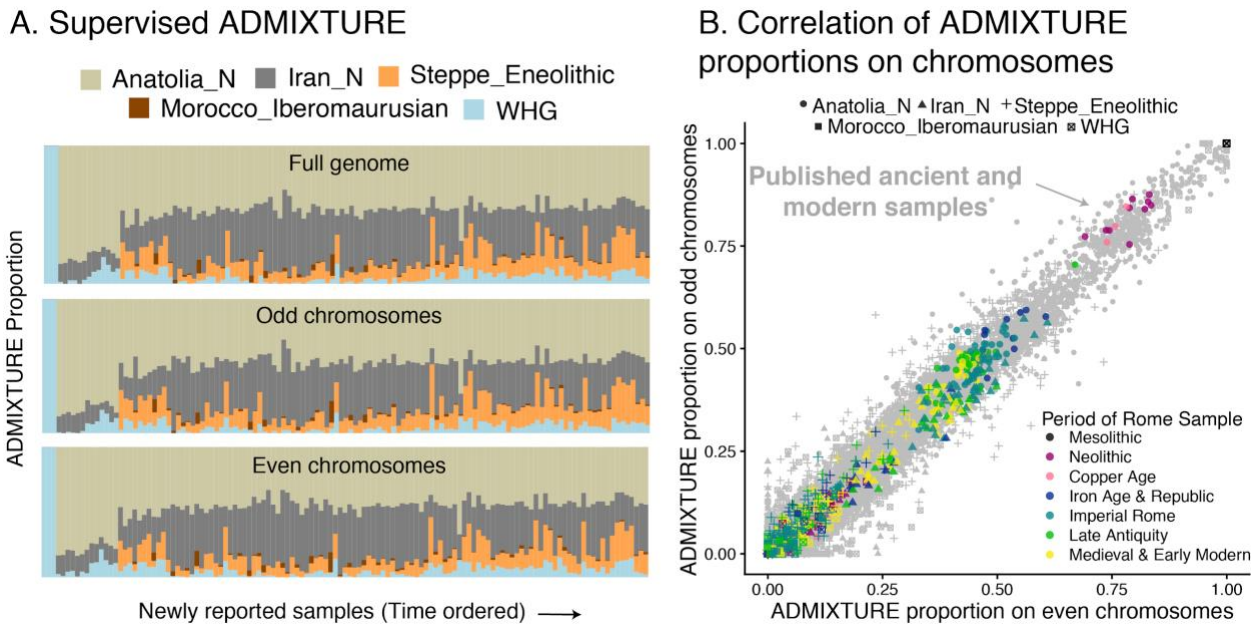

Fig. S13. Consistency of Supervised ADMIXTURE proportions across odd and even chromosomes. Supervised ADMIXTURE was run on both odd and even chromosomes of pseudohaploid genotypes for the study samples (127 ancient Romans and 7 ancient Sardinians) and reference samples (varying genotyping methods, but consistent across both runs). (**A**) Admixture proportions are shown for only study samples for simplicity. (**B**) Corresponding ADMIXTURE proportions (for same sample and source population) across the two runs are shown with points for study samples colored by time period, and published samples in gray.

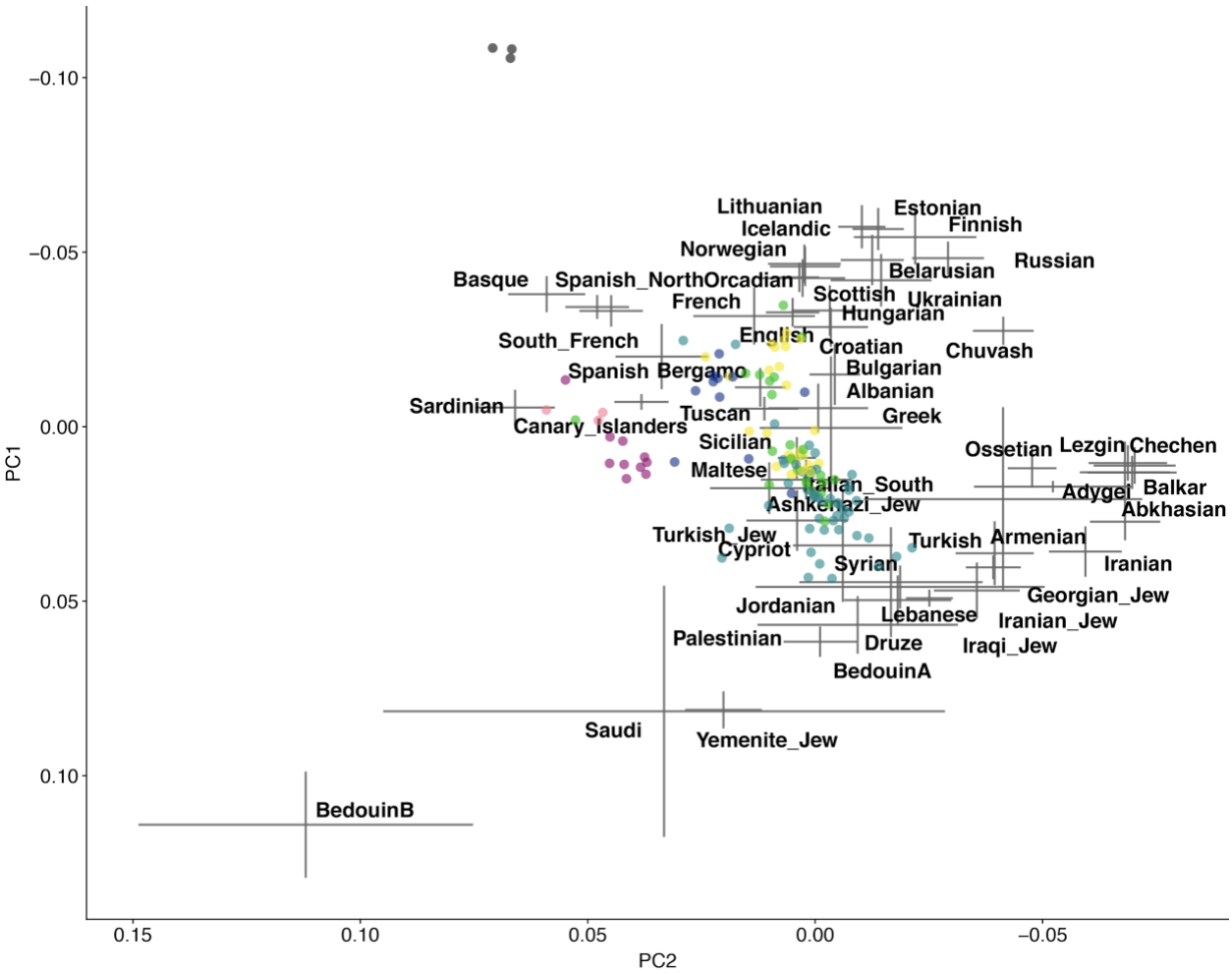

Fig. S14. Modern reference space for principal component analysis. Modern populations used to create the principal component (PC) space for projection of ancient samples are represented by 2 standard deviations of each PC for a given population. Study samples from central Italy are represented by the circular points for reference.

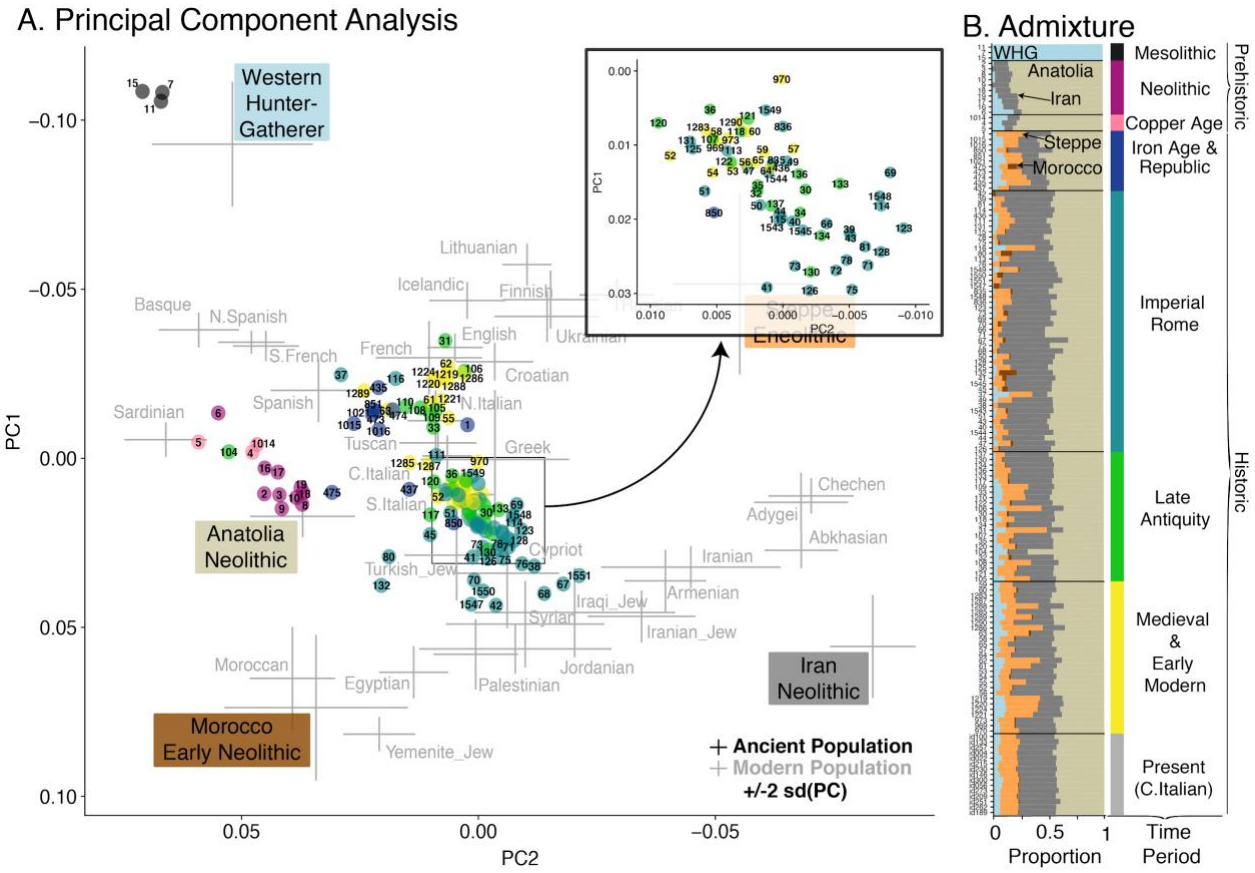

Fig. S15. PCA and ADMIXTURE analysis for ancient individuals in the time series. This figure is the same as Fig. 2 of the main paper except that all study samples are labeled. (**A**) Ancient Italian samples, some modern samples, and five previously reported ancient populations were projected onto a PC space determined by modern samples shown in Fig. S14. Color labels of ancient populations correspond to colors in the panel (**B**). Colors of study samples correspond to each time period shown in panel B. (**B**) Supervised ADMIXTURE analysis for ancient study samples.

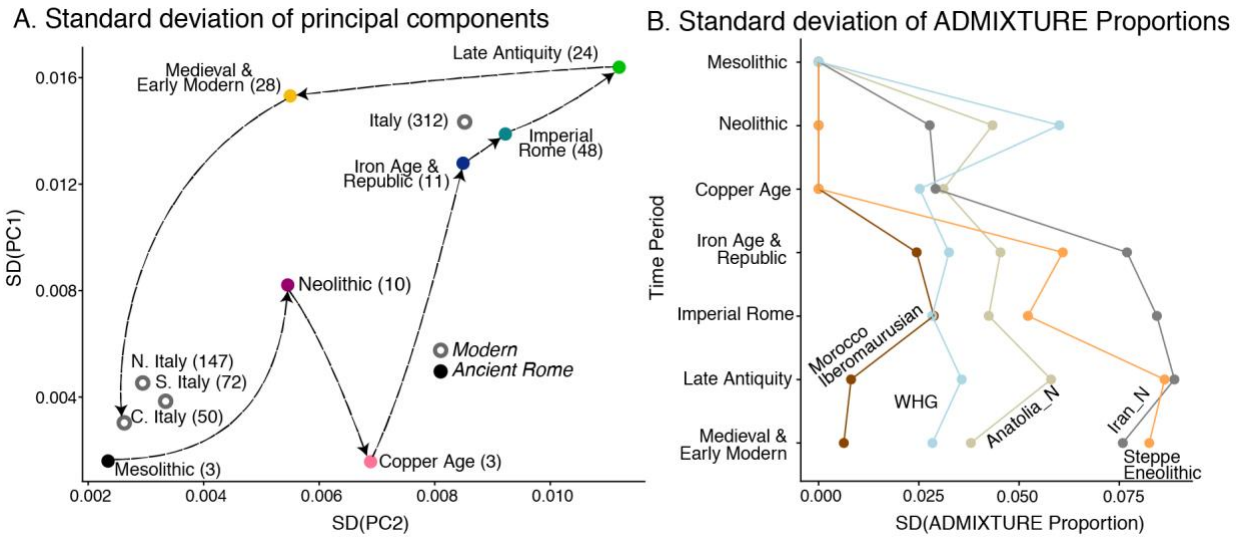

Fig. S16. Ancestry diversity within each time period measured by standard deviation across individuals in PCA. (**A**) Standard deviation of PC coordinates from the analysis shown in Figs. 2 and 4 is plotted for each time period group in the study population and for present-day Italian populations. Arrows depict temporal order for samples from mainland central Italy. (**B**) Standard deviation of ADMIXTURE proportions (x-axis) at each time period (y-axis) is shown for the source populations used in supervised ADMIXTURE in Fig. 2.

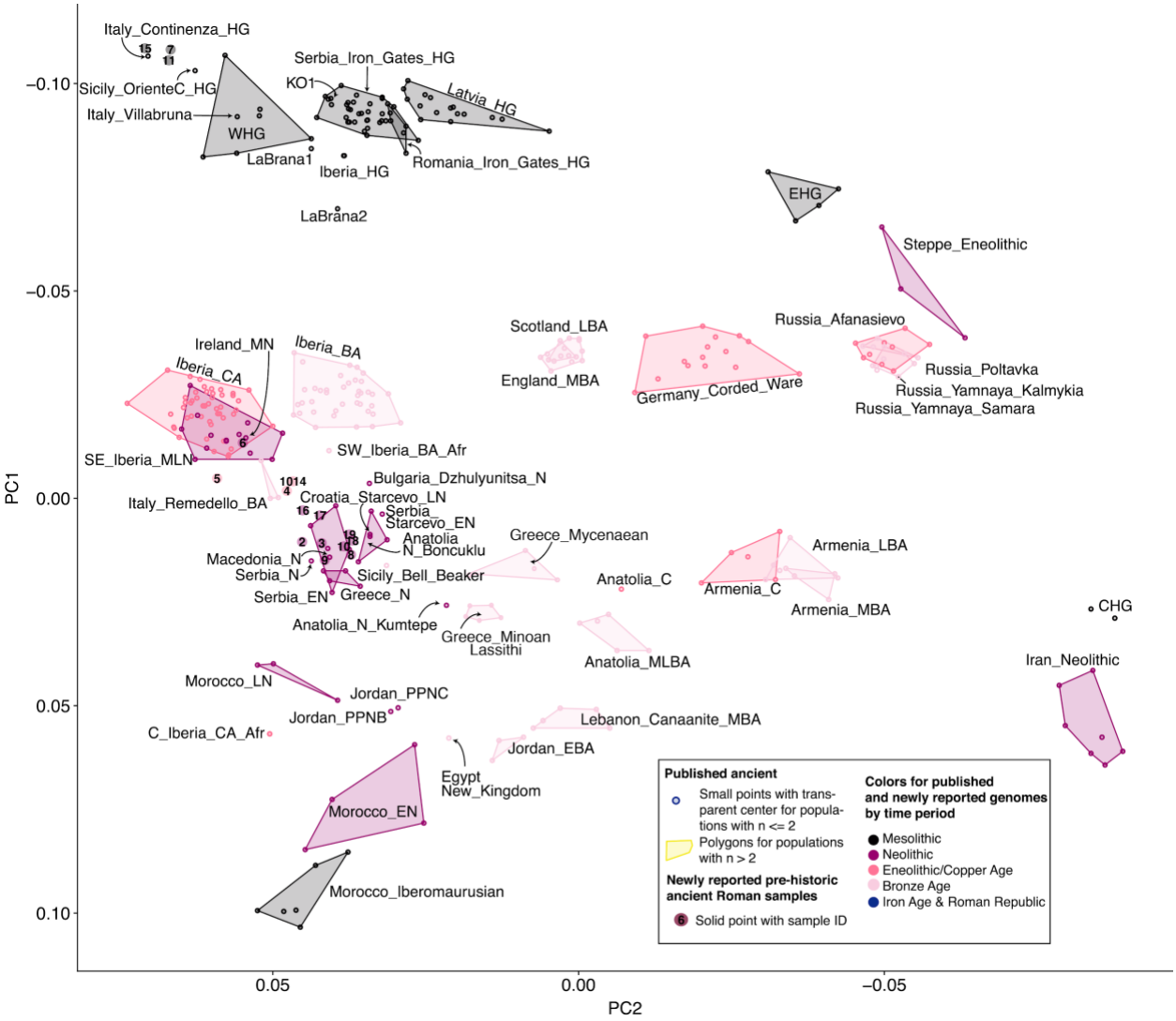

Fig. S17. PCA with ancient Individuals from central Italy and published prehistoric populations. Prehistoric ancient samples were projected onto a PC space created with select modern-day populations (Fig. S14). Polygons encompass all individuals from a given published ancient population. Published populations with n < 2 are denoted with small circular points. Study samples are shown by large, solid, labeled points. Colors represent the general time period to which the individuals and populations belong.

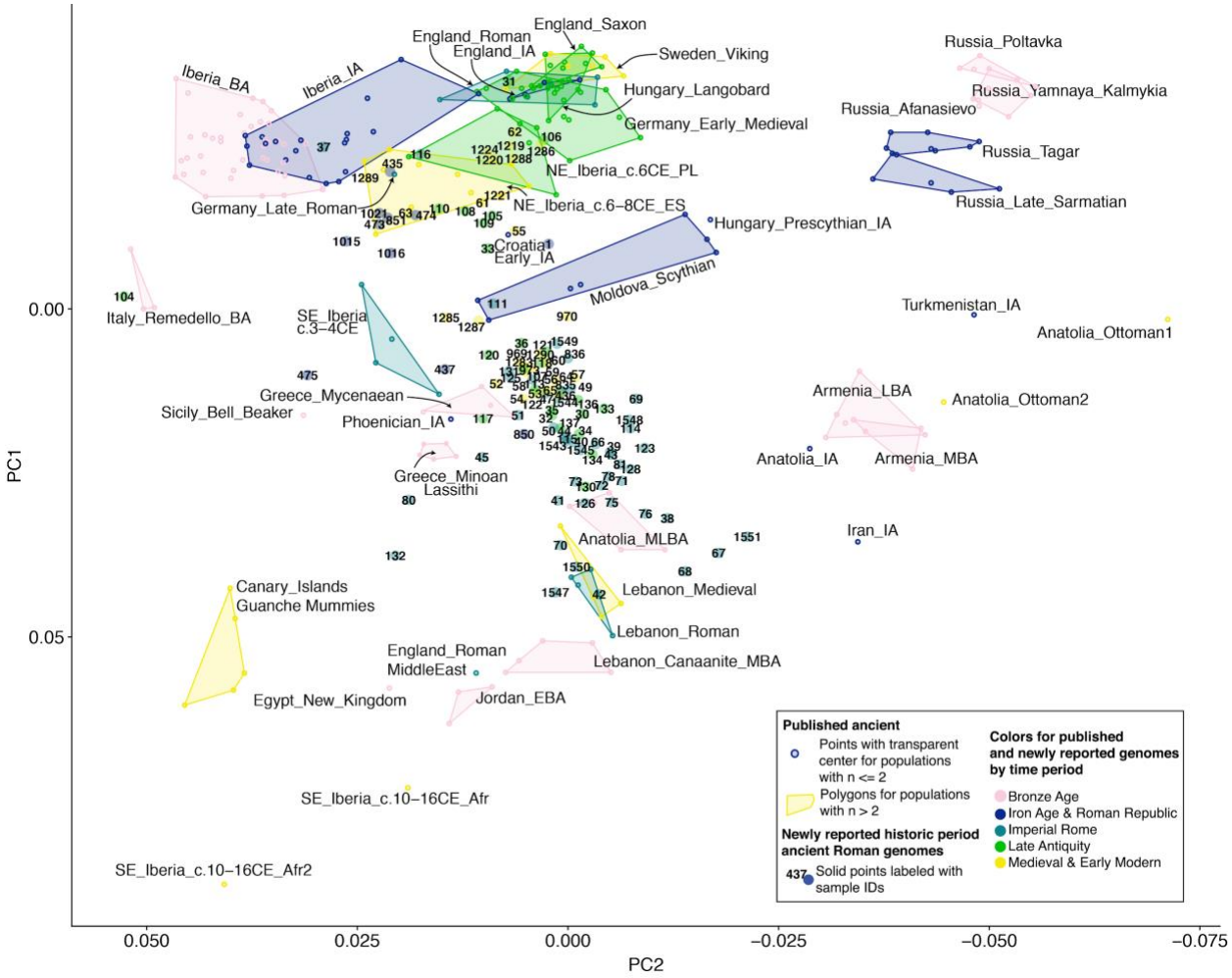

Fig. S18. PCA with ancient Individuals from central Italy and published historic populations labeled. Historic (Iron Age onward) samples from central Italy and published post-Neolithic ancient individuals were projected onto a PC space created with select modern-day populations (Fig. S14). Polygons encompass all individuals from a given published population. Study samples are shown by large, solid, labeled points. Colors represent the general time period to which the individuals and populations belong.

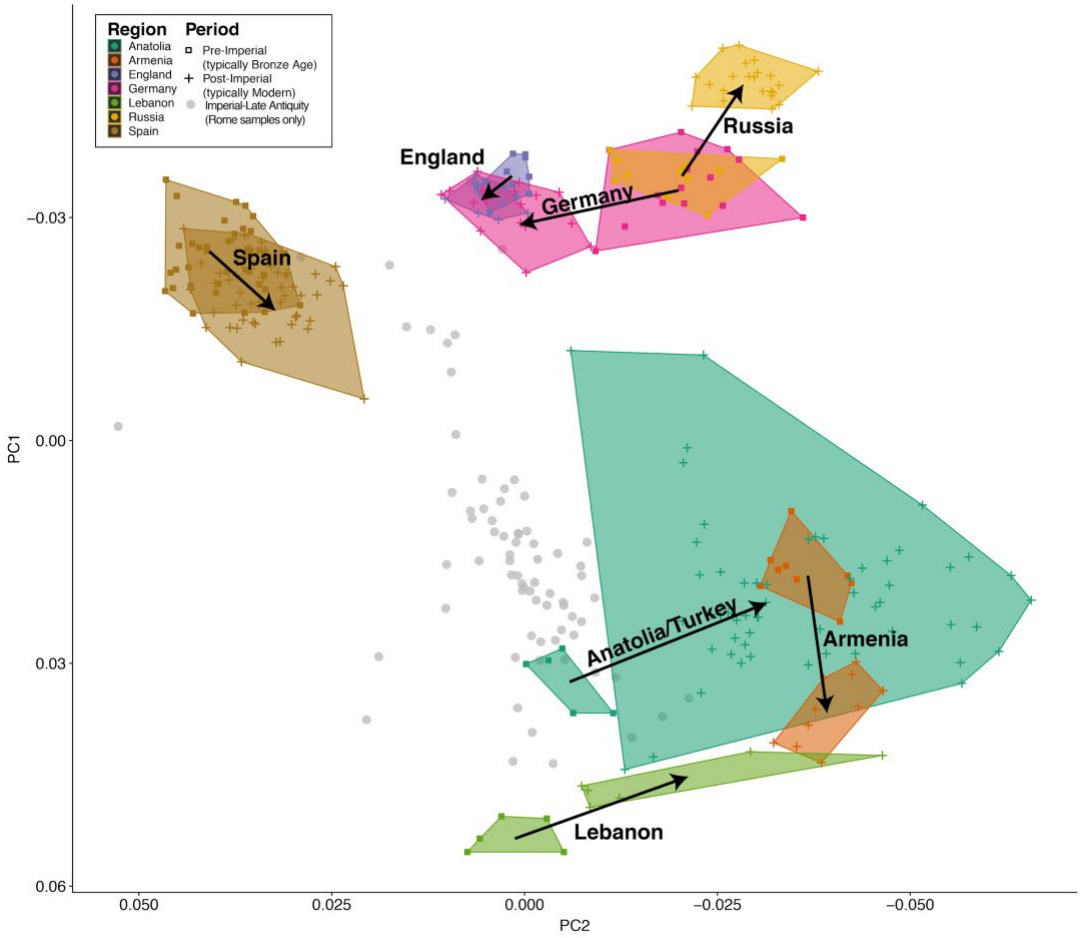

Fig. S19. PCA highlighting geographical regions for which samples from pre- and post-Imperial Rome are available. Where data was available, pre-Imperial (Bronze Age) and post-Imperial (Modern day, with the exception of Early Medieval for Germany) samples are shown for seven regions. Arrows are drawn from the approximate center of the pre-Imperial to the center of the post-Imperial population for a given region to highlight lack or presence of continuity in the PC space. Light gray points represent ancient Italian samples from Imperial to Late Antiquity for reference. All samples were projected onto the same PC space shown in Fig. S14.

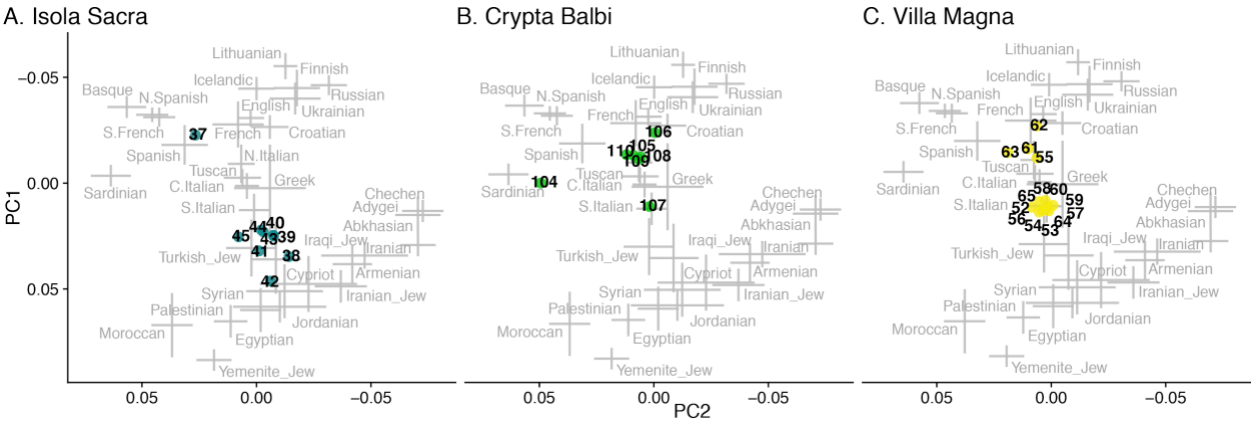

Fig. S20. Sites of interest in principal component analysis. Sites mentioned in the text, and individuals belonging to those sites, are shown in principal component analysis. Ancient individuals (points with sample IDs) are projected onto a principal component as in Fig. S14. Pseudo-haploid genotypes are used for ancient samples. Colors correspond to ancient Roman time periods used elsewhere in the study. (**A**) Isola Sacra was the necropolis of port town of Portus Romae, which was a key trading center for Rome in the Imperial Period. (**B**) The Late Antique burials from Crypta Balbi are contemporaneous with finds of a metal workshop producing belt buckles, seals and jewelry found in Lombard burials elsewhere in Italy (*195*). (**C**) The burials from Villa Magna in this study are from the Medieval period, when the site former Imperial villa housed a monastery and lay community.

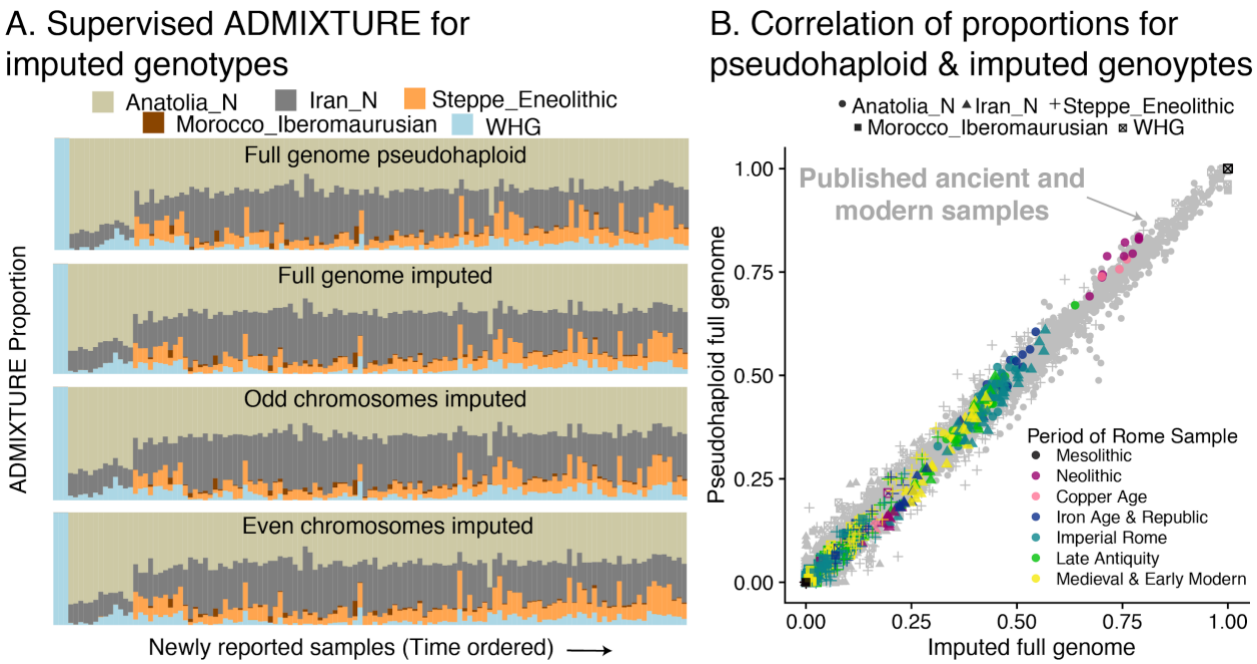

Fig. S21. Consistency of ADMIXTURE proportions for imputed and pseudohaploid genotypes. Supervised ADMIXTURE was run for 127 ancient Italian samples with either imputed diploid genotypes or pseudohaploid genotypes. All other samples (published ancient and modern) remained the same in both runs. (**A**) Admixture proportions are shown for Italian samples only for simplicity. (**B**) Corresponding ADMIXTURE proportions (for same sample and source population) across the two runs are shown with points for Italian samples colored by time period, and published samples in gray. Correlation was > 0.99 for the Italian samples across all proportions.

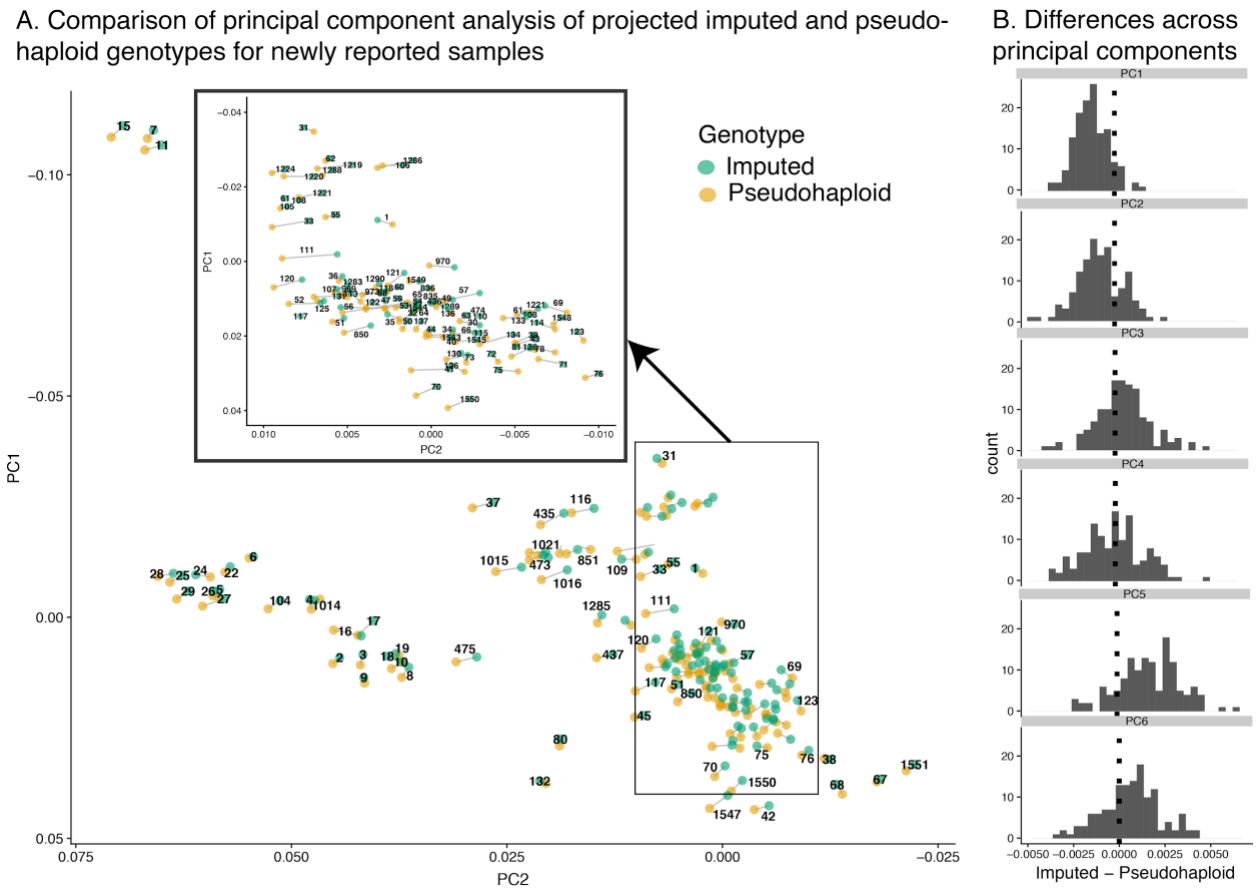

Fig. S22. Comparison of imputed and pseudohaploid genotypes by principal component analysis. **(A)** Imputed and pseudohaploid genotypes for 13 reported samples (127 ancient Romans and 7 ancient Sardinians) were projected onto the same principal coordinate space (Fig. S14). Line segments are drawn between a given sample's two data points (pseudohaploid and imputed genotypes). (**B**) Distributions of the differences between imputed and pseudohaploid coordinates for principal components 1-6 are shown.

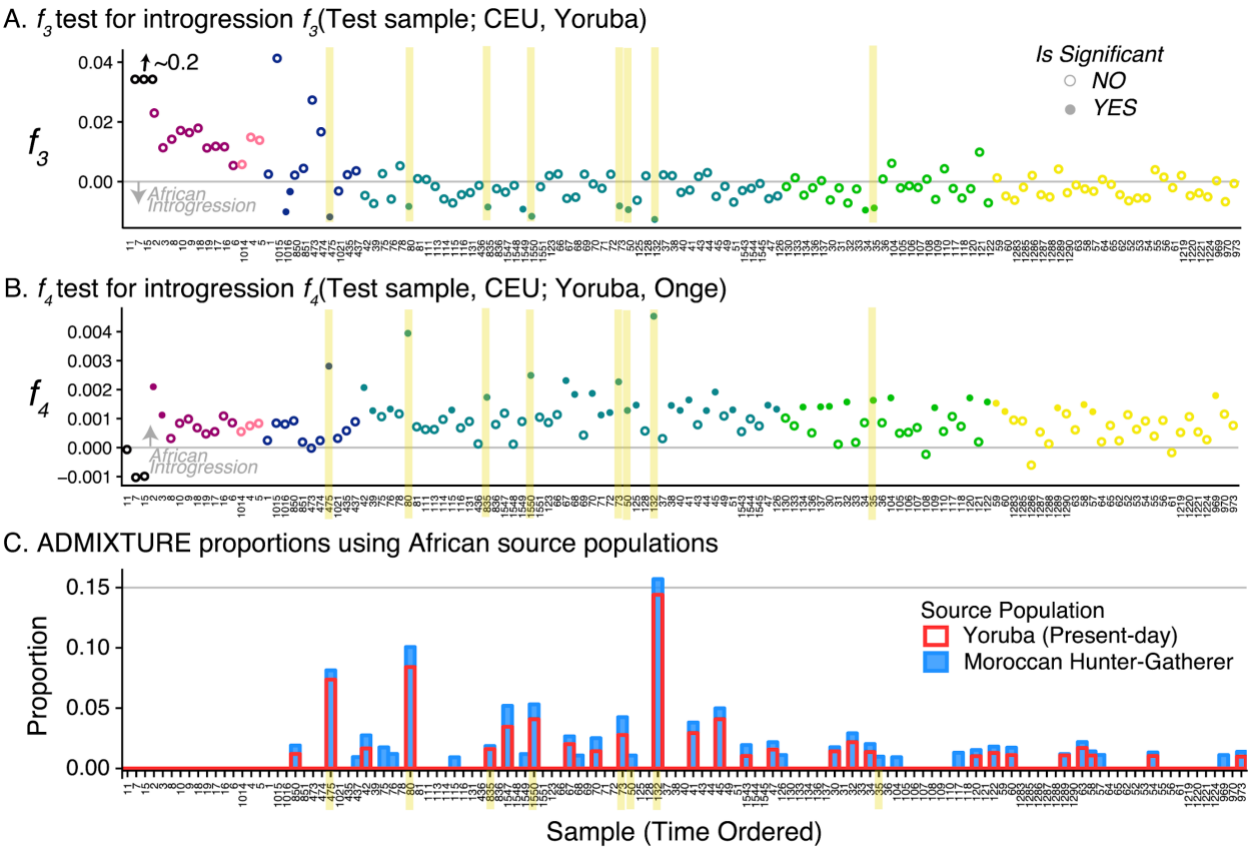

Fig. S23. Tests for African introgression in the ancient Roman population. Results from f_3(Test sample; CEU, Yoruba) and f_4(Test sample, CEU; Yoruba, Onge) tests and proportions from ADMIXTURE in panels (**A**), (**B**), and (**C**), respectively, are shown for each sample (time ordered on the x-axis). Individuals considered to confidently have African ancestry based on having a Z-score < -3 for the f_3 test and Z-score > 3 for the f_4 test are labeled with their sample ID and highlighted yellow across the three panels.

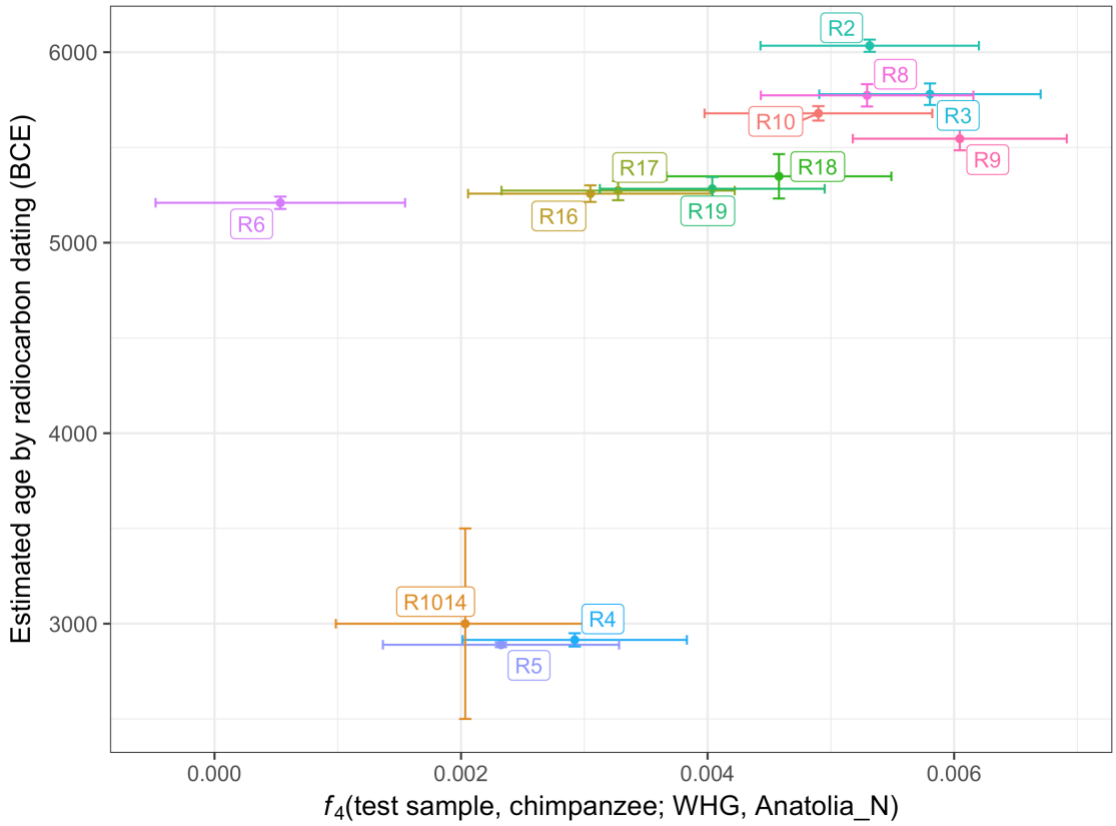

Fig. S24. Rebound of WHG ancestry in later Neolithic and Copper Ages illustrated by f_4(test sample, chimpanzee ; WHG, Anatolia_N). Horizontal bars represent two times standard deviation in the f_4-statistic evaluated by jackknife (roughly corresponding to 95% confidence interval); vertical bars denote the upper and lower bounds of the estimated age by radiocarbon dating. Compared to early Neolithic individuals (e.g., R2, R8, R3), later Neolithic individuals (e.g., R16, R17, R18, R19, R5) and Copper Age individuals (R4, R5, R1014) significantly shifted towards WHG and away from Anatolia farmers, suggesting an increase in WHG ancestry with time.

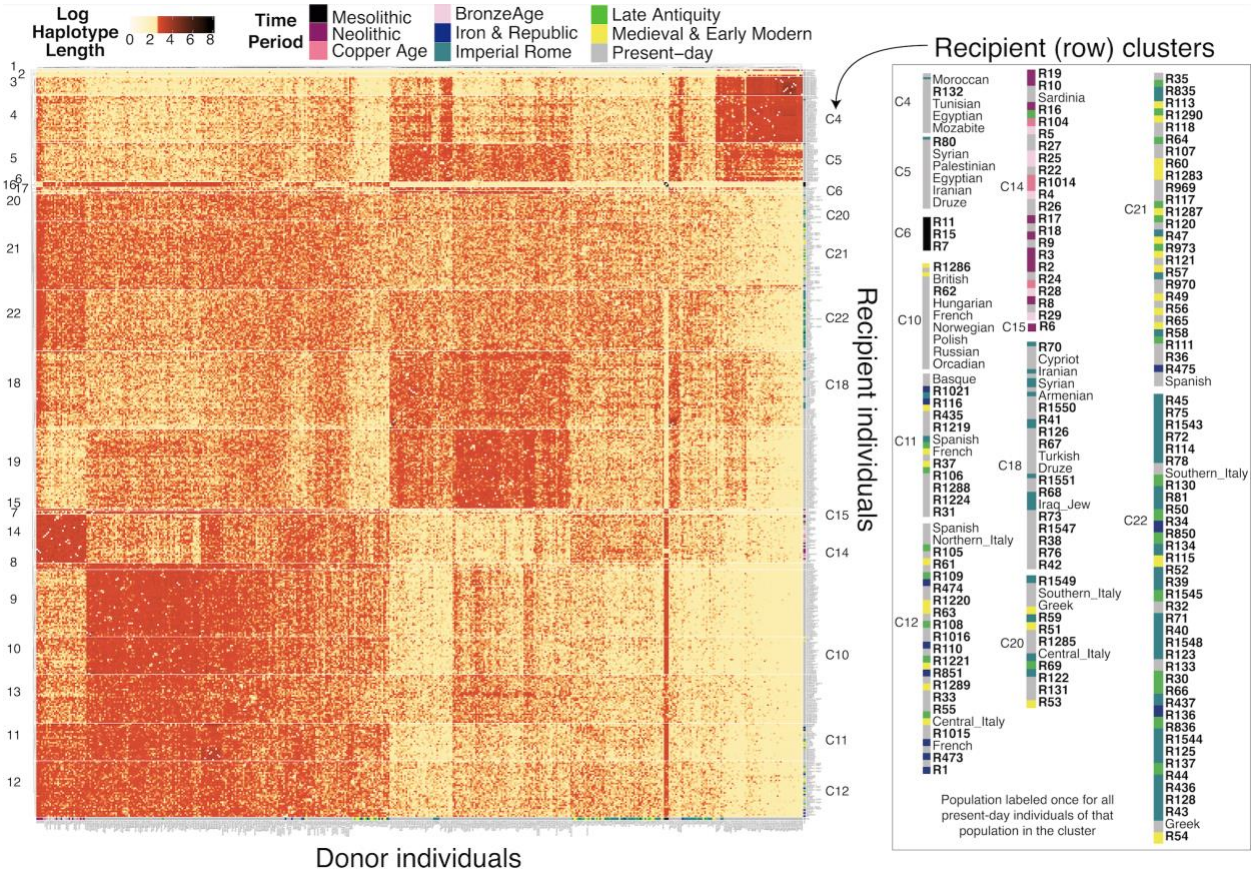

Fig. S25. Haplotype sharing between all modern individuals and ancient individuals from central Italy analyzed by ChromoPainter. Imputed and phased genotypes from eleven individuals for each of 32 present-day populations in Europe, the Mediterranean, the Levant, the Caucuses, and North Africa along with 134 ancient Italians (127 Roman/mainland Italy + 7 Sardinian) were analyzed for haplotype sharing. The resulting co-ancestry matrix displays all 475 donor individuals (columns, labeled on bottom) and 475 recipient individuals (rows, labeled on left side), along with an annotation bar for the time period of the individual. Each tile in the matrix represents the total length (cM) of haplotype segments "copied" from a donor individual to a recipient individual. K-means clustering was performed on the rows (recipients). For clarity, recipient clusters containing ancient individuals are enlarged on the right hand side.

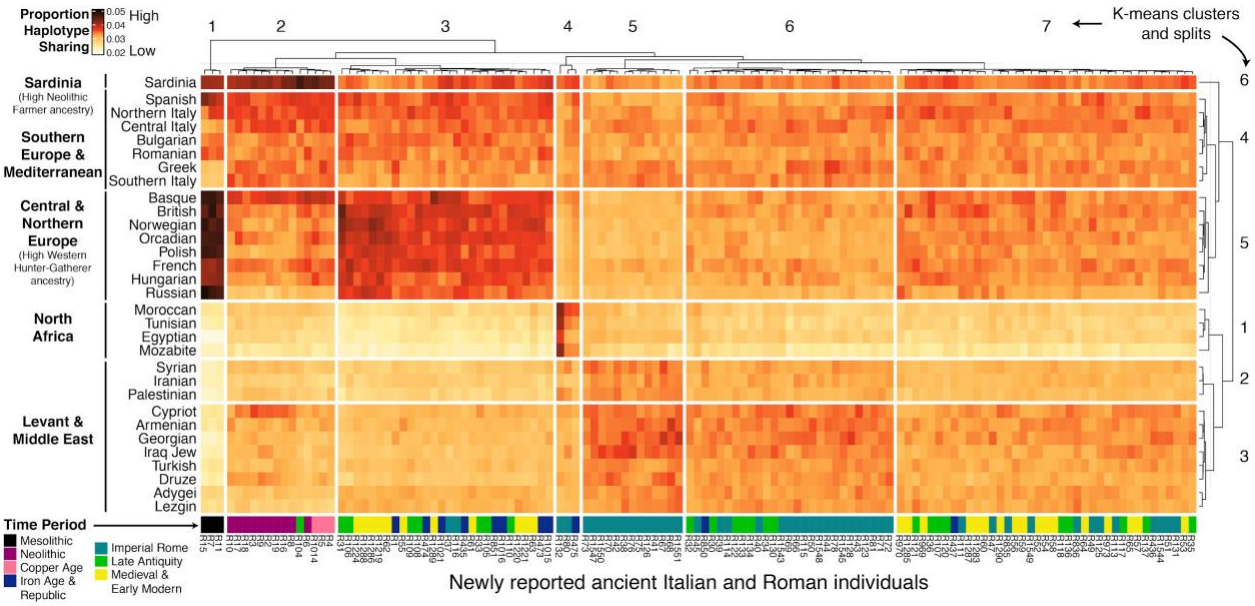

Fig. S26. Haplotype sharing between modern populations and ancient individuals from central Italy. Individual-level haplotype sharing represented in the co-ancestry matrix (Fig. S22) was summarized by summing the total length of copied haplotypes from individuals in a present-day population (rows, labeled on left side) to study ancient individuals (columns, labeled on bottom). Each tile in the matrix represents the total proportion of the ancient individual's haplotypes that are copied from that population. K-means was performed on the columns and rows of the resulting matrix. The time period of ancient individuals is shown by the annotation bar on the bottom. This figure is identical to Fig. 4A, except that it includes the sample labels and dendrogram.

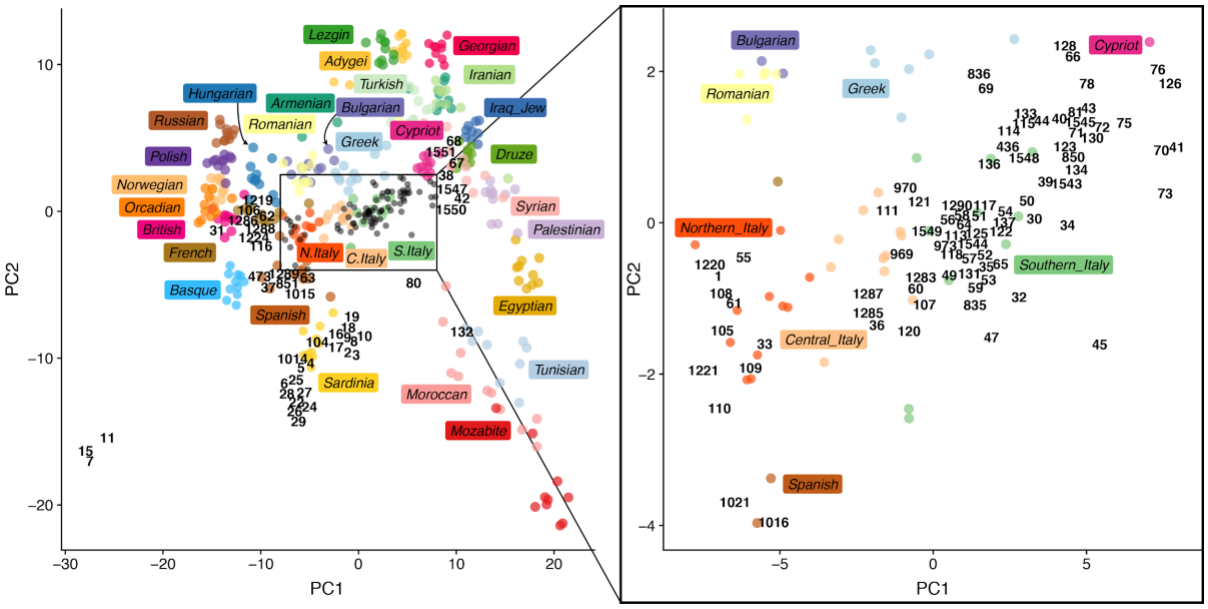

Fig. S27. Principal component analysis of haplotype sharing between modern populations and ancient individuals from central Italy. PCA was performed on the full co-ancestry matrix (total length of haplotypes copied from donor to recipient) shown in Fig. S25 with the exception of 8 outliers (2 Tunisian, 2 Iraqi Jew, 1 Mozabite, 1 Egyptian). The first two principal components are shown for all individuals on the left side and a zoomed in portion is shown on the right. Present-day individuals (colored points) and populations labels are shown in color. Study individuals are represented only by their numeric sample IDs or by small black points.

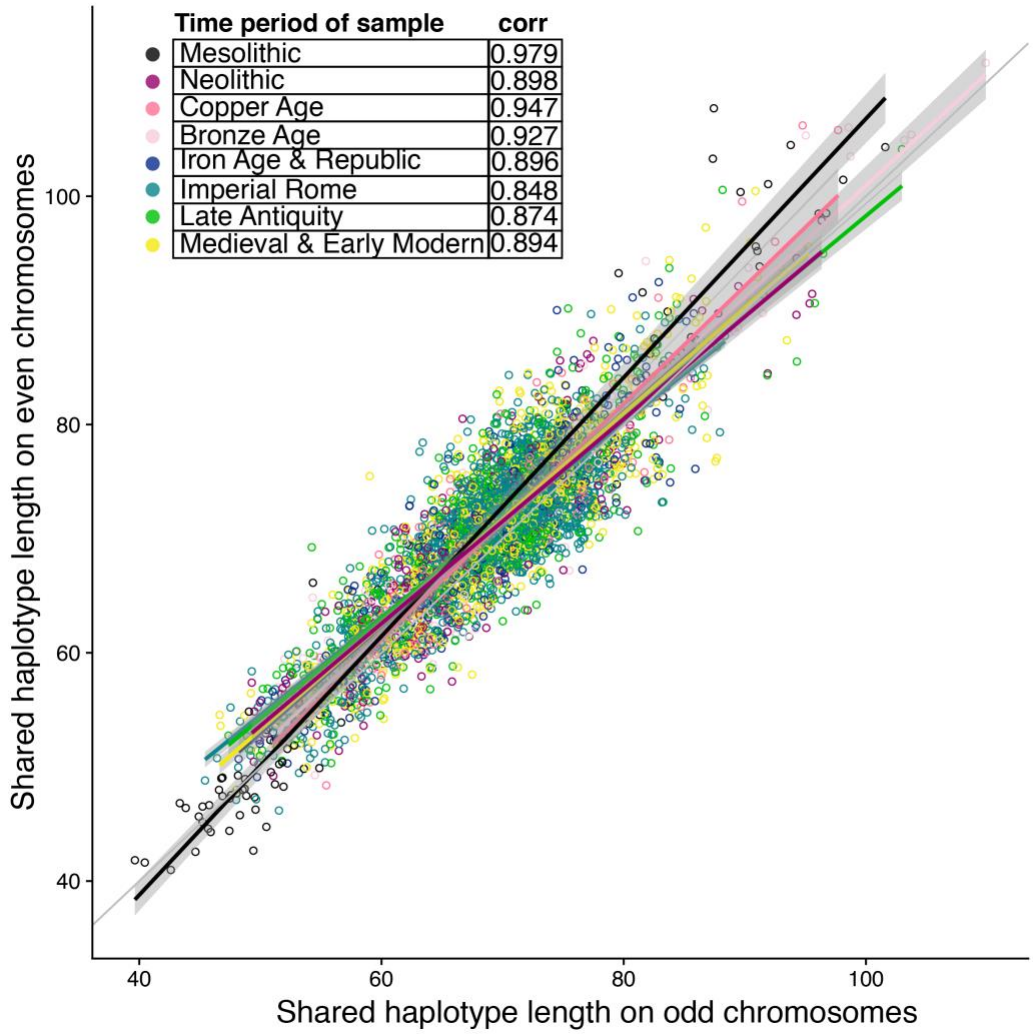

Fig. S28. Correlation of haplotype sharing for odd and even chromosomes. Total shared haplotype length between an ancient individual and a modern population across even and odd chromosomes . Each point represents shared haplotype length for one ancient individual and one modern population. Linear fits are shown for each time period. Points and lines are colored based on the ancient individual's time period. Correlations between odd and even chromosomes are shown in the table inset.

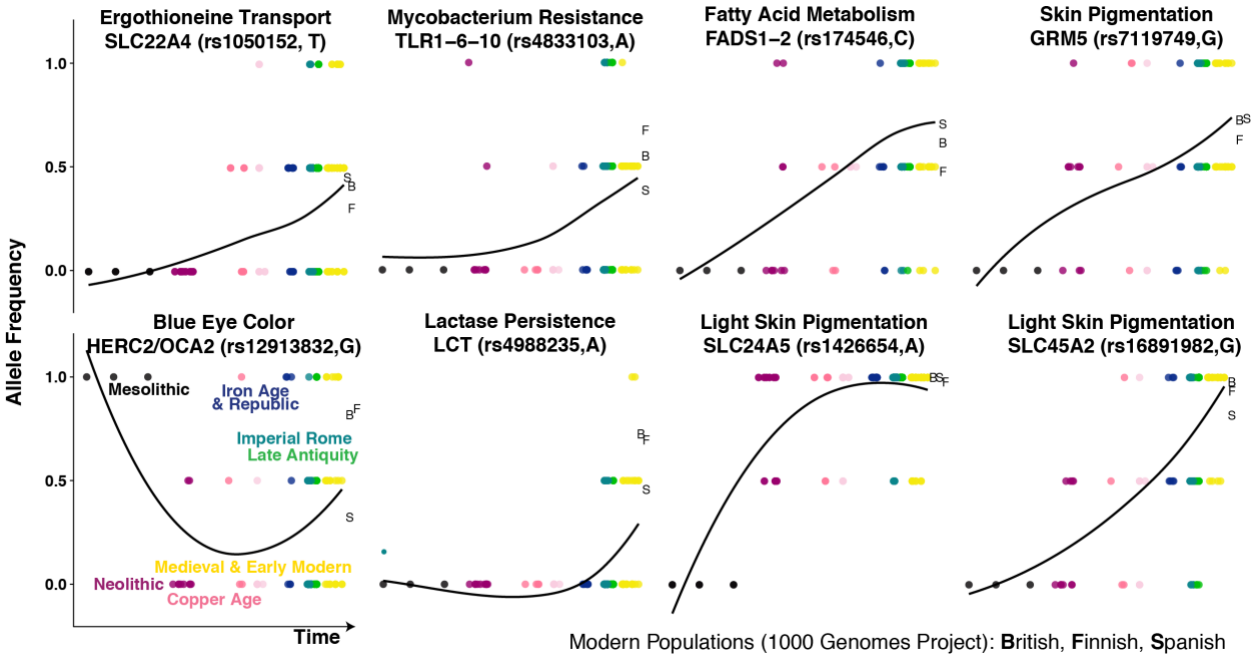

Fig. S29. Allele frequencies for alleles of functional importance. Imputed genotypes for alleles previously shown to be of functional importance (and under selection), denoted by putative function, associated gene, variant ID, and derived allele, are shown for study individuals from central Italy, ordered by time on the x-axis. For reference, the population allele frequency for three present-day populations in the 1000 Genomes Project (British/GBR, Finnish/FIN, Spanish/IBS) are designated by the first letter of the population name. Sample points for study individuals are colored by their time period. For each variant, a LOESS (locally weighted smoothing line) is plotted all points excluding the three modern populations.

Fig. S30. Silver bowl excavated from the Bernardini Tomb at Praeneste dating to the 8th/7th century BCE.

Supplementary Tables

Table S1. Archaeological site information (Excel file)

Table S2. Sample information (Excel files)

Table S3. Radiocarbon Dating and deltaC and deltaN Measurements (Excel files)

Table S4. Published samples used in this study (Excel files)

Table S5. Y-chromosome haplogroups of individuals in Mesolithic period to Iron Age

Period	Sample ID	Site	Date	Y-chr Haplogroup	Characteristic derived allele(s) carried	Other ancient individuals belonging to the haplogroup (earlier or around the same time)
ME	R11	Grotta Continenza	10100 - 9816 calBCE	I-M436 (I2a2)	L503, P217	Falkenstein (Germany 7460-7040 calBCE) I5401 (Serbia 7076-6699 calBCE calBCE) I4596 (Latvia 6061-5990 calBCE)
ME	R7	Grotta Continenza	8821 - 8642 calBCE	I-M223 (I2a2a)	L503, M436, M223	Falkenstein (Germany 7460-7040 calBCE) I4881 (Serbia 6570-6255 calBCE calBCE) I4596 (Latvia 6061-5990 calBCE)
ME	R15	Grotta Continenza	7284 - 7065 calBCE	I-M223 (I2a2a)	M438, L460, P217, P223	Falkenstein (Germany 7460-7040 calBCE) I4881 (Serbia 6570-6255 calBCE calBCE) I4596 (Latvia 6061-5990 calBCE)
NE	R9	Grotta Continenza	5607 - 5485 calBCE	G-L91 (G2a2a1a2)	P15, PF3177, L91, Z6177	I1583 (Turkey 6426-6236 calBCE) I0698 (Bulgaria 6000-5900 BCE) Klei10 (Greece 4230-3995 calBCE) Otzi (Italy 3484-3104 calBCE)
NE	R19	Ripabianca di Monterado	5345 - 5221 calBCE	J-L26 (J2a1)	L134, L228, M410, L27	KK1 (Georgia 7940-7600 calBCE) I0708 (Turkey 6221-6073 calBCE) I5078 (Croatia 4692-4546 calBCE) I5207 (Austria 5500-4500 BCE)
NE	R17	Ripabianca di Monterado	5324 - 5223 calBCE	J-M304 (J)	M304, PF4622	N.A.
NE	R6	Grotta Continenza	5242 - 5177 calBCE	R-M343 (R1b)	M306, M343	Villabruna (Italy 12230-11830 calBCE) I5235 (Serbia 9221-8548 calBCE) I5411 (Romania 7000-6300 BCE) I4630 (Latvia 7465-7078 calBCE) I5890 (Ukraine 5286-5062 calBCE) I0410 (Spain 5294-5066 calBCE)
CA	R1014	Monte San Biagio	3500 - 2500 BCE	H-L901 (H)	M2936	I0867 (Israel 7300-6200 BCE) I0745 (Turkey 6374-6227 calBCE) I2520 (Bulgaria 3336-3028 calBCE)
CA	R4	Grotta Continenza	2950 - 2880 calBCE	G-F1193 (G2a2b2b1)	CTS9605, CTS2488, PF3359	Bon004 (Turkey 8300-7952 BCE) I2532 (Romania 5715-5626 calBCE) I0676 (Macedonia 5979-5735 calBCE) I2521 (Bulgaria 5619-5491 calBCE) I1314 (Spain 3363-1903 calBCE)
IA	R1016	Castel di Decima	900-700 BCE	R-M269 (R1b1a2)	P238, M343, M269, CTS8591	I0429 (Russia 3339-2918 calBCE) TV32032 (Portugal 1750-1510 calBCE)
IA	R850	Ardea	800-500 BCE	T-L208 (T1a1a)	M70, L299, L905	I0700 (Bulgaria 5800-5400 calBCE) I0797 (Germany 5500-4850 BCE)
IA	R851	Ardea	800-500 BCE	R-P311 (R1b1a2a1a)	P238, L278, M269, CTS8591, P310	I0443 (Russia 3300-2700 BCE) RISE563 (Germany 2572-2512 calBCE)

						RISE566 (Czech 2279-2033 calBCE) RISE98 (Sweden 2275-2032 calBCE) TV3831 (Portugal 1750-1510 calBCE)
IA	R1021	Boville Ernica	700-600 BCE	R-PF7589 (R1b1a2a1b)	M207, P238, PF6505, PF6509, CTS5981	I0439 (Russia 3321-2921 calBCE) I0805 (Germany 2467-2142 calBCE) RISE47 (Denmark 1499-1324 calBCE)
IA	R474	Civitavecchia	700-600 BCE	J-M12 (J2b)	M172, M12, M314	I4331 (Croatia 1631-1521 calBCE)
IA	R435	Palestrina Colombella	600-200 BCE	R-P312 (R1b1a2a1a2)	M173, P238, L278, M269, CTS8591, P311, P312	I0443 (Russia 3300-2700 BCE) RISE563 (Germany 2572-2512 calBCE) RISE566 (Czech 2279-2033 calBCE) RISE98 (Sweden 2275-2032 calBCE) TV3831 (Portugal 1750-1510 calBCE)
IA	R437	Palestrina Selciata	400-200 BCE	R-P312 (R1b1a2a1a2)	M207, P238, M173, M269, CTS8591, P311, P312	I0443 (Russia 3300-2700 BCE) RISE563 (Germany 2572-2512 calBCE) RISE566 (Czech 2279-2033 calBCE) RISE98 (Sweden 2275-2032 calBCE) TV3831 (Portugal 1750-1510 calBCE)

Table S6. Summary of ROH segments of 5Mb or longer in ancient Italian individuals

Sample ID	Total length of ROH (Mb)	Length of the longest ROH (Mb)	Number of ROH ≥5Mb
R7	256.6	24.8	26
R1015	157.0	15.4	21
R473	85.2	32.4	7
R474	47.8	8.8	6
R15	44.2	7.6	7
R11	32.2	7.8	5
R1286	12.0	12.0	1
R973	11.0	5.6	2
R2	10.0	10.0	1
R80	9.6	9.6	1
R3	8.2	8.2	1
R121	7.4	7.4	1
R1	7.0	7.0	1
R435	6.8	6.8	1
R18	6.0	6.0	1
R56	5.8	5.8	1
R65	5.6	5.6	1
R110	5.4	5.4	1
R10	5.0	5.0	1

Table S7. Working 2-way admixture models for Neolithic individuals from central Italy (RMPR_NE)

Target	Source 1	Source 2	dof	Chisq	p-value	Prop.1 (SE)	Prop.2 (SE)	Nested p-value for RMPR_ME component
RMPR_NE (10, 402871)	RMPR_ME (3, 402697)	Greece_N (3, 398289)	15	11.784	0.695	0.043 (0.007)	0.957 (0.007)	4.84E-10
RMPR_NE (10, 402871)	RMPR_ME (3, 402697)	Croatia_Starcevo_LN (1, 294565)	15	14.706	0.473	0.028 (0.011)	0.972 (0.011)	0.0147
RMPR_NE (10, 402871)	RMPR_ME (3, 402697)	Anatolia_N_Bonc uklu.SG (4, 383699)	15	16.202	0.369	0.030 (0.010)	0.970 (0.010)	0.00252
RMPR_NE (10, 402871)	RMPR_ME (3, 402697)	Macedonia_N (1, 343544)	15	17.727	0.277	0.073 (0.009)	0.927 (0.009)	5.28E-14
RMPR_NE (10, 402871)	RMPR_ME (3, 402697)	Serbia_EN (5, 382370)	15	23.358	0.077	0.035 (0.007)	0.965 (0.007)	3.23E-06
RMPR_NE (10, 402871)	RMPR_ME (3, 402697)	Serbia_N (1, 74328)	15	24.141	0.063	0.032 (0.007)	0.968 (0.007)	1.28E-05

Table S8. Working 1-way models for Copper Age individuals from central Italy (RMPR_CA)

Target	Source 1	dof	Chisq	p-value
RMPR_CA (3, 402376)	Bulgaria_Dzhulyunitsa_N (1, 94162)	16	26.613	0.046
RMPR_CA (3, 402376)	RMPR_CA_Sar (7, 399185)	16	26.889	0.043

Table S9. Significant admixture signals for Copper Age individuals from central Italy based on tests in the form of f_3(RMPR_CA; RMPR_NE, test population). A significant negative f_3 statistic indicates admixture signal with the test population.

Test population	f_3	**SE**	**z-score**	**Number of sites used**	**p-value after Bonferroni correction**
RMPR_ME	-0.006492	0.001532	-4.238	254634	0.00262

Table S10. Significant results in f_4 tests in the form of f_4(RMPR_CA, RMPR_NE; test population, Onge). A significant positive f_4 statistic indicates that Copper Age central Italians share more alleles with the test population than Neolithic Age individuals do.

Test population	f_4	SE	z-score	BABA	ABBA	Number of sites used	p-value after Bonferroni correction
RMPR_ME	0.002251	0.000369	6.108	21953	21048	402201	1.170e-07
WHG	0.001851	0.000370	5.002	21706	20963	400947	6.582e-05
LaBrana1	0.001936	0.000401	4.826	18847	18170	349584	0.000162
Serbia_Iron_Gates_HG	0.001291	0.000283	4.564	21726	21208	401096	0.000582
Italy_Villabruna	0.001878	0.000420	4.467	18579	17939	340751	0.000920
Latvia_HG	0.001246	0.000298	4.183	20813	20333	385356	0.00334
NW_Iberia_Meso	0.001610	0.000395	4.078	19139	18568	354891	0.00527
Romania_Iron_Gates_HG	0.001286	0.000318	4.051	21625	21109	400783	0.00592
KO1	0.001748	0.000433	4.038	15662	15160	287073	0.00625

Table S11. Working 2-way admixture models for Copper individuals from central Italy (RMPR_CA) under model competition with N_Iberia_MLN added to the "right" set.

Target	Source 1	Source 2	dof	Chisq	p-value	Prop.1 (SE)	Prop.2 (SE)
RMPR_CA (3, 402376)	RMPR_NE (10, 402871)	NE_Iberia_CA (1, 242452)	16	13.884	0.607	0.618 (0.048)	0.382 (0.048)
RMPR_CA (3, 402376)	RMPR_NE (10, 402871)	Iberia_C (40, 404079)	16	16.982	0.387	0.625 (0.040)	0.375 (0.040)
RMPR_CA (3, 402376)	RMPR_NE (10, 402871)	N_Iberia_CA (7, 368546)	16	18.068	0.320	0.672 (0.036)	0.328 (0.036)
RMPR_CA (3, 402376)	RMPR_NE (10, 402871)	RMPR_CA_Sar (7, 399185)	16	18.727	0.283	0.267 (0.094)	0.733 (0.094)
RMPR_CA (3, 402376)	RMPR_NE (10, 402871)	Ireland_MN.SG (1, 404027)	16	22.529	0.127	0.476 (0.091)	0.524 (0.091)
RMPR_CA (3, 402376)	RMPR_NE (10, 402871)	SE_Iberia_MLN (1, 358265)	16	23.441	0.102	0.539 (0.054)	0.461 (0.054)

Table S12. Working 1-way models for Iron Age individuals from central Italy (RMPR_IA)

Target	Source 1	dof	Chisq	p-value
RMPR_IA (11, 402869)	Croatia_Early_IA (1, 292206)	16	20.427	0.202

Table S13. Significant admixture signals for Iron Age individuals from central Italy based on tests in the form of f_3(RMPR_IA; RMPR_CA, test population). A significant negative f_3 statistic indicates admixture signal with the test population.

Test population	f_3	SE	z-score	Number of sites used	p-value after Bonferroni correction
Russia_Yamnaya_Samara	-0.009213	0.000714	-12.897	294241	5.80E-36
Russia_Okunevo_BA.SG	-0.009637	0.000771	-12.500	304967	9.26E-34
Russia_Yamnaya_Kalmykia.SG	-0.009471	0.000831	-11.399	281374	5.24E-28
Steppe_Eneolithic	-0.010791	0.001151	-9.375	196980	8.58E-19
Russia_IA.SG	-0.006878	0.000940	-7.320	285973	3.07E-11
Germany_Corded_Ware	-0.005242	0.000740	-7.087	289918	1.70E-10
Estonia_Corded_Ware.SG	-0.005145	0.000817	-6.297	281969	3.76E-08
Greenland_Saqqaq.SG	-0.008079	0.001289	-6.266	270816	4.59E-08
Moldova_Cimmerian.SG	-0.006507	0.001134	-5.740	185291	1.17E-06
England_Bell_Beaker	-0.003214	0.000565	-5.687	309761	1.60E-06
Czech_Corded_Ware	-0.006159	0.001086	-5.669	219778	1.78E-06
Poland_EBA	-0.004547	0.000836	-5.441	283880	6.57E-06
Turkmenistan_IA.SG	-0.006711	0.001267	-5.298	232626	1.45E-05
Netherlands_Bell_Beaker	-0.003600	0.000724	-4.971	265969	8.26E-05
Ukraine_Scythian.SG	-0.004792	0.001016	-4.715	266281	3.00E-04
Lithuania_BA	-0.005543	0.001203	-4.608	155271	5.04E-04
Latvia_BA	-0.003209	0.000722	-4.447	288506	0.0011
Scotland_CA_EBA	-0.003295	0.000771	-4.275	259220	0.0024
Armenia_LBA	-0.004836	0.001186	-4.077	138438	0.0057
Armenia_LchashenMetsamor.SG	-0.004425	0.001139	-3.884	208824	0.0127
Ireland_BA.SG	-0.003207	0.000857	-3.744	286883	0.0225
Armenia_C	-0.002895	0.000797	-3.635	268736	0.0345
Bulgaria_MLBA	-0.004573	0.001261	-3.628	204533	0.0354

Table S14. Significant results in f_4 tests in the form of f_4(RMPR_IA, RMPR_CA; test population, Onge). A significant positive f_4 statistic in this test indicates that Iron Age central Italians share more alleles with the test population than Copper Age individuals do.

Test population	f_4	**SE**	**z-score**	**BABA**	**ABBA**	**Number of sites used**	**p-value after Bonferroni correction**
Russia_Okunevo_BA.SG	0.001098	0.000235	4.679	21048	20607	402263	0.000357
Steppe_Eneolithic	0.001641	0.000359	4.577	15342	14881	280992	0.000585
Russia_Yamnaya_Samara	0.000987	0.00026	3.794	21751	21357	399270	0.0184
Russia_Yamnaya_Kalmykia.SG	0.001035	0.000286	3.616	21299	20894	391193	0.0371

Table S15. Working 2-way models for Iron Age individuals from central Italy (RMPR_IA)

Target	Source 1	Source 2	dof	Chisq	p-value	Prop.1 (SE)	Prop.2 (SE)
RMPR_IA (11, 402869)	RMPR_CA (3, 402376)	Turkmenistan_IA.SG (1, 337292)	15	17.451	0.292	0.575 (0.019)	0.425 (0.019)
RMPR_IA (11, 402869)	RMPR_CA (3, 402376)	Russia_Afanasievo.SG (2, 205779)	15	18.143	0.255	0.649 (0.014)	0.351 (0.014)
RMPR_IA (11, 402869)	RMPR_CA (3, 402376)	Moldova_Scythian.SG (7, 382478)	15	19.06	0.211	0.289 (0.027)	0.711 (0.027)
RMPR_IA (11, 402869)	RMPR_CA (3, 402376)	Russia_Yamnaya_Kalmykia.SG (6, 392837)	15	19.672	0.184	0.700 (0.011)	0.300 (0.011)
RMPR_IA (11, 402869)	RMPR_CA (3, 402376)	Russia_Late_Sarmatian.SG (5, 388147)	15	20.623	0.149	0.621 (0.014)	0.379 (0.014)
RMPR_IA (11, 402869)	RMPR_CA (3, 402376)	Hungary_Prescythian_IA.SG (1, 273636)	15	21.814	0.112	0.472 (0.025)	0.528 (0.025)
RMPR_IA (11, 402869)	RMPR_CA (3, 402376)	Russia_Poltavka (4, 396233)	15	22.013	0.107	0.698 (0.012)	0.302 (0.012)
RMPR_IA (11, 402869)	RMPR_CA (3, 402376)	Russia_Yamnaya_Samara (9, 400976)	14	21.285	0.0945	0.693 (0.013)	0.307 (0.013)

Table S16. *qpAdm* modeling of each Iron Age individual as mixture of preceding Copper Age ancestry (RMPR_CA) and Steppe-related ancestry (Russia_Yamnaya_Samara)

Target	Source 1	Source 2	dof	Chisq	p-value	Prop.1 (SE)	Prop.2 (SE)
R1015	RMPR_CA (3, 402376)	Russia_Yamnaya_Samara (9, 400976)	14	8.436	0.865	0.729 (0.030)	0.271 (0.030)
R851	RMPR_CA (3, 402376)	Russia_Yamnaya_Samara (9, 400976)	14	13.684	0.474	0.757 (0.029)	0.243 (0.029)
R474	RMPR_CA (3, 402376)	Russia_Yamnaya_Samara (9, 400976)	14	14.176	0.437	0.664 (0.029)	0.336 (0.029)
R1	RMPR_CA (3, 402376)	Russia_Yamnaya_Samara (9, 400976)	14	17.325	0.239	0.650 (0.027)	0.350 (0.027)
R473	RMPR_CA (3, 402376)	Russia_Yamnaya_Samara (9, 400976)	14	18.807	0.172	0.712 (0.037)	0.288 (0.037)
R1016	RMPR_CA (3, 402376)	Russia_Yamnaya_Samara (9, 400976)	14	20.848	0.106	0.749 (0.033)	0.251 (0.033)
R1021	RMPR_CA (3, 402376)	Russia_Yamnaya_Samara (9, 400976)	14	20.983	0.102	0.715 (0.031)	0.285 (0.031)
R435	RMPR_CA (3, 402376)	Russia_Yamnaya_Samara (9, 400976)	14	21.062	0.100	0.624 (0.030)	0.376 (0.030)
R437	RMPR_CA (3, 402376)	Russia_Yamnaya_Samara (9, 400976)	14	38.376	4.55E-04	0.725 (0.028)	0.275 (0.028)
R850	RMPR_CA (3, 402376)	Russia_Yamnaya_Samara (9, 400976)	14	60.787	8.53E-08	0.704 (0.028)	0.296 (0.028)
R475	RMPR_CA (3, 402376)	Russia_Yamnaya_Samara (9, 400976)	14	107.992	1.37E-16	0.754 (0.027)	0.246 (0.027)

Table S17. Working 1-way and 2-way models for Iron Age individual R437

Target	Source 1	Source 2	dof	Chisq	p-value	Prop.1 (SE)	Prop.2 (SE)
R437 (1, 326478)	Croatia_Early_IA (1, 292206)	--	16	21.301	0.167	--	--
R437 (1, 326478)	RMPR_CA (3, 402376)	Armenia_LBA (5, 199919)	15	15.225	0.435	0.467	0.533
R437 (1, 326478)	RMPR_CA (3, 402376)	Anatolia_IA.SG (2, 196601)	15	22.29	0.100	0.396	0.604

Table S18. Working 1-way and 2-way models for Iron Age individual R850

Target	Source 1	Source 2	dof	Chisq	p-value	Prop.1 (SE)	Prop.2 (SE)
R850 (1, 228460)	Anatolia_C (1, 208021)	--	16	25.541	0.0608	--	--
R850 (1, 228460)	RMPR_CA (3, 402376)	Armenia_LBA (5, 199919)	15	16.524	0.348	0.373	0.627
R850 (1, 228460)	RMPR_CA (3, 402376)	Anatolia_IA.SG (2, 196601)	15	22.234	0.102	0.237	0.763

Table S19. Working models for Iron Age individual R475

Target	Source 1	Source 2	Source 3	dof	Chisq	p-value	Prop.1 (SE)	Prop.2 (SE)	Prop.3 (SE)
R475 (1, 304539)	RMPR_CA (3, 402376)	Russia_Yamnaya_Samara (9, 400976)	Morocco_LN (3, 96211)	13	23.112	0.0404	0.309 (0.048)	0.161 (0.023)	0.531 (0.053)
R475 (1, 304539)	RMPR_CA (3, 402376)	Russia_Yamnaya_Samara (9, 400976)	Mota (1, 403973)	12	21.974	0.0378	0.699 (0.026)	0.109 (0.031)	0.192 (0.023)

Table S20. Significant results in f_4 tests in the form of f_4(RMPR_IR, RMPR_IA; test population, Onge). A significant positive f_4 statistic in this test indicates that Imperial individual from central Italy share more alleles with the test population than Iron Age individuals do.

Test population	f_4	**SE**	**z-score**	**BABA**	**ABBA**	**Number of sites used**	**p-value after Bonferroni correction**
Jordan_EBA	0.000724	0.000171	4.225	17980	17749	320398	0.000741
South_Africa_2000BP.SG	0.000599	0.000172	3.481	22613	22371	402857	0.0155
Yemenite_Jew	0.000600	0.000144	4.179	22466	22224	402868	0.00211
Yemeni	0.000524	0.000133	3.950	22365	22153	402868	0.00563
BedouinA	0.000473	0.000126	3.740	22403	22212	402868	0.0132
BedouinB	0.000492	0.000136	3.627	22452	22254	402868	0.0206
Balochi	0.000434	0.000121	3.601	21890	21715	402868	0.0228
Saudi	0.000493	0.000140	3.513	22429	22230	402868	0.0319
Iranian	0.000423	0.000122	3.457	22211	22040	402868	0.0393

Italic fonts indicate modern populations.

Table S21. Significant admixture signals for Imperial individuals from central Italy based on tests in the form of f_3(RMPR_IR; RMPR_IA, test population). A significant negative f_3 statistic indicates admixture signal with the test population.

Test population	f_3	**SE**	**z-score**	**Number of sites used**	**p-value after Bonferroni correction**
Jordan_EBA	-0.002309	0.000393	-5.868	266647	1.37E-07
South_Africa_2000BP.SG	-0.002125	0.000507	-4.190	353608	0.000865
Lebanon_Canaanite_MBA.SG	-0.001231	0.000334	-3.691	334355	0.00692
Iran_IA.SG	-0.002184	0.000633	-3.449	290910	0.0174

Table S22. Working 2-way models for central Italians in the Imperial Rome period (RMPR_IR)

Target	Source 1	Source 2	dof	Chisq	p-value	Prop.1 (SE)	Prop.2 (SE)	Outgroup set
RMPR_IR (48, 402898)	RMPR_IA (11, 402869)	Cypriot (8, 404087)	15	19.136	0.208	0.178 (0.031)	0.822 (0.031)	ANC17
RMPR_IR (48, 402898)	RMPR_IA (11, 402869)	Cypriot (8, 404087)	16	19.36	0.250	0.210 (0.022)	0.790 (0.022)	MOD18
RMPR_IR (48, 402898)	RMPR_IA (11, 402869)	Anatolia_MLBA.SG (5, 387406)	16	16.277	0.433	0.197 (0.034)	0.803 (0.034)	MOD18
RMPR_IR (48, 402898)	RMPR_IA (11, 402869)	Iraqi_Jew (10, 404087)	16	28.752	0.0257	0.424 (0.015)	0.576 (0.015)	MOD18

Table S23. Significant results in f_4 tests in the form of f_4(RMPR_LA, RMPR_IR; test population, Onge). A significant positive f_4 statistic in this test indicates that Late antiquity individuals from central Italy share more alleles with the test population than Imperial individuals do, and vice versa for negative f_4 statistics.

Test population	f_4	SE	z-score	BABA	ABBA	Number of sites used	p-value after Bonferroni correction
Sweden_Viking.SG	0.000531	0.000097	5.449	22402	22188	402881	1.570e-06
England_Saxon.SG	0.000531	0.000100	5.283	22409	22196	402877	3.940e-06
England_Roman.SG	0.000541	0.000103	5.232	22417	22199	401960	5.198e-06
E_Iberia_IA	0.000521	0.000112	4.656	20178	19991	359597	9.9957e-05
Germany_Early_Medieval.SG	0.000443	0.000097	4.566	22348	22169	402779	0.000154
Russia_Tagar.SG	0.000428	0.000101	4.237	21802	21631	400967	0.000702
England_IA.SG	0.000473	0.000114	4.138	22406	22216	402720	0.00109
NE_Iberia_c.6-8CE_ES	0.000558	0.000135	4.137	13910	13771	249106	0.00109
Hungary_Langobard	0.000367	0.000095	3.855	21992	21847	394303	0.00359
N_Iberia_IA	0.000500	0.000132	3.795	19023	18853	339230	0.00458
Hungary_Langobard.SG	0.000347	0.000098	3.537	22374	22234	402885	0.0125
Sweden_IA.SG	0.000545	0.000157	3.463	13658	13523	247116	0.0166
NE_Iberia_c.6CE_PL	0.000409	0.000120	3.408	17505	17377	313146	0.0203
Ukraine_Scythian.SG	0.000426	0.000129	3.296	21143	20981	379887	0.0304
Lithuanian	0.000611	0.000094	6.514	22379	22133	402889	5.269e-09
Norwegian	0.000589	0.000094	6.287	22427	22189	402889	2.330e-08
Finnish	0.000541	0.000089	6.066	22169	21951	402889	9.442e-08
Icelandic	0.000571	0.000095	6.032	22406	22176	402889	1.166e-07
Estonian	0.000551	0.000095	5.790	22339	22117	402889	5.068e-07
Orcadian	0.000529	0.000094	5.622	22411	22198	402889	1.359e-06
Russian	0.000493	0.000092	5.381	22217	22018	402889	5.333e-06
British	0.000477	0.000089	5.356	22335	22143	402889	6.126e-06
Mordovian	0.000501	0.000094	5.306	22245	22044	402889	8.068e-06
Belarusian	0.000484	0.000096	5.057	22346	22151	402889	3.067e-05
Ukrainian	0.000477	0.000095	5.042	22367	22175	402889	3.317e-05
French	0.000441	0.000090	4.913	22445	22268	402889	6.458e-05
Basque	0.000429	0.000092	4.670	22501	22329	402889	0.000217
Spanish_North	0.000467	0.000102	4.571	22494	22306	402889	0.000349

Czech	0.000425	0.000095	4.498	22425	22254	402889	0.000494
Hungarian	0.000402	0.000091	4.416	22409	22247	402889	0.000724
Chuvash	0.000331	0.000090	3.681	21893	21760	402889	0.0167
Croatian	0.000333	0.000095	3.514	22401	22267	402889	0.0318
Spanish	0.000313	0.000090	3.459	22449	22323	402889	0.0390
Palestinian	-0.00031	0.000090	-3.434	22312	22437	402889	0.0428

Italic fonts indicate modern populations.

Table S24. Working 2-way models for central Italian individuals in Late Antiquity (RMPR_LA)

Target	**Source 1**	**Source 2**	**dof**	**Chisq**	**p-value**	**Prop.1 (SE)**	**Prop.2 (SE)**
RMPR_LA (24, 402894)	RMPR_IR (48, 402898)	Germany_Late_Roman.SG (1, 379470)	16	21.219	0.170	0.593 (0.030)	0.407 (0.030)
RMPR_LA (24, 402894)	RMPR_IR (48, 402898)	*Central_Italy* (50, 404087)	16	19.075	0.265	0.157 (0.034)	0.843 (0.034)
RMPR_LA (24, 402894)	RMPR_IR (48, 402898)	*Basque* (29, 404087)	15	19.45	0.194	0.625 (0.016)	0.375 (0.016)
RMPR_LA (24, 402894)	RMPR_IR (48, 402898)	*Bergamo* (12, 404087)	16	26.468	0.0478	0.465 (0.024)	0.535 (0.024)
RMPR_LA (24, 402894)	RMPR_IR (48, 402898)	*Northern_Italy* (147, 404087)	16	26.812	0.0436	0.445 (0.021)	0.555 (0.021)

Italic fonts indicate modern populations.

Table S25. Significant admixture signals for Medieval and early modern individuals from central Italy based on tests in the form of f_3(RMPR_LA; RMPR_MD, test population). A significant negative f_3 statistic indicates admixture signal with the test population.

Test population	f_3	**SE**	**z-score**	**number of sites used**	**p-value after Bonferroni correction**
Sweden_Viking.SG	-0.000707	0.000197	-3.594	337198	0.0101
Hungary_Langobard.SG	-0.000711	0.000198	-3.587	334776	0.0104
England_Saxon.SG	-0.000692	0.000218	-3.174	333848	0.0466
Finnish	-0.000867	0.000157	-5.505	347306	2.658e-06
Chuvash	-0.000947	0.000191	-4.952	342236	5.289e-05
British	-0.000672	0.000136	-4.924	345825	6.105e-05
Estonian	-0.000931	0.000189	-4.924	338273	6.105e-05
Russian	-0.000694	0.000164	-4.237	344568	0.00163
Lithuanian	-0.000797	0.000189	-4.223	337945	0.00174
Icelandic	-0.000659	0.000184	-3.580	338435	0.0247

Italic fonts indicate modern populations.

Table S26. Working 2-way models for central Italian individuals in the Middle Ages and later (RMPR_MD)

Target	Source 1	Source 2	dof	Chisq	p-value	Prop.1 (SE)	Prop.2 (SE)
RMPR_MD (28, 402895)	RMPR_LA (24, 402894)	Germany_Early_Medieval_refined (17, 402345)	16	6.464	0.982	0.806 (0.020)	0.194 (0.020)
RMPR_MD (28, 402895)	RMPR_LA (24, 402894)	Germany_Early_Medieval.SG (27, 403968)	16	6.734	0.978	0.775 (0.022)	0.225 (0.022)
RMPR_MD (28, 402895)	RMPR_LA (24, 402894)	Sweden_Viking.SG (22, 404073)	16	7.825	0.954	0.845 (0.015)	0.155 (0.015)
RMPR_MD (28, 402895)	RMPR_LA (24, 402894)	England_Saxon.SG (8, 404065)	16	8.670	0.926	0.817 (0.018)	0.183 (0.018)
RMPR_MD (28, 402895)	RMPR_LA (24, 402894)	Hungary_Langobard_refined (11, 404079)	16	8.894	0.918	0.819 (0.018)	0.881 (0.018)
RMPR_MD (28, 402895)	RMPR_LA (24, 402894)	Hungary_Langobard.SG (9, 404070)	16	9.673	0.883	0.756 (0.024)	0.244 (0.024)
RMPR_MD (28, 402895)	RMPR_LA (24, 402894)	England_Roman.SG (6, 403143)	16	9.747	0.880	0.811 (0.019)	0.189 (0.019)
RMPR_MD (28, 402895)	RMPR_LA (24, 402894)	Sweden_Viking_refined (5, 386951)	16	10.148	0.859	0.858 (0.015)	0.142 (0.015)
RMPR_MD (28, 402895)	RMPR_LA (24, 402894)	Italy_Langobard_refined (9, 392345)	16	11.019	0.808	0.810 (0.020)	0.190 (0.020)
RMPR_MD (28, 402895)	RMPR_LA (24, 402894)	NE_Iberia_c.6CE_PL (9, 314121)	16	11.673	0.766	0.712 (0.034)	0.288 (0.034)
RMPR_MD (28, 402895)	RMPR_LA (24, 402894)	*Orcadian* (13, 404087)	16	6.250	0.985	0.806 (0.019)	0.194 (0.019)
RMPR_MD (28, 402895)	RMPR_LA (24, 402894)	Czech (10, 404087)	16	6.853	0.976	0.808 (0.019)	0.192 (0.019)
RMPR_MD (28, 402895)	RMPR_LA (24, 402894)	*Lithuanian* (10, 404087)	16	7.143	0.970	0.872 (0.013)	0.128 (0.013)
RMPR_MD (28, 402895)	RMPR_LA (24, 402894)	*Norwegian* (11, 404087)	16	7.356	0.966	0.823 (0.017)	0.177 (0.017)
RMPR_MD (28, 402895)	RMPR_LA (24, 402894)	*Icelandic* (12, 404087)	16	8.761	0.923	0.826 (0.017)	0.174 (0.017)
RMPR_MD (28, 402895)	RMPR_LA (24, 402894)	*Scottish* (1, 403205)	16	8.94	0.916	0.817 (0.022)	0.183 (0.022)
RMPR_MD (28, 402895)	RMPR_LA (24, 402894)	*Hungarian* (20, 404087)	16	9.248	0.903	0.786 (0.021)	0.214 (0.021)
RMPR_MD (28, 402895)	RMPR_LA (24, 402894)	*Estonian* (10, 404087)	16	9.466	0.893	0.874 (0.013)	0.126 (0.013)
RMPR_MD (28, 402895)	RMPR_LA (24, 402894)	*Croatian* (10, 404087)	16	9.791	0.877	0.748 (0.025)	0.252 (0.025)
RMPR_MD (28, 402895)	RMPR_LA (24, 402894)	*British* (92, 404087)	16	9.791	0.877	0.801 (0.019)	0.199 (0.019)
RMPR_MD (28, 402895)	RMPR_LA (24, 402894)	*French* (54, 404087)	16	10.383	0.846	0.759 (0.023)	0.241 (0.023)
RMPR_MD (28, 402895)	RMPR_LA (24, 402894)	*Belarusian* (10, 404087)	16	11.608	0.770	0.857 (0.015)	0.143 (0.015)
RMPR_MD (28, 402895)	RMPR_LA (24, 402894)	*Ukrainian* (10, 404087)	16	11.611	0.770	0.844 (0.016)	0.156 (0.016)

RMPR_MD (28, 402895)	RMPR_LA (24, 402894)	*Bulgarian* (10, 404087)	16	15.436	0.493	0.621 (0.040)	0.379 (0.040)
RMPR_MD (28, 402895)	RMPR_LA (24, 402894)	*Finnish* (99, 404087)	16	22.654	0.123	0.887 (0.012)	0.113 (0.012)
RMPR_MD (28, 402895)	RMPR_LA (24, 402894)	*Russian* (22, 404087)	15	23.837	0.0679	0.910 (0.016)	0.090 (0.016)
RMPR_MD (28, 402895)	RMPR_LA (24, 402894)	*Mordovian* (10, 404087)	16	28.373	0.0285	0.884 (0.014)	0.116 (0.014)

Italic fonts indicate modern populations. Groups with the label "refined" represent subsets of the original samples, who form more genetically homogenous populations (based on PCA location).

Table S27. Significant genetic outliers for each time period identified by f_4 statistics

Time period	Sample ID	Site	Ancestry	Z-score	*p*-value after Bonferroni correction
Neolithic	R6	Grotta Continenza	WHG	4.656	1.93E-04
Iron Age	R475	Civitavecchia	Morocco_Iberomaurusian	5.257	9.66E-06
Imperial	R37	Isola Sacra	WHG	9.347	<1E-12
Imperial	R116	Via Paisiello	WHG	7.750	2.57E-12
Imperial	R80	Viale Rossini	Morocco_Iberomaurusian	7.494	1.84E-11
Imperial	R132	Marcellino & Pietro	Morocco_Iberomaurusian	7.517	1.51E-11
Late Antiquity	R31	Mausoleo di Augusto	WHG	6.280	4.88E-08
Late Antiquity	R104	Crypta Balbi	Anatolia_N	5.807	8.78E-07
Late Antiquity	R106	Crypta Balbi	WHG	5.589	3.01E-06
Medieval and early modern	R64	Villa Magna	WHG	-5.627*	2.57E-06
Medieval and early modern	R1286	Cancelleria	Natufian	-4.564*	8.13E-04

*A negative z-score indicates that the test sample carries less of the corresponding ancestry than their contemporaries do.

Table S28. Working *qpAdm* models for genetic outliers in each time period

Time period	Sample ID	Source 1	Source 2	dof	Chisq	p-value	Prop.1 (SE)	Prop.2 (SE)
Imperial	R132 (1, 339591)	RMPR_IR_core (44, 402895)	Algerian (7, 404087)	16	23.333	0.105	0.543 (0.035)	0.457 (0.035)
		RMPR_IR_core (44, 402895)	Mozabite (21, 404087)	16	26.008	0.054	0.545 (0.034)	0.455 (0.034)
		RMPR_IR_core (44, 402895)	Tunisian (8, 404087)	16	26.331	0.050	0.499 (0.038)	0.501 (0.038)
		RMPR_IR_core (44, 402895)	Canary_Islands_Guanche_mummy.SG (5, 401795)	16	17.685	0.343	0.477 (0.039)	0.523 (0.039)
		RMPR_IR_core (44, 402895)	C_Iberia_CA_Afr (1, 244679)	16	19.315	0.253	0.501 (0.040)	0.499 (0.040)
Imperial	R80 (1, 363278)	RMPR_IR_core (44, 402895)	Morocco_LN (3, 96211)	16	9.658	0.884	0.453 (0.060)	0.547 (0.060)
		RMPR_IR_core (44, 402895)	C_Iberia_CA_Afr (1, 244679)	16	15.468	0.491	0.684 (0.036)	0.316 (0.036)
		RMPR_IR_core (44, 402895)	Canary_Islands_Guanche_mummy.SG (5, 401795)	16	22.719	0.121	0.694 (0.034)	0.306 (0.034)
Imperial	R116 (1, 291967)	French (54, 404087)	--	17	11.421	0.834	1	--
Imperial	R37 (1, 271897)	Basque (29, 404087)	--	16	11.062	0.806	1	--
Late Antiquity	R106 (1, 291306)	French (54, 404087)	--	17	25.144	0.092	1	--
		Scottish (1, 403205)	--	17	19.586	0.296	1	--
		British (92, 404087)	--	17	22.674	0.160	1	--
		RMPR_LA_core (21, 402893)	Icelandic (12, 404087)	16	17.718	0.341	0.258 (0.066)	0.742 (0.066)
		RMPR_LA_core (21, 402893)	Orcadian (13, 404087)	16	19.749	0.232	0.193 (0.072)	0.807 (0.072)
		RMPR_LA_core (21, 402893)	Czech (10, 404087)	16	21.278	0.168	0.200 (0.075)	0.800 (0.075)
		RMPR_LA_core (21, 402893)	Norwegian (11, 404087)	16	25.105	0.068	0.273 (0.066)	0.727 (0.066)
Late Antiquity	R31 (1, 366364)	Scottish (1, 403205)	--	17	13.283	0.717	1	--
		British (92, 404087)	--	17	21.378	0.210	1	--
		Czech (10, 404087)	--	17	23.447	0.135	1	--
		Orcadian (13, 404087)	--	17	26.043	0.074	1	--

Late Antiquity	R104 (1, 258740)	Sardinia (21, 404087)	--	17	20.637	0.243	1	--
		Sardinian (27, 404087)	--	17	21.058	0.176	1	--
Medieval and early modern	R64 (1, 365079)	Italian_South (4, 403969)	--	17	17.854	0.398	1	--
		Southern_Italy (72, 404087)	--	17	24.888	0.097	1	--
		RMPR_MD_core (26, 402895)	Cypriot (8, 404087)	16	19.474	0.245	0.577 (0.090)	0.423 (0.090)
		RMPR_MD_core (26, 402895)	Druze (39, 404087)	16	21.470	0.161	0.685 (0.068)	0.315 (0.068)
Medieval and early modern	R1286 (1, 293660)	Croatian (10, 404087)	--	17	15.433	0.564	1	--
		Hungarian (20, 404087)	--	17	17.978	0.390	1	--
		French (54, 404087)	--	17	16.784	0.469	1	--
		RMPR_MD_core (26, 402895)	Norwegian (11, 404087)	16	9.383	0.897	0.364 (0.083)	0.636 (0.083)
		RMPR_MD_core (26, 402895)	Scottish (1, 403205)	16	10.083	0.862	0.297 (0.110)	0.703 (0.110)
		RMPR_MD_core (26, 402895)	Orcadian (13, 404087)	16	12.824	0.686	0.305 (0.097)	0.695 (0.097)
		RMPR_MD_core (26, 402895)	Icelandic (12, 404087)	16	12.946	0.677	0.385 (0.082)	0.615 (0.082)
		RMPR_MD_core (26, 402895)	British (92, 404087)	16	13.626	0.627	0.270 (0.099)	0.730 (0.099)
		RMPR_MD_core (26, 402895)	Czech (10, 404087)	16	14.687	0.548	0.323 (0.096)	0.677 (0.096)
		RMPR_MD_core (26, 402895)	Lithuanian (10, 404087)	16	17.990	0.324	0.590 (0.059)	0.410 (0.059)
		RMPR_MD_core (26, 402895)	Estonian (10, 404087)	16	18.385	0.302	0.600 (0.057)	0.400 (0.057)
		RMPR_MD_core (26, 402895)	Ukrainian (9, 404087)	16	20.456	0.200	0.493 (0.075)	0.507 (0.075)
		RMPR_MD_core (26, 402895)	Belarusian (10, 404087)	16	21.337	0.166	0.543 (0.068)	0.457 (0.068)
		RMPR_MD_core (26, 402895)	Finnish (99 404087)	16	21.779	0.150	0.644 (0.052)	0.356 (0.052)
		RMPR_MD_core (26, 402895)	Mordovian (10, 404087)	16	25.968	0.054	0.631 (0.058)	0.369 (0.058)

References and Notes

1. K. Harper, *The Fate of Rome: Climate, Disease, and the End of an Empire* (Princeton Univ. Press, Princeton, 2017).

2. P. Horden, N. Purcell, *The Corrupting Sea: A Study of Mediterranean History* (Bl6, ackwell, Oxford, U.K.; Malden, Mass, 2000).

3. D. Abulafia, *The Great Sea: A Human History of the Mediterranean* (Oxford Univ. Press, New York, 2011).

4. D. Petkova, J. Novembre, M. Stephens, Visualizing spatial population structure with estimated effective migration surfaces. *Nat. Genet.* **48**, 94–100 (2016). doi:10.1038/ng.3464 Medline

5. A. Raveane, S. Aneli, F. Montinaro, G. Athanasiadis, S. Barlera, G. Birolo, G. Boncoraglio, A. M. Di Blasio, C. Di Gaetano, L. Pagani, S. Parolo, P. Paschou, A. Piazza, G. Stamatoyannopoulos, A. Angius, N. Brucato, F. Cucca, G. Hellenthal, A. Mulas, M. Peyret-Guzzon, M. Zoledziewska, A. Baali, C. Bycroft, M. Cherkaoui, J. Chiaroni, J. Di Cristofaro, C. Dina, J. M. Dugoujon, P. Galan, J. Giemza, T. Kivisild, S. Mazieres, M. Melhaoui, M. Metspalu, S. Myers, L. Pereira, F. X. Ricaut, F. Brisighelli, I. Cardinali, V. Grugni, H. Lancioni, V. L. Pascali, A. Torroni, O. Semino, G. Matullo, A. Achilli, A. Olivieri, C. Capelli, Population structure of modern-day Italians reveals patterns of ancient and archaic ancestries in Southern Europe. *Sci. Adv.* **5**, w3492 (2019). doi:10.1126/sciadv.aaw3492 Medline

6. C. Broodbank, *The Making of the Middle Sea: A History of the Mediterranean from the Beginning to the Emergence of the Classical World* (Oxford Univ. Press, 2013).

7. Supplementary materials.

8. D. H. Alexander, J. Novembre, K. Lange, Fast model-based estimation of ancestry in unrelated individuals. *Genome Res.* **19**, 1655–1664 (2009). doi:10.1101/gr.094052.109 Medline

9. N. Patterson, P. Moorjani, Y. Luo, S. Mallick, N. Rohland, Y. Zhan, T. Genschoreck, T. Webster, D. Reich, Ancient admixture in human history. *Genetics* **192**, 1065–1093 (2012). doi:10.1534/genetics.112.145037 Medline

10. W. Haak, I. Lazaridis, N. Patterson, N. Rohland, S. Mallick, B. Llamas, G. Brandt, S. Nordenfelt, E. Harney, K. Stewardson, Q. Fu, A. Mittnik, E. Bánffy, C. Economou, M. Francken, S. Friederich, R. G. Pena, F. Hallgren, V. Khartanovich, A. Khokhlov, M. Kunst, P. Kuznetsov, H. Meller, O. Mochalov, V. Moiseyev, N. Nicklisch, S. L. Pichler, R. Risch, M. A. Rojo Guerra, C. Roth, A. Szécsényi-Nagy, J. Wahl, M. Meyer, J. Krause, D. Brown, D. Anthony, A. Cooper, K. W. Alt, D. Reich, Massive migration from the steppe was a source for Indo-European languages in Europe. *Nature* **522**, 207–211 (2015). doi:10.1038/nature14317 Medline

11. D. J. Lawson, G. Hellenthal, S. Myers, D. Falush, Inference of population structure using dense haplotype data. *PLOS Genet.* **8**, e1002453 (2012). doi:10.1371/journal.pgen.1002453 Medline

12. I. Lazaridis, N. Patterson, A. Mittnik, G. Renaud, S. Mallick, K. Kirsanow, P. H. Sudmant, J. G. Schraiber, S. Castellano, M. Lipson, B. Berger, C. Economou, R. Bollongino, Q. Fu, K. I. Bos, S. Nordenfelt, H. Li, C. de Filippo, K. Prüfer, S. Sawyer, C. Posth, W. Haak, F. Hallgren, E. Fornander, N. Rohland, D. Delsate, M. Francken, J.-M. Guinet, J. Wahl, G. Ayodo, H. A. Babiker, G. Bailliet, E. Balanovska, O. Balanovsky, R. Barrantes, G. Bedoya, H. Ben-Ami, J. Bene, F. Berrada, C. M. Bravi, F. Brisighelli, G. B. J. Busby, F. Cali, M. Churnosov, D. E. C. Cole, D. Corach, L. Damba, G. van Driem, S. Dryomov, J.-M. Dugoujon, S. A. Fedorova, I. Gallego Romero, M. Gubina, M. Hammer, B. M. Henn, T. Hervig, U. Hodoglugil, A. R. Jha, S. Karachanak-Yankova, R. Khusainova, E. Khusnutdinova, R. Kittles, T. Kivisild, W. Klitz, V. Kučinskas, A. Kushniarevich, L. Laredj, S. Litvinov, T. Loukidis, R. W. Mahley, B. Melegh, E. Metspalu, J. Molina, J. Mountain, K. Näkkäläjärvi, D. Nesheva, T. Nyambo, L. Osipova, J. Parik, F. Platonov, O. Posukh, V. Romano, F. Rothhammer, I. Rudan, R. Ruizbakiev, H. Sahakyan, A. Sajantila, A. Salas, E. B. Starikovskaya, A. Tarekegn, D. Toncheva, S. Turdikulova, I. Uktveryte, O. Utevska, R. Vasquez, M. Villena, M. Voevoda, C. A. Winkler, L. Yepiskoposyan, P. Zalloua, T. Zemunik, A. Cooper, C. Capelli, M. G. Thomas, A. Ruiz-Linares, S. A. Tishkoff, L. Singh, K. Thangaraj, R. Villems, D. Comas, R. Sukernik, M. Metspalu, M. Meyer, E. E. Eichler, J. Burger, M. Slatkin, S. Pääbo, J. Kelso, D. Reich, J. Krause, Ancient human genomes suggest three ancestral populations for present-day Europeans. *Nature* **513**, 409–413 (2014). doi:10.1038/nature13673 Medline

13. I. Mathieson, I. Lazaridis, N. Rohland, S. Mallick, N. Patterson, S. A. Roodenberg, E. Harney, K. Stewardson, D. Fernandes, M. Novak, K. Sirak, C. Gamba, E. R. Jones, B. Llamas, S. Dryomov, J. Pickrell, J. L. Arsuaga, J. M. B. de Castro, E. Carbonell, F. Gerritsen, A. Khokhlov, P. Kuznetsov, M. Lozano, H. Meller, O. Mochalov, V. Moiseyev, M. A. R. Guerra, J. Roodenberg, J. M. Vergès, J. Krause, A. Cooper, K. W. Alt, D. Brown, D. Anthony, C. Lalueza-Fox, W. Haak, R. Pinhasi, D. Reich, Genome-wide patterns of selection in 230 ancient Eurasians. *Nature* **528**, 499–503 (2015). doi:10.1038/nature16152 Medline

14. I. Mathieson, S. Alpaslan-Roodenberg, C. Posth, A. Szécsényi-Nagy, N. Rohland, S. Mallick, I. Olalde, N. Broomandkhoshbacht, F. Candilio, O. Cheronet, D. Fernandes, M. Ferry, B. Gamarra, G. G. Fortes, W. Haak, E. Harney, E. Jones, D. Keating, B. Krause-Kyora, I. Kucukkalipci, M. Michel, A. Mittnik, K. Nägele, M. Novak, J. Oppenheimer, N. Patterson, S. Pfrengle, K. Sirak, K. Stewardson, S. Vai, S. Alexandrov, K. W. Alt, R. Andreescu, D. Antonović, A. Ash, N. Atanassova, K. Bacvarov, M. B. Gusztáv, H. Bocherens, M. Bolus, A. Boroneanţ, Y. Boyadzhiev, A. Budnik, J. Burmaz, S. Chohadzhiev, N. J. Conard, R. Cottiaux, M. Čuka, C. Cupillard, D. G. Drucker, N. Elenski, M. Francken, B. Galabova, G. Ganetsovski, B. Gély, T. Hajdu, V. Handzhyiska, K. Harvati, T. Higham, S. Iliev, I. Janković, I. Karavanić, D. J. Kennett, D. Komšo, A. Kozak, D. Labuda, M. Lari, C. Lazar, M. Leppek, K. Leshtakov, D. L. Vetro, D. Los, I. Lozanov, M. Malina, F. Martini, K. McSweeney, H. Meller, M. Menđušić, P. Mirea, V. Moiseyev, V. Petrova, T. D. Price, A. Simalcsik, L. Sineo, M. Šlaus, V. Slavchev, P. Stanev, A. Starović, T. Szeniczey, S. Talamo, M. Teschler-Nicola, C. Thevenet, I. Valchev, F. Valentin, S. Vasilyev, F. Veljanovska, S. Venelinova, E. Veselovskaya, B. Viola, C. Virag, J. Zaninović, S. Zäuner, P. W. Stockhammer, G. Catalano, R. Krauß, D. Caramelli, G. Zariņa, B. Gaydarska, M. Lillie, A. G. Nikitin, I. Potekhina, A. Papathanasiou, D. Borić, C. Bonsall, J. Krause, R. Pinhasi, D. Reich, The genomic

history of southeastern Europe. *Nature* **555**, 197–203 (2018). doi:10.1038/nature25778 Medline

15. Q. Fu, C. Posth, M. Hajdinjak, M. Petr, S. Mallick, D. Fernandes, A. Furtwängler, W. Haak, M. Meyer, A. Mittnik, B. Nickel, A. Peltzer, N. Rohland, V. Slon, S. Talamo, I. Lazaridis, M. Lipson, I. Mathieson, S. Schiffels, P. Skoglund, A. P. Derevianko, N. Drozdov, V. Slavinsky, A. Tsybankov, R. G. Cremonesi, F. Mallegni, B. Gély, E. Vacca, M. R. G. Morales, L. G. Straus, C. Neugebauer-Maresch, M. Teschler-Nicola, S. Constantin, O. T. Moldovan, S. Benazzi, M. Peresani, D. Coppola, M. Lari, S. Ricci, A. Ronchitelli, F. Valentin, C. Thevenet, K. Wehrberger, D. Grigorescu, H. Rougier, I. Crevecoeur, D. Flas, P. Semal, M. A. Mannino, C. Cupillard, H. Bocherens, N. J. Conard, K. Harvati, V. Moiseyev, D. G. Drucker, J. Svoboda, M. P. Richards, D. Caramelli, R. Pinhasi, J. Kelso, N. Patterson, J. Krause, S. Pääbo, D. Reich, The genetic history of Ice Age Europe. *Nature* **534**, 200–205 (2016). doi:10.1038/nature17993 Medline

16. M. Beard, *SPQR: A history of Ancient Rome* (Liveright, New York, ed. 1, 2015).

17. I. Lazaridis, A. Mittnik, N. Patterson, S. Mallick, N. Rohland, S. Pfrengle, A. Furtwängler, A. Peltzer, C. Posth, A. Vasilakis, P. J. P. McGeorge, E. Konsolaki-Yannopoulou, G. Korres, H. Martlew, M. Michalodimitrakis, M. Özsait, N. Özsait, A. Papathanasiou, M. Richards, S. A. Roodenberg, Y. Tzedakis, R. Arnott, D. M. Fernandes, J. R. Hughey, D. M. Lotakis, P. A. Navas, Y. Maniatis, J. A. Stamatoyannopoulos, K. Stewardson, P. Stockhammer, R. Pinhasi, D. Reich, J. Krause, G. Stamatoyannopoulos, Genetic origins of the Minoans and Mycenaeans. *Nature* **548**, 214–218 (2017). doi:10.1038/nature23310 Medline

18. Z. Hofmanová, S. Kreutzer, G. Hellenthal, C. Sell, Y. Diekmann, D. Díez-Del-Molino, L. van Dorp, S. López, A. Kousathanas, V. Link, K. Kirsanow, L. M. Cassidy, R. Martiniano, M. Strobel, A. Scheu, K. Kotsakis, P. Halstead, S. Triantaphyllou, N. Kyparissi-Apostolika, D. Urem-Kotsou, C. Ziota, F. Adaktylou, S. Gopalan, D. M. Bobo, L. Winkelbach, J. Blöcher, M. Unterländer, C. Leuenberger, Ç. Çilingiroğlu, B. Horejs, F. Gerritsen, S. J. Shennan, D. G. Bradley, M. Currat, K. R. Veeramah, D. Wegmann, M. G. Thomas, C. Papageorgopoulou, J. Burger, Early farmers from across Europe directly descended from Neolithic Aegeans. *Proc. Natl. Acad. Sci. U.S.A.* **113**, 6886–6891 (2016). doi:10.1073/pnas.1523951113 Medline

19. I. Olalde, S. Mallick, N. Patterson, N. Rohland, V. Villalba-Mouco, M. Silva, K. Dulias, C. J. Edwards, F. Gandini, M. Pala, P. Soares, M. Ferrando-Bernal, N. Adamski, N. Broomandkhoshbacht, O. Cheronet, B. J. Culleton, D. Fernandes, A. M. Lawson, M. Mah, J. Oppenheimer, K. Stewardson, Z. Zhang, J. M. Jiménez Arenas, I. J. Toro Moyano, D. C. Salazar-García, P. Castanyer, M. Santos, J. Tremoleda, M. Lozano, P. García Borja, J. Fernández-Eraso, J. A. Mujika-Alustiza, C. Barroso, F. J. Bermúdez, E. Viguera Mínguez, J. Burch, N. Coromina, D. Vivó, A. Cebrià, J. M. Fullola, O. García-Puchol, J. I. Morales, F. X. Oms, T. Majó, J. M. Vergès, A. Díaz-Carvajal, I. Ollich-Castanyer, F. J. López-Cachero, A. M. Silva, C. Alonso-Fernández, G. Delibes de Castro, J. Jiménez Echevarría, A. Moreno-Márquez, G. Pascual Berlanga, P. Ramos-García, J. Ramos-Muñoz, E. Vijande Vila, G. Aguilella Arzo, Á. Esparza Arroyo, K. T. Lillios, J. Mack, J. Velasco-Vázquez, A. Waterman, L. Benítez de Lugo Enrich, M. Benito Sánchez, B. Agustí, F. Codina, G. de Prado, A. Estalrrich, Á. Fernández Flores, C.

Finlayson, G. Finlayson, S. Finlayson, F. Giles-Guzmán, A. Rosas, V. Barciela González, G. García Atiénzar, M. S. Hernández Pérez, A. Llanos, Y. Carrión Marco, I. Collado Beneyto, D. López-Serrano, M. Sanz Tormo, A. C. Valera, C. Blasco, C. Liesau, P. Ríos, J. Daura, M. J. de Pedro Michó, A. A. Diez-Castillo, R. Flores Fernández, J. Francès Farré, R. Garrido-Pena, V. S. Gonçalves, E. Guerra-Doce, A. M. Herrero-Corral, J. Juan-Cabanilles, D. López-Reyes, S. B. McClure, M. Merino Pérez, A. Oliver Foix, M. Sanz Borràs, A. C. Sousa, J. M. Vidal Encinas, D. J. Kennett, M. B. Richards, K. Werner Alt, W. Haak, R. Pinhasi, C. Lalueza-Fox, D. Reich, The genomic history of the Iberian Peninsula over the past 8000 years. *Science* **363**, 1230–1234 (2019). doi:10.1126/science.aav4040 Medline

20. D. M. Fernandes, D. Strapagiel, P. Borówka, B. Marciniak, E. Żądzińska, K. Sirak, V. Siska, R. Grygiel, J. Carlsson, A. Manica, W. Lorkiewicz, R. Pinhasi, A genomic Neolithic time transect of hunter-farmer admixture in central Poland. *Sci. Rep.* **8**, 14879 (2018). doi:10.1038/s41598-018-33067-w Medline

21. D. W. Anthony, *The Horse, the Wheel, and Language: How Bronze-Age Riders from the Eurasian Steppes Shaped the Modern World* (Princeton Univ. Press, Princeton, N.J., 2007).

22. M. E. Allentoft, M. Sikora, K.-G. Sjögren, S. Rasmussen, M. Rasmussen, J. Stenderup, P. B. Damgaard, H. Schroeder, T. Ahlström, L. Vinner, A.-S. Malaspinas, A. Margaryan, T. Higham, D. Chivall, N. Lynnerup, L. Harvig, J. Baron, P. Della Casa, P. Dąbrowski, P. R. Duffy, A. V. Ebel, A. Epimakhov, K. Frei, M. Furmanek, T. Gralak, A. Gromov, S. Gronkiewicz, G. Grupe, T. Hajdu, R. Jarysz, V. Khartanovich, A. Khokhlov, V. Kiss, J. Kolář, A. Kriiska, I. Lasak, C. Longhi, G. McGlynn, A. Merkevicius, I. Merkyte, M. Metspalu, R. Mkrtchyan, V. Moiseyev, L. Paja, G. Pálfi, D. Pokutta, Ł. Pospieszny, T. D. Price, L. Saag, M. Sablin, N. Shishlina, V. Smrčka, V. I. Soenov, V. Szeverényi, G. Tóth, S. V. Trifanova, L. Varul, M. Vicze, L. Yepiskoposyan, V. Zhitenev, L. Orlando, T. Sicheritz-Pontén, S. Brunak, R. Nielsen, K. Kristiansen, E. Willerslev, Population genomics of Bronze Age Eurasia. *Nature* **522**, 167–172 (2015). doi:10.1038/nature14507 Medline

23. D. M. Fernandes *et al*., The Arrival of Steppe and Iranian related ancestry in the islands of the western Mediterranean. *bioRxiv* 584714 (2019). https://doi.org/10.1101/584714

24. A. Fraschetti, Romolo il fondatore (GLF editori Laterza, 2002).

25. M. Pallottino, Origini e storia primitiva di Roma: Texte imprimé (Rusconi, 1993).

26. A. Grandazzi, The Foundation of Rome: Myth and History (Cornell Univ. Press, 1997).

27. R. Miles, *Carthage Must Be Destroyed: The Rise and Fall of an Ancient Mediterranean Civilization* (Allen Lane, London, 2010).

28. M. Haber, C. Doumet-Serhal, C. L. Scheib, Y. Xue, R. Mikulski, R. Martiniano, B. Fischer-Genz, H. Schutkowski, T. Kivisild, C. Tyler-Smith, A Transient Pulse of Genetic Admixture from the Crusaders in the Near East Identified from Ancient Genome Sequences. *Am. J. Hum. Genet.* **104**, 977–984 (2019). doi:10.1016/j.ajhg.2019.03.015 Medline

29. D. Noy, Immigrants in Late Imperial Rome, in *Ethnicity and Culture in Late Antiquity*, S. Mitchell, G. Greatrex, Eds. (David Brown Book Co., 2000).

30. G. E. Rickman, The Grain Trade under the Roman Empire. *Mem. Am. Acad. Rome.* **36**, 261–275 (1980). doi:10.2307/4238709

31. S. Alcock, in *The Cambridge Economic History of the Greco-Roman World*, W. Scheidel, I. Morris, R. P. Saller, Eds. (Cambridge Univ. Press, 2007).

32. P. Zalloua, C. J. Collins, A. Gosling, S. A. Biagini, B. Costa, O. Kardailsky, L. Nigro, W. Khalil, F. Calafell, E. Matisoo-Smith, Ancient DNA of Phoenician remains indicates discontinuity in the settlement history of Ibiza. *Sci. Rep.* **8**, 17567 (2018). doi:10.1038/s41598-018-35667-y Medline

33. P. Garnsey, Osteodental biology of the people of Portus Romae (necropolis of Isola Sacra, 2nd–3rd cent. AD), enamel microstructure and developmental defects of the primary dentition. Rome: National Prehistoric Ethnographic "'L. Pigorini'"Museum (CD-ROM) (1999).

34. T. L. Prowse, H. P. Schwarcz, P. Garnsey, M. Knyf, R. Macchiarelli, L. Bondioli, Isotopic evidence for age-related immigration to imperial Rome. *Am. J. Phys. Anthropol.* **132**, 510–519 (2007). doi:10.1002/ajpa.20541 Medline

35. C. E. G. Amorim, S. Vai, C. Posth, A. Modi, I. Koncz, S. Hakenbeck, M. C. La Rocca, B. Mende, D. Bobo, W. Pohl, L. P. Baricco, E. Bedini, P. Francalacci, C. Giostra, T. Vida, D. Winger, U. von Freeden, S. Ghirotto, M. Lari, G. Barbujani, J. Krause, D. Caramelli, P. J. Geary, K. R. Veeramah, Understanding 6th-century barbarian social organization and migration through paleogenomics. *Nat. Commun.* **9**, 3547 (2018). doi:10.1038/s41467-018-06024-4 Medline

36. D. Abulafia, *The Two Italies: Economic Relations Between the Norman Kingdom of Sicily and the Northern Communes* (Cambridge Univ. Press, 2005).

37. R. Pinhasi, D. M. Fernandes, K. Sirak, O. Cheronet, Isolating the human cochlea to generate bone powder for ancient DNA analysis. *Nat. Protoc.* **14**, 1194–1205 (2019). doi:10.1038/s41596-019-0137-7 Medline

38. R. Pinhasi, D. Fernandes, K. Sirak, M. Novak, S. Connell, S. Alpaslan-Roodenberg, F. Gerritsen, V. Moiseyev, A. Gromov, P. Raczky, A. Anders, M. Pietrusewsky, G. Rollefson, M. Jovanovic, H. Trinhhoang, G. Bar-Oz, M. Oxenham, H. Matsumura, M. Hofreiter, Optimal Ancient DNA Yields from the Inner Ear Part of the Human Petrous Bone. *PLOS ONE* **10**, e0129102 (2015). doi:10.1371/journal.pone.0129102 Medline

39. N. Rohland, M. Hofreiter, Ancient DNA extraction from bones and teeth. *Nat. Protoc.* **2**, 1756–1762 (2007). doi:10.1038/nprot.2007.247 Medline

40. J. Dabney, M. Knapp, I. Glocke, M.-T. Gansauge, A. Weihmann, B. Nickel, C. Valdiosera, N. García, S. Pääbo, J.-L. Arsuaga, M. Meyer, Complete mitochondrial genome sequence of a Middle Pleistocene cave bear reconstructed from ultrashort DNA fragments. *Proc. Natl. Acad. Sci. U.S.A.* **110**, 15758–15763 (2013). doi:10.1073/pnas.1314445110 Medline

41. N. Rohland, E. Harney, S. Mallick, S. Nordenfelt, D. Reich, Partial uracil-DNA-glycosylase treatment for screening of ancient DNA. *Philos. Trans. R. Soc. Lond. B Biol. Sci.* **370**, 20130624 (2015). doi:10.1098/rstb.2013.0624 Medline

42. M. Meyer, M. Kircher, Illumina sequencing library preparation for highly multiplexed target capture and sequencing. *Cold Spring Harb. Protoc.* **2010**, t5448 (2010). doi:10.1101/pdb.prot5448 Medline

43. M. Martin, *EMBnet.journal* **17**, 10 (2011).

44. H. Li, R. Durbin, Fast and accurate short read alignment with Burrows-Wheeler transform. *Bioinformatics* **25**, 1754–1760 (2009). doi:10.1093/bioinformatics/btp324 Medline

45. H. Li, B. Handsaker, A. Wysoker, T. Fennell, J. Ruan, N. Homer, G. Marth, G. Abecasis, R. Durbin; 1000 Genome Project Data Processing Subgroup, The Sequence Alignment/Map format and SAMtools. *Bioinformatics* **25**, 2078–2079 (2009). doi:10.1093/bioinformatics/btp352 Medline

46. H. Jónsson, A. Ginolhac, M. Schubert, P. L. F. Johnson, L. Orlando, mapDamage2.0: Fast approximate Bayesian estimates of ancient DNA damage parameters. *Bioinformatics* **29**, 1682–1684 (2013). doi:10.1093/bioinformatics/btt193 Medline

47. G. Renaud, V. Slon, A. T. Duggan, J. Kelso, Schmutzi: Estimation of contamination and endogenous mitochondrial consensus calling for ancient DNA. *Genome Biol.* **16**, 224 (2015). doi:10.1186/s13059-015-0776-0 Medline

48. T. S. Korneliussen, A. Albrechtsen, R. Nielsen, ANGSD: Analysis of Next Generation Sequencing Data. *BMC Bioinformatics* **15**, 356 (2014). doi:10.1186/s12859-014-0356-4 Medline

49. S. Mallick, D. Reich, Compiled published present-day and ancient DNA genotypes (2019), (available at https://reich.hms.harvard.edu/downloadable-genotypes-present-day-and-ancient-dna-data-compiled-published-papers).

50. A. Auton, L. D. Brooks, R. M. Durbin, E. P. Garrison, H. M. Kang, J. O. Korbel, J. L. Marchini, S. McCarthy, G. A. McVean, G. R. Abecasis; 1000 Genomes Project Consortium, A global reference for human genetic variation. *Nature* **526**, 68–74 (2015). doi:10.1038/nature15393 Medline

51. D. M. Behar, B. Yunusbayev, M. Metspalu, E. Metspalu, S. Rosset, J. Parik, S. Rootsi, G. Chaubey, I. Kutuev, G. Yudkovsky, E. K. Khusnutdinova, O. Balanovsky, O. Semino, L. Pereira, D. Comas, D. Gurwitz, B. Bonne-Tamir, T. Parfitt, M. F. Hammer, K. Skorecki, R. Villems, The genome-wide structure of the Jewish people. *Nature* **466**, 238–242 (2010). doi:10.1038/nature09103 Medline

52. G. Fiorito, C. Di Gaetano, S. Guarrera, F. Rosa, M. W. Feldman, A. Piazza, G. Matullo, The Italian genome reflects the history of Europe and the Mediterranean basin. *Eur. J. Hum. Genet.* **24**, 1056–1062 (2016). doi:10.1038/ejhg.2015.233 Medline

53. G. Hellenthal, G. B. J. Busby, G. Band, J. F. Wilson, C. Capelli, D. Falush, S. Myers, A genetic atlas of human admixture history. *Science* **343**, 747–751 (2014). doi:10.1126/science.1243518 Medline

54. C. Gamba, E. R. Jones, M. D. Teasdale, R. L. McLaughlin, G. Gonzalez-Fortes, V. Mattiangeli, L. Domboróczki, I. Kővári, I. Pap, A. Anders, A. Whittle, J. Dani, P. Raczky, T. F. G. Higham, M. Hofreiter, D. G. Bradley, R. Pinhasi, Genome flux and stasis in a five millennium transect of European prehistory. *Nat. Commun.* **5**, 5257 (2014). doi:10.1038/ncomms6257 Medline

55. B. Pasaniuc, N. Rohland, P. J. McLaren, K. Garimella, N. Zaitlen, H. Li, N. Gupta, B. M. Neale, M. J. Daly, P. Sklar, P. F. Sullivan, S. Bergen, J. L. Moran, C. M. Hultman, P. Lichtenstein, P. Magnusson, S. M. Purcell, D. W. Haas, L. Liang, S. Sunyaev, N. Patterson, P. I. W. de Bakker, D. Reich, A. L. Price, Extremely low-coverage sequencing and imputation increases power for genome-wide association studies. *Nat. Genet.* **44**, 631–635 (2012). doi:10.1038/ng.2283 Medline

56. R. Martiniano, L. M. Cassidy, R. Ó'Maoldúin, R. McLaughlin, N. M. Silva, L. Manco, D. Fidalgo, T. Pereira, M. J. Coelho, M. Serra, J. Burger, R. Parreira, E. Moran, A. C. Valera, E. Porfirio, R. Boaventura, A. M. Silva, D. G. Bradley, The population genomics of archaeological transition in west Iberia: Investigation of ancient substructure using imputation and haplotype-based methods. *PLOS Genet.* **13**, e1006852 (2017). doi:10.1371/journal.pgen.1006852 Medline

57. M. A. DePristo, E. Banks, R. Poplin, K. V. Garimella, J. R. Maguire, C. Hartl, A. A. Philippakis, G. del Angel, M. A. Rivas, M. Hanna, A. McKenna, T. J. Fennell, A. M. Kernytsky, A. Y. Sivachenko, K. Cibulskis, S. B. Gabriel, D. Altshuler, M. J. Daly, A framework for variation discovery and genotyping using next-generation DNA sequencing data. *Nat. Genet.* **43**, 491–498 (2011). doi:10.1038/ng.806 Medline

58. S. R. Browning, B. L. Browning, Rapid and accurate haplotype phasing and missing-data inference for whole-genome association studies by use of localized haplotype clustering. *Am. J. Hum. Genet.* **81**, 1084–1097 (2007). doi:10.1086/521987 Medline

59. H. Weissensteiner, D. Pacher, A. Kloss-Brandstätter, L. Forer, G. Specht, H.-J. Bandelt, F. Kronenberg, A. Salas, S. Schönherr, HaploGrep 2: Mitochondrial haplogroup classification in the era of high-throughput sequencing. *Nucleic Acids Res.* **44**, W58–W63 (2016). doi:10.1093/nar/gkw233 Medline

60. Q. Fu, P. Rudan, S. Pääbo, J. Krause, Complete mitochondrial genomes reveal neolithic expansion into Europe. *PLOS ONE* **7**, e32473 (2012). doi:10.1371/journal.pone.0032473 Medline

61. N. Isern, J. Fort, V. L. de Rioja, The ancient cline of haplogroup K implies that the Neolithic transition in Europe was mainly demic. *Sci. Rep.* **7**, 11229 (2017). doi:10.1038/s41598-017-11629-8 Medline

62. P. Brotherton, W. Haak, J. Templeton, G. Brandt, J. Soubrier, C. Jane Adler, S. M. Richards, C. Der Sarkissian, R. Ganslmeier, S. Friederich, V. Dresely, M. van Oven, R. Kenyon, M. B. Van der Hoek, J. Korlach, K. Luong, S. Y. W. Ho, L. Quintana-Murci, D. M. Behar, H. Meller, K. W. Alt, A. Cooper; Genographic Consortium, Neolithic mitochondrial haplogroup H genomes and the genetic origins of Europeans. *Nat. Commun.* **4**, 1764 (2013). doi:10.1038/ncomms2656 Medline

63. A. Szécsényi-Nagy, C. Roth, G. Brandt, C. Rihuete-Herrada, C. Tejedor-Rodríguez, P. Held, Í. García-Martínez-de-Lagrán, H. Arcusa Magallón, S. Zesch, C. Knipper, E. Bánffy, S.

Friederich, H. Meller, P. Bueno Ramírez, R. Barroso Bermejo, R. de Balbín Behrmann, A. M. Herrero-Corral, R. Flores Fernández, C. Alonso Fernández, J. Jiménez Echevarria, L. Rindlisbacher, C. Oliart, M.-I. Fregeiro, I. Soriano, O. Vicente, R. Micó, V. Lull, J. Soler Díaz, J. A. López Padilla, C. Roca de Togores Muñoz, M. S. Hernández Pérez, F. J. Jover Maestre, J. Lomba Maurandi, A. Avilés Fernández, K. T. Lillios, A. M. Silva, M. Magalhães Ramalho, L. M. Oosterbeek, C. Cunha, A. J. Waterman, J. Roig Buxó, A. Martínez, J. Ponce Martínez, M. Hunt Ortiz, J. C. Mejías-García, J. C. Pecero Espín, R. Cruz-Auñón Briones, T. Tomé, E. Carmona Ballestero, J. L. Cardoso, A. C. Araújo, C. Liesau von Lettow-Vorbeck, C. Blasco Bosqued, P. Ríos Mendoza, A. Pujante, J. I. Royo-Guillén, M. A. Esquembre Beviá, V. M. Dos Santos Goncalves, R. Parreira, E. Morán Hernández, E. Méndez Izquierdo, J. Vega Y Miguel, R. Menduiña García, V. Martínez Calvo, O. López Jiménez, J. Krause, S. L. Pichler, R. Garrido-Pena, M. Kunst, R. Risch, M. A. Rojo-Guerra, W. Haak, K. W. Alt, The maternal genetic make-up of the Iberian Peninsula between the Neolithic and the Early Bronze Age. *Sci. Rep.* **7**, 15644 (2017). doi:10.1038/s41598-017-15480-9 Medline

64. M. V. Emery, A. T. Duggan, T. J. Murchie, R. J. Stark, J. Klunk, J. Hider, K. Eaton, E. Karpinski, H. P. Schwarcz, H. N. Poinar, T. L. Prowse, Ancient Roman mitochondrial genomes and isotopes reveal relationships and geographic origins at the local and pan-Mediterranean scales. *J. Archaeol. Sci. Rep.* **20**, 200–209 (2018). doi:10.1016/j.jasrep.2018.04.036

65. T. L. Prowse, J. L. Barta, T. E. von Hunnius, A. V. Small, Stable isotope and mtDNA evidence for geographic origins at the site of Vagnari (2nd–4th centuries AD), Italy. *J. Roman Archaeol. Suppl.* **78**, 175–198 (2010).

66. E. A. Matisoo-Smith, A. L. Gosling, J. Boocock, O. Kardailsky, Y. Kurumilian, S. Roudesli-Chebbi, L. Badre, J.-P. Morel, L. L. Sebaï, P. A. Zalloua, A European Mitochondrial Haplotype Identified in Ancient Phoenician Remains from Carthage, North Africa. *PLOS ONE* **11**, e0155046 (2016). doi:10.1371/journal.pone.0155046 Medline

67. A. Non, thesis, University of Florida (2010).

68. L. Rishishwar, I. K. Jordan, Implications of human evolution and admixture for mitochondrial replacement therapy. *BMC Genomics* **18**, 140 (2017). doi:10.1186/s12864-017-3539-3 Medline

69. G. D. Poznik, Identifying Y-chromosome haplogroups in arbitrarily large samples of sequenced or genotyped men. *bioRxiv* 088716 (2016). https://doi.org/10.1101/088716

70. E. R. Jones, G. Gonzalez-Fortes, S. Connell, V. Siska, A. Eriksson, R. Martiniano, R. L. McLaughlin, M. Gallego Llorente, L. M. Cassidy, C. Gamba, T. Meshveliani, O. Bar-Yosef, W. Müller, A. Belfer-Cohen, Z. Matskevich, N. Jakeli, T. F. G. Higham, M. Currat, D. Lordkipanidze, M. Hofreiter, A. Manica, R. Pinhasi, D. G. Bradley, Upper Palaeolithic genomes reveal deep roots of modern Eurasians. *Nat. Commun.* **6**, 8912 (2015). doi:10.1038/ncomms9912 Medline

71. A. Keller, A. Graefen, M. Ball, M. Matzas, V. Boisguerin, F. Maixner, P. Leidinger, C. Backes, R. Khairat, M. Forster, B. Stade, A. Franke, J. Mayer, J. Spangler, S. McLaughlin, M. Shah, C. Lee, T. T. Harkins, A. Sartori, A. Moreno-Estrada, B. Henn, M. Sikora, O. Semino, J. Chiaroni, S. Rootsi, N. M. Myres, V. M. Cabrera, P. A.

Underhill, C. D. Bustamante, E. E. Vigl, M. Samadelli, G. Cipollini, J. Haas, H. Katus, B. D. O'Connor, M. R. J. Carlson, B. Meder, N. Blin, E. Meese, C. M. Pusch, A. Zink, New insights into the Tyrolean Iceman's origin and phenotype as inferred by whole-genome sequencing. *Nat. Commun.* **3**, 698 (2012). doi:10.1038/ncomms1701 Medline

72. I. Olalde, S. Brace, M. E. Allentoft, I. Armit, K. Kristiansen, T. Booth, N. Rohland, S. Mallick, A. Szécsényi-Nagy, A. Mittnik, E. Altena, M. Lipson, I. Lazaridis, T. K. Harper, N. Patterson, N. Broomandkhoshbacht, Y. Diekmann, Z. Faltyskova, D. Fernandes, M. Ferry, E. Harney, P. de Knijff, M. Michel, J. Oppenheimer, K. Stewardson, A. Barclay, K. W. Alt, C. Liesau, P. Ríos, C. Blasco, J. V. Miguel, R. M. García, A. A. Fernández, E. Bánffy, M. Bernabò-Brea, D. Billoin, C. Bonsall, L. Bonsall, T. Allen, L. Büster, S. Carver, L. C. Navarro, O. E. Craig, G. T. Cook, B. Cunliffe, A. Denaire, K. E. Dinwiddy, N. Dodwell, M. Ernée, C. Evans, M. Kuchařík, J. F. Farré, C. Fowler, M. Gazenbeek, R. G. Pena, M. Haber-Uriarte, E. Haduch, G. Hey, N. Jowett, T. Knowles, K. Massy, S. Pfrengle, P. Lefranc, O. Lemercier, A. Lefebvre, C. H. Martínez, V. G. Olmo, A. B. Ramírez, J. L. Maurandi, T. Majó, J. I. McKinley, K. McSweeney, B. G. Mende, A. Modi, G. Kulcsár, V. Kiss, A. Czene, R. Patay, A. Endrődi, K. Köhler, T. Hajdu, T. Szeniczey, J. Dani, Z. Bernert, M. Hoole, O. Cheronet, D. Keating, P. Velemínský, M. Dobeš, F. Candilio, F. Brown, R. F. Fernández, A.-M. Herrero-Corral, S. Tusa, E. Carnieri, L. Lentini, A. Valenti, A. Zanini, C. Waddington, G. Delibes, E. Guerra-Doce, B. Neil, M. Brittain, M. Luke, R. Mortimer, J. Desideri, M. Besse, G. Brücken, M. Furmanek, A. Hałuszko, M. Mackiewicz, A. Rapiński, S. Leach, I. Soriano, K. T. Lillios, J. L. Cardoso, M. P. Pearson, P. Włodarczak, T. D. Price, P. Prieto, P.-J. Rey, R. Risch, M. A. Rojo Guerra, A. Schmitt, J. Serralongue, A. M. Silva, V. Smrčka, L. Vergnaud, J. Zilhão, D. Caramelli, T. Higham, M. G. Thomas, D. J. Kennett, H. Fokkens, V. Heyd, A. Sheridan, K.-G. Sjögren, P. W. Stockhammer, J. Krause, R. Pinhasi, W. Haak, I. Barnes, C. Lalueza-Fox, D. Reich, The Beaker phenomenon and the genomic transformation of northwest Europe. *Nature* **555**, 190–196 (2018). doi:10.1038/nature25738 Medline

73. F. Cruciani, R. La Fratta, B. Trombetta, P. Santolamazza, D. Sellitto, E. B. Colomb, J.-M. Dugoujon, F. Crivellaro, T. Benincasa, R. Pascone, P. Moral, E. Watson, B. Melegh, G. Barbujani, S. Fuselli, G. Vona, B. Zagradisnik, G. Assum, R. Brdicka, A. I. Kozlov, G. D. Efremov, A. Coppa, A. Novelletto, R. Scozzari, Tracing past human male movements in northern/eastern Africa and western Eurasia: New clues from Y-chromosomal haplogroups E-M78 and J-M12. *Mol. Biol. Evol.* **24**, 1300–1311 (2007). doi:10.1093/molbev/msm049 Medline

74. R. Fregel, F. L. Méndez, Y. Bokbot, D. Martín-Socas, M. D. Camalich-Massieu, J. Santana, J. Morales, M. C. Ávila-Arcos, P. A. Underhill, B. Shapiro, G. Wojcik, M. Rasmussen, A. E. R. Soares, J. Kapp, A. Sockell, F. J. Rodríguez-Santos, A. Mikdad, A. Trujillo-Mederos, C. D. Bustamante, Ancient genomes from North Africa evidence prehistoric migrations to the Maghreb from both the Levant and Europe. *Proc. Natl. Acad. Sci. U.S.A.* **115**, 6774–6779 (2018). doi:10.1073/pnas.1800851115 Medline

75. T. Lappalainen, S. Koivumäki, E. Salmela, K. Huoponen, P. Sistonen, M.-L. Savontaus, P. Lahermo, Regional differences among the Finns: A Y-chromosomal perspective. *Gene* **376**, 207–215 (2006). doi:10.1016/j.gene.2006.03.004 Medline

76. T. Lappalainen, U. Hannelius, E. Salmela, U. von Döbeln, C. M. Lindgren, K. Huoponen, M.-L. Savontaus, J. Kere, P. Lahermo, Population structure in contemporary Sweden—A Y-chromosomal and mitochondrial DNA analysis. *Ann. Hum. Genet.* **73**, 61–73 (2009). doi:10.1111/j.1469-1809.2008.00487.x Medline

77. P. A. Underhill *et al*., Rethinking the Human Revolution. Cambridge, UK: McDonald Institute Monographs, 33–42 (2007).

78. A. Boattini, B. Martinez-Cruz, S. Sarno, C. Harmant, A. Useli, P. Sanz, D. Yang-Yao, J. Manry, G. Ciani, D. Luiselli, L. Quintana-Murci, D. Comas, D. Pettener; Genographic Consortium, Uniparental markers in Italy reveal a sex-biased genetic structure and different historical strata. *PLOS ONE* **8**, e65441 (2013). doi:10.1371/journal.pone.0065441 Medline

79. C. Batini, P. Hallast, D. Zadik, P. M. Delser, A. Benazzo, S. Ghirotto, E. Arroyo-Pardo, G. L. Cavalleri, P. de Knijff, B. M. Dupuy, H. A. Eriksen, T. E. King, A. L. de Munain, A. M. López-Parra, A. Loutradis, J. Milasin, A. Novelletto, H. Pamjav, A. Sajantila, A. Tolun, B. Winney, M. A. Jobling, Large-scale recent expansion of European patrilineages shown by population resequencing. *Nat. Commun.* **6**, 7152 (2015). doi:10.1038/ncomms8152 Medline

80. G. M. Kılınç, A. Omrak, F. Özer, T. Günther, A. M. Büyükkarakaya, E. Bıçakçı, D. Baird, H. M. Dönertaş, A. Ghalichi, R. Yaka, D. Koptekin, S. C. Açan, P. Parvizi, M. Krzewińska, E. A. Daskalaki, E. Yüncü, N. D. Dağtaş, A. Fairbairn, J. Pearson, G. Mustafaoğlu, Y. S. Erdal, Y. G. Çakan, İ. Togan, M. Somel, J. Storå, M. Jakobsson, A. Götherström, The Demographic Development of the First Farmers in Anatolia. *Curr. Biol.* **26**, 2659–2666 (2016). doi:10.1016/j.cub.2016.07.057 Medline

81. P. Skoglund, H. Malmström, A. Omrak, M. Raghavan, C. Valdiosera, T. Günther, P. Hall, K. Tambets, J. Parik, K.-G. Sjögren, J. Apel, E. Willerslev, J. Storå, A. Götherström, M. Jakobsson, Genomic diversity and admixture differs for Stone-Age Scandinavian foragers and farmers. *Science* **344**, 747–750 (2014). doi:10.1126/science.1253448 Medline

82. C. C. Chang, C. C. Chow, L. C. A. M. Tellier, S. Vattikuti, S. M. Purcell, J. J. Lee, Second-generation PLINK: Rising to the challenge of larger and richer datasets. *Gigascience* **4**, 7 (2015). doi:10.1186/s13742-015-0047-8 Medline

83. A. Manichaikul, J. C. Mychaleckyj, S. S. Rich, K. Daly, M. Sale, W.-M. Chen, Robust relationship inference in genome-wide association studies. *Bioinformatics* **26**, 2867–2873 (2010). doi:10.1093/bioinformatics/btq559 Medline

84. A. L. Price, N. J. Patterson, R. M. Plenge, M. E. Weinblatt, N. A. Shadick, D. Reich, Principal components analysis corrects for stratification in genome-wide association studies. *Nat. Genet.* **38**, 904–909 (2006). doi:10.1038/ng1847 Medline

85. N. Patterson, A. L. Price, D. Reich, Population structure and eigenanalysis. *PLOS Genet.* **2**, e190 (2006). doi:10.1371/journal.pgen.0020190 Medline

86. P. C. Sereno, E. A. A. Garcea, H. Jousse, C. M. Stojanowski, J.-F. Saliège, A. Maga, O. A. Ide, K. J. Knudson, A. M. Mercuri, T. W. Stafford Jr., T. G. Kaye, C. Giraudi, I. M. N'siala, E. Cocca, H. M. Moots, D. B. Dutheil, J. P. Stivers, Lakeside cemeteries in the

Sahara: 5000 years of holocene population and environmental change. *PLOS ONE* **3**, e2995 (2008). doi:10.1371/journal.pone.0002995 Medline

87. I. Lazaridis, D. Nadel, G. Rollefson, D. C. Merrett, N. Rohland, S. Mallick, D. Fernandes, M. Novak, B. Gamarra, K. Sirak, S. Connell, K. Stewardson, E. Harney, Q. Fu, G. Gonzalez-Fortes, E. R. Jones, S. A. Roodenberg, G. Lengyel, F. Bocquentin, B. Gasparian, J. M. Monge, M. Gregg, V. Eshed, A.-S. Mizrahi, C. Meiklejohn, F. Gerritsen, L. Bejenaru, M. Blüher, A. Campbell, G. Cavalleri, D. Comas, P. Froguel, E. Gilbert, S. M. Kerr, P. Kovacs, J. Krause, D. McGettigan, M. Merrigan, D. A. Merriwether, S. O'Reilly, M. B. Richards, O. Semino, M. Shamoon-Pour, G. Stefanescu, M. Stumvoll, A. Tönjes, A. Torroni, J. F. Wilson, L. Yengo, N. A. Hovhannisyan, N. Patterson, R. Pinhasi, D. Reich, Genomic insights into the origin of farming in the ancient Near East. *Nature* **536**, 419–424 (2016). doi:10.1038/nature19310 Medline

88. M. Lipson, A. Szécsényi-Nagy, S. Mallick, A. Pósa, B. Stégmár, V. Keerl, N. Rohland, K. Stewardson, M. Ferry, M. Michel, J. Oppenheimer, N. Broomandkhoshbacht, E. Harney, S. Nordenfelt, B. Llamas, B. Gusztáv Mende, K. Köhler, K. Oross, M. Bondár, T. Marton, A. Osztás, J. Jakucs, T. Paluch, F. Horváth, P. Csengeri, J. Koós, K. Sebők, A. Anders, P. Raczky, J. Regenye, J. P. Barna, S. Fábián, G. Serlegi, Z. Toldi, E. Gyöngyvér Nagy, J. Dani, E. Molnár, G. Pálfi, L. Márk, B. Melegh, Z. Bánfai, L. Domboróczki, J. Fernández-Eraso, J. Antonio Mujika-Alustiza, C. Alonso Fernández, J. Jiménez Echevarría, R. Bollongino, J. Orschiedt, K. Schierhold, H. Meller, A. Cooper, J. Burger, E. Bánffy, K. W. Alt, C. Lalueza-Fox, W. Haak, D. Reich, Parallel palaeogenomic transects reveal complex genetic history of early European farmers. *Nature* **551**, 368–372 (2017). doi:10.1038/nature24476 Medline

89. S. Schiffels, W. Haak, P. Paajanen, B. Llamas, E. Popescu, L. Loe, R. Clarke, A. Lyons, R. Mortimer, D. Sayer, C. Tyler-Smith, A. Cooper, R. Durbin, Iron Age and Anglo-Saxon genomes from East England reveal British migration history. *Nat. Commun.* **7**, 10408 (2016). doi:10.1038/ncomms10408 Medline

90. P. B. Damgaard, N. Marchi, S. Rasmussen, M. Peyrot, G. Renaud, T. Korneliussen, J. V. Moreno-Mayar, M. W. Pedersen, A. Goldberg, E. Usmanova, N. Baimukhanov, V. Loman, L. Hedeager, A. G. Pedersen, K. Nielsen, G. Afanasiev, K. Akmatov, A. Aldashev, A. Alpaslan, G. Baimbetov, V. I. Bazaliiskii, A. Beisenov, B. Boldbaatar, B. Boldgiv, C. Dorzhu, S. Ellingvag, D. Erdenebaatar, R. Dajani, E. Dmitriev, V. Evdokimov, K. M. Frei, A. Gromov, A. Goryachev, H. Hakonarson, T. Hegay, Z. Khachatryan, R. Khaskhanov, E. Kitov, A. Kolbina, T. Kubatbek, A. Kukushkin, I. Kukushkin, N. Lau, A. Margaryan, I. Merkyte, I. V. Mertz, V. K. Mertz, E. Mijiddorj, V. Moiyesev, G. Mukhtarova, B. Nurmukhanbetov, Z. Orozbekova, I. Panyushkina, K. Pieta, V. Smrčka, I. Shevnina, A. Logvin, K.-G. Sjögren, T. Štolcová, A. M. Taravella, K. Tashbaeva, A. Tkachev, T. Tulegenov, D. Voyakin, L. Yepiskoposyan, S. Undrakhbold, V. Varfolomeev, A. Weber, M. A. Wilson Sayres, N. Kradin, M. E. Allentoft, L. Orlando, R. Nielsen, M. Sikora, E. Heyer, K. Kristiansen, E. Willerslev, 137 ancient human genomes from across the Eurasian steppes. *Nature* **557**, 369–374 (2018). doi:10.1038/s41586-018-0094-2 Medline

91. K. R. Veeramah, A. Rott, M. Groß, L. van Dorp, S. López, K. Kirsanow, C. Sell, J. Blöcher, D. Wegmann, V. Link, Z. Hofmanová, J. Peters, B. Trautmann, A. Gairhos, J.

Haberstroh, B. Päffgen, G. Hellenthal, B. Haas-Gebhard, M. Harbeck, J. Burger, Population genomic analysis of elongated skulls reveals extensive female-biased immigration in Early Medieval Bavaria. *Proc. Natl. Acad. Sci. U.S.A.* **115**, 3494–3499 (2018). doi:10.1073/pnas.1719880115 Medline

92. M. Krzewińska, A. Kjellström, T. Günther, C. Hedenstierna-Jonson, T. Zachrisson, A. Omrak, R. Yaka, G. M. Kılınç, M. Somel, V. Sobrado, J. Evans, C. Knipper, M. Jakobsson, J. Storå, A. Götherström, Genomic and Strontium Isotope Variation Reveal Immigration Patterns in a Viking Age Town. *Curr. Biol.* **28**, 2730–2738.e10 (2018). doi:10.1016/j.cub.2018.06.053 Medline

93. W. Scheidel, Human Mobility in Roman Italy, II: The Slave Population. *J. Roman Stud.* **95**, 64–79 (2005). doi:10.3815/000000005784016270

94. Virgil, *The Aeneid* (Penguin, 2006).

95. T. Prowse, H. P. Schwarcz, S. Saunders, R. Macchiarelli, L. Bondioli, Isotopic paleodiet studies of skeletons from the Imperial Roman-age cemetery of Isola Sacra, Rome, Italy. *J. Archaeol. Sci.* **31**, 259–272 (2004). doi:10.1016/j.jas.2003.08.008

96. A. Andrén, Scavi e scoperte sull'Acropoli di Ardea (1961).

97. F. Di Mario, in *Atti della Conferenza Nazionale* (2010), pp. 213–226.

98. E. H. Richardson, P. G. Gierow, The Iron Age Culture of Latium: II. Excavations and Finds. I. The Alban Hills. *Am. J. Archaeol.* **70**, 391 (1966). doi:10.2307/502345

99. P. C. Sestieri, Il Museo della preistoria e protostoria del Lazio: (Roma, E. U. R.) (Museo Luigi Pigorini) (1964).

100. M. Rubini, F. Mallegni, *Arch. Antropol. Etnol.* **CXXVI-CXXVII**, 125–135 (1997).

101. L. Crescenzi, E. Tortorici, Ardea, immagini di una ricerca: Biblioteca nazionale centrale "Vittorio Emanuele II": Roma, giugno 1983 (De Luca, Roma, 1983).

102. R. Peroni, *Bull. Paletnol. Ital.* **75**, 175–197 (1966).

103. S. Modica, *Atti della Accademia Lancisiana di Roma.* **118**, 279–288 (2011).

104. E. S. Shuckburgh, Ed., *The Histories of Polybius* (Cambridge Univ. Press, 2012), vol. 2.

105. S. Gatti, *Quaderni di archeologia etrusco-italica* **24**, 603–613 (1995).

106. F. Coarelli, Guida Archeologica del Lazio, Edizioni Laterza (1984).

107. P. D'Arpino, Boville Ernica storia dell' arte tradizioni: Passeggiate Archeologiche (2003).

108. M. Cancellieri, in Bollettino dell'Istituto di Storia e di Arte del Lazio Meridionale IX (Roma, 1976-1977).

109. R. Vargiu, A. Cucina, M. Mancinelli, M. Lucci, A. Coppa, in L'antica Basilica di San Lorenzo in Damaso indagini archeologiche nel Palazzo della Cancelleria, 1988-1993, C. L. Frommel, Ed. (De Luca, Roma, 2009), vol. II.

110. M. T. Cecchelli, Materiali e tecniche dell'edilizia paleocristiana a Roma (De Luca Editori d'Arte, 2001).

111. A. Coppa, A. Cucina, D. Mancinelli, M. Lucci, R. Vargiu, in Popolazione e Società a Roma dal Medioevo dell'Età Contemporanea, E. Sonnino, Ed. (Il Calamo, Roma, 1998), pp. 435–481.

112. M. Salamon, A. Coppa, M. McCormick, M. Rubini, R. Vargiu, N. Tuross, The consilience of historical and isotopic approaches in reconstructing the medieval Mediterranean diet. *J. Archaeol. Sci.* **35**, 1667–1672 (2008). doi:10.1016/j.jas.2007.11.015

113. A. Guidi, P. Pascucci, in Dives Anagnia: archeologia nella valle del Sacco, S. Gatti, Ed. (Roma, 1993), pp. 57–60.

114. A. Coppa, P. P. Petrone, M. Rubini, R. Vargiu, L. Bernardi, A. Cucina, L. Fattore, M. Lucci, D. Mancinelli, E. Papagiannopoulo, C. Signoretti, in Casale del Dolce. Ambiente, economia e cultura di una comunità preistorica della Valle del Sacco, A. Zarattini, L. Petrassi, Eds. (Ministero per i beni Culturali e Ambientali, Soprintendenza Archeologica per il Lazio, Roma, Roma, 1997), pp. 209–226.

115. Vargiu R., Cucina A., Lucci M., Petrone P.P., Rampa R., Rubini M., Signoretti C., Coppa A., "Relazione Antropologica, documentazione grafica e fotografica delle sepolture rinvenute durante lo scavo del cantiere di scavo archeologico in località 'Casale del Dolce', Anagni (FR), linea alta velocità Milano-Roma Napoli" (Internal Report on Archaeological Superintendence for Lazio, 1996).

116. J. Robb, *The Early Mediterranean Village: Agency, Material Culture, and Social Change in Neolithic Italy* (Cambridge Univ. Press, 2007).

117. M. Rubini, P. Zaio, Bone Changes in an Italian Ancient Human Skeleton—Possibly Caused by Leprosy. *Indian J. Lepr.* **87**, 91–99 (2015). Medline

118. E. K. Nitsch, thesis, University of Oxford (2012).

119. A. Bedini, Castel di Decima. Enciclopedia dell' Arte Antica (1994), p. Vol.II 35–36.

120. M. Bedello Tata, in Roma città del Lazio (2002).

121. A. Bedini, Mélanges de l'École française de Rome. Antiquité, 277–281 (2018).

122. C. Pavolini, G. Spinola, La Collezione Casali e le nuove indagini sul Celio - Rita Santolini Giordani, Antichità Casali. la Collezione di Villa Casali a Roma (Studi Miscellanei 27, L'Erma di Bretschneider, Roma 1989). Pagine 254, 31 figure e 57 tavole fuori testo. ISBN 88-7062-658-X. Lit. 333.000. *J. Roman Archaeol.* **4**, 215–218 (1991). doi:10.1017/S1047759400015646

123. P. Palazzo, C. Pavolini, Ed., Gli dèi propizi. La Basilica Hilariana nel contesto dello scavo dell'Ospedale Militare Celio (1987-2000) (Edizioni Quasar, Roma, 2013).

124. L. Salvadei, A. Nava, G. Tartaglia, Le sepolture dell'area S.5: i dati antropologici, in *Centocelle: Roma S.D.O. le Indagini Archeologiche*, R. Volpe, Ed. (Rubbettino Editore, Roma, 2007).

125. L. Salvadei, A. Nava, G. Tartaglia, Analisi antropologica dei resti umani rinvenuti nel sepolcro a tempietto della villa delle Terme (T.493), in *Centocelle: Roma S.D.O. le Indagini Archeologiche*, R. Volpe, Ed. (Rubbettino Editore, Roma, 2007).

126. L. Salvadei, A. Nava, G. Tartaglia, Considerazioni antropologiche sulle sepolture di età tardoantica, in *Centocelle: Roma S.D.O. le Indagini Archeologiche*, R. Volpe, Ed. (Rubbettino Editore, Roma, 2007).

127. G. Tartaglia, A. Nava, L. Salvadei, in Centocelle: Roma S.D.O. le indagini archeologiche, R. Volpe, Ed. (Rubbettino Editore, Roma, 2007).

128. C. Corrain, G. Erspamer, M. Capitanio, Alcune necropoli romane delle Marche (1982), vol. CXII.

129. F. Capuani, *Bollettino di Informazione dell'Associazione Archeologica Centumcellae* **V**, 56–68 (1971).

130. P. Pascucci, L'Insediamento Costiero Della Prima Età Del Ferro De "La Mattonara (Civitavecchia). *Archeologia Classica* **50**, 69–115 (1998).

131. S. Bastianelli, Appunti di campagna (Roma, 1988).

132. M. S. Arena, P. Delogu, L. Paroli, M. Ricci, L. Saguì, Roma dall'antichità al Medioevo: archeologia e storia nel Museo nazionale romano, Crypta Balbi. I (Electa, 2001).

133. D. Manacorda, Crypta Balbi: archeologia e storia di un paesaggio urbano (Mondadori Electa, 2001).

134. I. Paroli, Roma dall'antichità al Medioevo II: Contesti tardi antichi e altomedievali (Electa, Milano, 2004), vol. 222–278.

135. M. Serradimigni, M. Colombo, R. Grifoni, Atti del IV Convegno di Archeologia "Il Fucino e le aree limitrofe nell'antichita". Archeoclub d'Italia, Avezzano, 49–57 (2016).

136. G. Boschian, M. Serradimigni, M. Colombo, S. Ghislandi, R. Grifoni Cremonesi, Change fast or change slow? Late Glacial and Early Holocene cultures in a changing environment at Grotta Continenza, Central Italy. *Quat. Int.* **450**, 186–208 (2017). doi:10.1016/j.quaint.2016.12.027

137. R. Grifoni Cremonesi, S. M. Borgognini Tarli, V. Formicola, G. Paoli, La sepoltura epigravettiana scoperta nel 1993 nella Grotta Continenza di Trasacco (L'Aquila). *Rivista di Antropologia* **73**, 225–236 (1995).

138. R. Grifoni Cremonesi, in *Congresso Internazionale "Préhistoire des pratiques mortuaires*", E. Derwich, Ed. (2003), pp. 107–110.

139. A. Sperduti, L. Bondioli, P. Garnsey, Skeletal evidence for occupational structure at the coastal towns of Portus and Velia (1st–3rd c. AD), in *More than just numbers? The Role of Science in Roman Archaeology*, I. Schrufer-Kolb, Ed. (Journal of Roman Archaeology Supplement, 2012), vol. **91**, pp. 53–70.

140. A. Sperduti, thesis, Sapienza University of Rome (1995).

141. T. L. Prowse, S. R. Saunders, H. P. Schwarcz, P. Garnsey, R. Macchiarelli, L. Bondioli, Isotopic and dental evidence for infant and young child feeding practices in an imperial Roman skeletal sample. *Am. J. Phys. Anthropol.* **137**, 294–308 (2008). doi:10.1002/ajpa.20870 Medline

142. T. L. Prowse, H. P. Schwarcz, S. R. Saunders, R. Macchiarelli, L. Bondioli, Isotopic evidence for age-related variation in diet from Isola Sacra, Italy. *Am. J. Phys. Anthropol.* **128**, 2–13 (2005). doi:10.1002/ajpa.20094 Medline

143. F. Crowe, A. Sperduti, T. C. O'Connell, O. E. Craig, K. Kirsanow, P. Germoni, R. Macchiarelli, P. Garnsey, L. Bondioli, Water-related occupations and diet in two Roman coastal communities (Italy, first to third century AD): Correlation between stable carbon and nitrogen isotope values and auricular exostosis prevalence. *Am. J. Phys. Anthropol.* **142**, 355–366 (2010). doi:10.1002/ajpa.21229 Medline

144. A. Nava, D. W. Frayer, L. Bondioli, *J. Archaeol. Sci. Rep.* **23**, 406–415 (2019).

145. C. FitzGerald, S. Saunders, L. Bondioli, R. Macchiarelli, Health of infants in an Imperial Roman skeletal sample: Perspective from dental microstructure. *Am. J. Phys. Anthropol.* **130**, 179–189 (2006). doi:10.1002/ajpa.20275 Medline

146. P. F. Rossi, L. Bondioli, G. Geusa, R. Macchiarelli, Osteodental biology of the people of Portus Romae (Necropolis of Isola Sacra, 2nd–3rd Cent. AD). I. Enamel microstructure and developmental defects of the primary dentition, in *Digital Archives of Human Paleobiology*, L. Bondioli, R. Macchiarelli, Eds. (National Prehistoric Ethnographic ''L. Pigorini'' Museum, Rome, 1999).

147. L. Bondioli, A. Nava, P. F. Rossi, A. Sperduti, Diet and health in Central-Southern Italy during the Roman Imperial time. *Acta IMEKO* **5**, 19–25 (2016). doi:10.21014/acta_imeko.v5i2.333

148. K. C. Hoover, R. S. Corruccini, L. Bondioli, R. Macchiarelli, Exploring the relationship between hypoplasia and odontometric asymmetry in Isola Sacra, an imperial Roman necropolis. *Am. J. Hum. Biol.* **17**, 752–764 (2005). doi:10.1002/ajhb.20436 Medline

149. S. Marciniak, T. L. Prowse, D. A. Herring, J. Klunk, M. Kuch, A. T. Duggan, L. Bondioli, E. C. Holmes, H. N. Poinar, Plasmodium falciparum malaria in 1^{st}-2^{nd} century CE southern Italy. *Curr. Biol.* **26**, R1220–R1222 (2016). doi:10.1016/j.cub.2016.10.016 Medline

150. S. Kacki, H. Réveillas, G. Sachau-Carcel, R. Giuliani, P. Blanchard, D. Castex, Réévaluation des arguments de simultanéité des dépôts de cadavres : L'exemple des sépultures plurielles de la catacombe des Saints Pierre-et-Marcellin (Rome). *BMSAP* **26**, 88–97 (2014). doi:10.1007/s13219-013-0092-8

151. D. Mancinelli, R. Vargiu, Gli inumati nella regione I della Catacomba dei SS. Pietro e Marcellino. *Rivista di Archeologia Cristiana* **70**, 43–60 (1994).

152. F. Bisconti, Materiale epigrafici dal cimitero dei SS. Pietro e Marcellino, spunti e conferme per la cronologia della regione I. *Rivista di Archeologia Cristiana* **70**, 7–42 (1994).

153. F. Bisconti, R. Giuliani, F. Tommasi, Archeologia Laziale XII, 1 (Quaderni del centro di studio per l'archeologia etrusco-italica). 23 (1995).

154. T. Di Fraia, in Proceedings of the XXXVIII Scientific Meeting. Italian Institute of Prehistory and Protohistory (2005), pp. 755–765.

155. D. Gatti, *BAR Int. Ser.* **1452**, 482 (2005).

156. A. J. Nijboer, Bollettino di Archeologia online I-2010 (2010).

157. N. Agnoli, E. Carnabuci, G. Caruso, E. Loreti, Apoteosi. Da uomini a Dei. Il Mausoleo di Adriano (Rome, 2014), 114–135 (2014).

158. P. Chini, "Il mausoleo di Augusto," Forma Urbis: itinerari Nascosti Roma Antica, vol. 2, Roma E. E. S. (2002).

159. M. Clemente, thesis, Università di Roma Sapienza (2011).

160. C. M. Coletti, E. M. Loreti, *MAAR* **61**, 304–325 (2016).

161. R. Vargiu, in Internal Report on Archaeological Superintendence of Southern Etrutria (Roma, 2001).

162. M. A. De Lucia Brolli, J. Tabolli, M. Pacifici, M. J. Becker, N. Pagani, *Bollettino Di Archeologia. Online* **7**, 1 (2016).

163. M. C. Biella, Note su Falerii Veteres: a proposito di alcune "nuove" sepolture in località Scasato. *Etruscan Studies: Journal of the Etruscan Foundation* **73**, 17–29 (2009).

164. J. Tabolli, thesis, Sapienza Università di Roma (2011).

165. S. Paoli, T. Sgrulloni, in L'area archeologica della via Nomentum-Eretum in località Tor Mancina, all'interno della Riserva Naturale Macchia di Gattaceca e Macchia del Barco, Archeoclub D'italia Sede, Ed. (Palombara Sabina, 2007).

166. S. Paoli, T. Sgrulloni, La via Nomentum-Eretum e il suo sepolcreto (2013).

167. M. Rubini, Cranial supernumerary ossicles in central-southern Italian populations from the Neolithic up to today. *Anthropol. Anz.* **53**, 33–44 (1995). Medline

168. M. Rubini, P. Zaio, S. Mogliazza, in Il fenomeno antropologico della facies del Gaudo in XLIII Riunione Scientifica - L'età del rame in Italia (2008), pp. 409–424.

169. A. De Bonis, C. Casale, C. R. Russo, Sviluppi storici nelle terre del basso Lazio. Dalla preistoria all'avvento dei Longobardi (Tre Bit, 2019).

170. J. M. Turfa, *The Etruscan World* (Routledge, 2014).

171. M. Silvestrini, G. Pignocchi, in *Le ceramiche impresse nel neolitico antico: Italia e Mediterraneo*, V. Tiné, Ed. (Studi di Paletnologia I, 2002), pp. 469–478.

172. D. G. Lollini, in *Atti VI Congr. Intern. Sc. Preist. Protost.* (Union Internationale des Sciences, 1965), II, pp. 309–315.

173. D. G. Lollini, in *Monterado (AN) – Loc. Ripabianca*, D. G. Lollini, Ed. (1991), pp. 58–63.

174. M. Rosini, M. Silvestrini, L. Sarti, *Rivista di Scienze Preistoriche.* **55**, 225–263 (2005).

175. M. Silvestrini, G. Pignocchi, in *La Neolitizzazione fra Oriente ed Occidente,Atti del Convegno di Studi*, G. Muscio, Ed. (Udine, April 23-24, 2000), pp. 341–354.

176. M. Silvestrini, G. Pignocchi, in *Settemila anni fa il primo pane: ambienti e culture delle società neolitiche: Comune di Udine, Museo friulano di storia naturale*, A. Pessina, G. Muscio, Museo friulano di storia naturale, Eds. (1998), pp. 70–77.

177. S. Pannuzi, Viabilità e utilizzo del territorio. Il suburbio sud-orientale di Ostia alla luce dei recenti rinvenimenti archeologici. Ricerche su Ostia e il suo territorio (2018).

178. P. Pergola, in Archeologia Laziale X (Quaderni del centro di studio per l'archeologia etrusco-italica, 18-19), S. Quilici Gigli, Ed. (C.N.R. (Istituto per l'archeologia etrusco-italica)., Rome, Italy, 1990), pp. 173–176.

179. G. Bartoloni, V. Acconcia, L'abitato etrusco di Veio: ricerche dell'Università di Roma "La Sapienza" (Sapienza Università di Roma, 2012).

180. C. Moffa, C. Rambelli, F. Salamone, *Bullettino della Commissione Archeologica Comunale di Roma* **117**, 322–326 (2016).

181. G. Bartoloni, F. Delpino, Introduzione allo studio delle necropoli arcaiche di Veio. Il sepolcreto di Valle La Fata. *Accad. Naz. Lincei (Rome)* (1979).

182. A. Kahane, L. Murray-Threipland, J. B. Ward-Perkins, *Pap. Br. Sch. Rome* **36**, 1–218 (1968). doi:10.1017/S006824620001103X

183. J. B. Ward-Perkins, I. Introduction. *Pap. Br. Sch. Rome* **29**, 1–119 (1961). doi:10.1017/S0068246200010916

184. P. Hemphill, Archaeological Investigations in Southern Etruria (Acta Instituti Romani Regni Sueciaem, 2000).

185. H. Patterson *et al.*, Bridging the Tiber. Approaches to regional archaeology in the Tiber Valley. *Archaeological monograph.* **13**, 11–28 (2004).

186. P. Brocato, La tomba delle Anatre di Veio (Universita della Calabria, 2012), Ricerche (Università degli studi della Calabria. Dipartimento di archeologia e storia delle arti).

187. C. Torri, A. De Loof, *Bollettino di Archeologia on line* **3**, 87–107 (2012).

188. P. Santoro, *Bollettino di Archeologia on line* **3**, 107–110 (2012).

189. M. Marrucci, M. Summa, *Bollettino di Archeologia on line* **3**, 58–86 (2012).

190. C. Goodson *et al*., in *Villa Magna: an imperial estate and its legacies: excavations 2006–10*, E. Fentress, C. Goodson, M. Maiuro, M. Andrews, A. Dufton, Eds. (British School at Rome, Rome, Italy, 2016), Archaeological Monographs of the British School at Rome, pp. 265–441.

191. T. M. Trombley, S. C. Agarwal, P. D. Beauchesne, C. Goodson, F. Candilio, A. Coppa, M. Rubini, Making sense of medieval mouths: Investigating sex differences of dental pathological lesions in a late medieval Italian community. *Am. J. Phys. Anthropol.* **169**, 253–269 (2019). doi:10.1002/ajpa.23821 Medline

192. S. Hay *et al*., in *Villa Magna: an imperial estate and its legacies: excavations 2006–10*, E. Fentress, C. Goodson, M. Maiuro, M. Andrews, A. Dufton, Eds. (British School at Rome, Rome, Italy, 2016), Archaeological Monographs of the British School at Rome, pp. 61–203.

193. E. Fentress, in *Villa Magna: an imperial estate and its legacies: excavations 2006–10*, E. Fentress, C. Goodson, M. Maiuro, M. Andrews, A. Dufton, Eds. (British School at Rome, Rome, Italy, 2016), vol. 22 of Archaeological Monographs of the British School at Rome, pp. 443–454.

194. E. Fentress, C. Goodson, *Archeologia medievale* **39**, 57–86 (2012).

195. N. Christie, Intelligible Beauty: recent research on Byzantine jewellery, The Trustees of the British Museum, 113–122 (2010).